UNIVERSITY OF SOUTHAMPTON

Faculty of Medicine

Clinical and Experimental Sciences

Characterisation of lipid specific T cell responses in Macaque and Human *Mycobacterium tuberculosis* infection

by

Andrew Chancellor

Thesis for the degree of Doctor of Philosophy

October 2016

UNIVERSITY OF SOUTHAMPTON

ABSTRACT

Mycobacterium tuberculosis (Mtb) continues to cause a global health pandemic and the emergence of new drug-resistant strains requires new therapeutic interventions. Mtb is characterised by a lipid-rich cell wall, thus T cells that respond to lipid antigens are likely to play a critical role in host immunity. I investigate the hypothesis that lipid-responsive CD1b- and CD1d-restricted T cells may play critical roles in host immunity to tuberculosis (TB). Invariant natural killer T cells (iNKTs) are a CD1d restricted T cell population found in humans and macaques and previous *in vitro* and *in vivo* studies have identified their key anti-Mtb roles. I focus on the macaque model of Mtb infection, due to their accurate recapitulation of human disease, to identify iNKT correlates of protection. Using validated methods to identify iNKTs, and systematic analyses across four genetically distinct groups, I first demonstrate that peripheral blood iNKT frequency associates with disease susceptibility. I also observe skewed iNKT $CD4^+/CD8^+$ subsets in animals more susceptible to Mtb. Furthermore, I demonstrate that $CD8^+$ iNKTs associate with better disease outcome in both the Chinese cynomolgus and Indian Rhesus macaque. My results warrant further investigation into the mechanisms behind the observed iNKT based correlates in macaque TB infection. CD1b, the second lipid presenting molecule that I have focused on, is expressed on the surface of professional antigen presenting cells (APCs) and I show for the first time its expression in the human lung granuloma. It presents mycolic acids (MA) from the Mtb cell wall to Germ-line-Encoded-Mycolyl lipid specific T cells (GEMs). I use multiple *in vitro* cellular models to study the structure-function relationships of a large panel (>20) of synthetic Mtb MAs, representative of the major families of MAs in the Mtb cell wall. My results demonstrate that structurally diverse MA lipid tails vary in their ability to stimulate GEM T cells in a mechanism which is independent of antigen processing. The mycolic acid antigenic potential is dictated by the type of meromycolate tail functional group and relative stereochemistry. *In silico* molecular modelling of MAs onto CD1b support my *in vitro* observations and suggest that stimulatory MAs form seemingly more stable CD1b lipid complexes. Finally, my observations are further corroborated in *ex vivo* T cell responses from TB patient clinical samples and increased cytokine responses after stimulation with different mycolic acids. Taken together, our findings delineate immunogenic Mtb lipids which paves the way for lipid based anti-Mtb vaccines and therapeutics targeting GEM T cells.

Table of Contents

List of Tables

List of Figures

List of Accompanying Materials

DECLARATION OF AUTHORSHIP

I, ...[please print name]

declare that this thesis and the work presented in it are my own and has been generated by me as the result of my own original research.

[title of thesis] .....

.....

I confirm that:

1. This work was done wholly or mainly while in candidature for a research degree at this University;
2. Where any part of this thesis has previously been submitted for a degree or any other qualification at this University or any other institution, this has been clearly stated;
3. Where I have consulted the published work of others, this is always clearly attributed;
4. Where I have quoted from the work of others, the source is always given. With the exception of such quotations, this thesis is entirely my own work;
5. I have acknowledged all main sources of help;
6. Where the thesis is based on work done by myself jointly with others, I have made clear exactly what was done by others and what I have contributed myself;
7. [Delete as appropriate] None of this work has been published before submission [or] Parts of this work have been published as: [please list references below]:

Signed:.....

Date:.....

Acknowledgements

I gratefully acknowledge the support and funding from Public Health England who have provided all the resources I required. In particular, I'd like to thank Dr Sally Sharpe and Dr Andrew White who gave careful guidance throughout. I also would like to thank Mark Baird for providing the lipids and helpful discussion.

I thank both Professor Stephan Gadola for initiating the project and continual mentoring and Professor Tim Elliott for advice and valuable conversation.

I'd particularly like to thank Professor Paul Elkington for leading the group so charismatically and for expert guidance, whose enthusiasm, ambition and passion for the subject are highly contagious. Dr Liku Tezera who has been a reliable source of inspiration, knowledge and friendship. Finally, Dr Salah Mansour to whom I remind, 'chi byth yn anghofio eich cyntaf'. I will always be grateful for your 24/7 availability, knowledge of the field and friendship from day one. Your attitude and considered approach sets you apart.

Definitions and Abbreviations

Ag	Antigen
αGC	Alpha galactosylceramide
APC	Antigen Presenting Cell
BCG	Bacille Calmette Geurin
BCR	B cell receptor
β-GlcCer	Beta-glucosylceramide
β_2M	Beta-2-microglobulin
CD1	Cluster differentiation 1
dNKT	Diverse Natural Killer T cell
ER	Endoplasmic Reticulum
ESAT-6	Early Secreted Antigenic Target 6kDa
FasL	FAS Ligand
GEM	Germline-encoded Mycolyl Specific T cell
GM-CSF	Granulocyte Monocyte – Colony Stimulating Factor
GMM	Glucose monomycolate
Gro-MM	Glycerol monomycolate
HIV	Human Immunodeficiency Virus
HLA	Human Leukocyte Antigen
iGb3	Isoglobotrihexosylceramide
IFN-γ	Interferon - Gamma

IL	Interleukin
iNKT	Invariant Natural Killer T cell
LAM	Lipoarabinomannan
LM	Lipomannan
MAIT	Mucosal Associated Invariant T cell
MCP-1	Monocyte Chemoattractant Protein-1
MFI	Median Fluorescent Intensity
MHC	Major Histocompatibility Complex
MIIC	MHC Class II Compartments
MIG	Monokine Induced by Gamma-Interferon
moDCs	Monocyte derived Dendritic cells
Mtb	*Mycobacterium tuberculosis*
PAMPs	Pathogen associated molecular patterns
PBS	Phosphate Buffered Saline
PIM	Phosphatidylmyo-inositol mannosides
PRR	Pattern Recognition Receptor
RAC2	Ras-related C3 2
RAG	Recombinase activating gene
RANTES	Regulated on Activation, Normal T cell Expressed and Secreted
ROI	Reactive Oxygen Intermediates
RNI	Reactive Nitrogen Intermediates
SIV	Simian Immunodeficiency Virus

STAT4	Signal Transducer and Activator of Transcription 4
TDM	Trehalose Dimycolate
TLRs	Toll-like Receptors
TMM	Trehalose monomycolate
TNF-α	Tumour Necrosis Factor - Alpha

Chapter 1: Introduction

Cellular adaptive immunity in higher vertebrates is critically dependent on T lymphocytes and their specific interactions with antigen (Ag) presenting molecules on the surface of antigen presenting cells (APCs). The two major families of antigen presenting molecules in mammals are the peptide binding HLA class I and II molecules, which are highly polymorphic, and the non-polymorphic, lipid binding CD1a-CD1e proteins. In contrast to the HLA system, relatively little is known about CD1 proteins, the spectrum of their presented antigens and the CD1 restricted lipid specific T cell repertoire. One member of the group two CD1 molecules, CD1d, is highly conserved in all mammals, including rats and mice, and has been the focus of intense global studies over the past 15 years. On the other hand, the three other CD1 molecules with antigen presenting function, CD1a, CD1b and CD1c, collectively known as group one CD1 proteins, are not present in mice and rats and remain largely unexplored due to a lack of a suitable animal model (1).

CD1 proteins present lipids and are therefore likely to be critical in host immunity to pathogens with lipid-rich cell walls. *Mycobacterium tuberculosis* (Mtb) is characterised by a complex, lipid-rich cell wall and is one of the most important human pathogens of the past centuries because of its current infection rate, responsible for the death of approximately 1.5 million people a year globally. Furthermore, there has been a significant increase in multidrug resistant (MDR-TB) and extremely drug resistant (XDR-TB) cases, with 92 countries having at least one case of XDR-TB and an estimated 9.6% of MDR-TB patients have XDR-TB, highlighting the global requirement for novel vaccines and tools for rapid diagnosis of TB.

The central research themes into Mtb specific T cell immunity have focused on HLA molecules and their presentation of peptide Ags derived from the Mtb proteome. This pathway results in a $CD4^+$ T cell response releasing interferon-γ (IFN-γ) that produces a host of downstream responses, principally the activation of macrophages to kill intracellular mycobacteria. This response often culminates in a state of latency where the organism cannot replicate, and contained within granulomas; an organised structure of macrophages, lymphocytes and fibroblasts (2). Although this immune response is

often enough to control growth of the pathogen, it rarely leads to sterilisation and in 5-10% of patients, reactivation of infection occurs frequently resulting in death. Bacille Calmette Guerin (BCG) is currently the only licensed vaccine available for Mtb infection and is an attenuated form of *M. bovis,* however despite its administration to around 3.5 billion people over the last century, BCG has done very little to eliminate the pathogen. Compounding the situation was the arrival of new antibiotics, which led to reduced scientific interest and study from the 1960s until 2 decades ago, so the pandemic continues.

Therefore, a greater understanding of immunological responses to Mtb is critical and further novel therapeutic, modelling and vaccination approaches need to be considered to eradicate the disease. Significantly, more appropriate animal models need to be explored to aid in the discovery of new vaccines and understand the immune response behind such a complex disease. This project explores the role of CD1 and their lipid specific T cells to identify possible cellular mechanisms of disease protection against Mtb. It will focus specifically on providing new insights into CD1 restricted T cell correlates of protection, T cell responses that may be harnessed to provide protection against Mtb infection and an understanding of T cell related mechanisms of pathology.

1.1 *Mycobacterium tuberculosis* pathology

Tuberculosis (TB) has a unique complex pathology, as interaction between the bacteria and the host could be considered both detrimental and beneficial to the organism. The large majority of infected individuals maintain life-long bacterial control and even sterilisation. However, bacteria persist in the lung and disease is evidenced only via a Ghon focus identified by a chest radiograph or an immune response to mycobacterial antigens (3). Secondary tuberculosis can still occur leading to dissemination, disease symptoms and ultimately transmission. Initial infection (primary) and secondary tuberculosis behave as two distinctive events, seemingly co-ordinated by Mtb to its advantage (4).

Mtb is transmitted via airborne droplets of less than 25μm, allowing passage to the lung alveoli (5). Once inhaled, Mtb is nearly always phagocytosed by alveolar resident macrophages or dendritic cells but evidence suggests type two pneumocytes may also permit infection in *ex vivo* studies (6). Phagocytosis occurs via the mannose receptor activity which is enhanced by surfactant protein A, in addition, complement protein C3 enhances macrophage phagocytosis (7, 8). The central dogma of Mtb pathology states that once engulfed, further macrophages aggregate around the primarily infected cell to form an organised focal lesion. Several mycobacterial peptides and lipid antigens have been implicated in generating this early granuloma, including ESAT-6, lipomannans (LM), phosphatidylmyo-inositol mannosides (PIMs) and trehalose dimycolate (TDM) (9). The phagosome, the organelle that Mtb inhabits within the macrophage, maintains retention of early endosome markers, normally cleared in maturing phagosomes. Late endosome markers are usually absent, allowing the organism to persist via acquisition of nutrients such as iron and preventing acidification of its environment (10). Activated macrophages in the presence of IFN-γ and tumor necrosis factor-α (TNF-α) are able to fuse phagosomes with lysosomes creating a hostile environment containing low pH, reactive oxygen intermediates (ROIs), lysosomal enzymes and toxic peptides that kill any live Mtb (11). Absence of this normal phagosome-lysosome fusion in activated macrophages accounts for one mechanism that allows Mtb to persist.

After the initial stages of granuloma formation, neutrophils and T cells are then recruited via cytokines and chemokines such as Chemokine motif ligand-1 (CCL-1), interleukin-8 (IL-8), MIG and RANTES to form a well organised structure. Giant foamy macrophages develop and are eventually killed by T cells forming a central necrotic core surrounded by fibroblasts, lymphocytes and monocytes. Mtb generally does not replicate within the central granuloma and can remain dormant for the life of the patient (11, 12). In immunocompromised patients, or during poorly understood circumstances in otherwise healthy patients, the fibrous wall is unable to hold the granuloma and necrotic tissue undergoes liquefaction leading to erosion of infected semi-liquid material into a bronchus for transmission. If dendritic cells are infected they can also migrate through the lymph to settle in new areas of the lung and form secondary granulomas (8). Clinical features of active tuberculosis include weight loss,

fatigue, low grade fever and wasting. Erosion of infection into bronchial arteries can lead to blood in sputum (13). Indeed, although thought of primarily as a pulmonary disease, around 20% of patients with active disease will develop extra-pulmonary symptoms. Infecting bones, genitourinary tract, joints and pleura with the most serious infection in the central nervous system resulting in meningitis (13).

A characteristic feature of tuberculosis infection is granuloma formation. Their presence can be considered a stalemate between the host and Mtb, where control but not clearance is achieved. There is a substantial body of work describing key regulators of granuloma formation and their function. The two most important cytokines are IFN-γ and TNF-α, which act in concert to activate macrophages and induce the maturation of phagosomes. Macrophages are much more capable of killing Mtb *in vitro* with prior addition of either of these cytokines added individually. They activate nitric oxide synthases and stimulate production of reactive nitrogen intermediates (RNIs) (8). Other cytokines such as IL-10 are negative regulators of granuloma formation and therefore establishing granulomas is a result of balance between pro- and anti-inflammatory signals (14).

1.2 Innate and adaptive cytokines in Mtb infection

Many cytokines are involved in the balance between disease control, exacerbation and inflammatory mediation in a prolonged interaction of pathogen and host within the lung. The role of many cytokines are well documented, some are unknown, literature regarding others is contradictory and of course many cytokines are pleiotropic with both a protective and pathogenic effect. Discussed below are a few of the major soluble players involved in Mtb infection.

The early macrophage response to Mtb is critical in host control of Mtb, therefore innate cytokine release is important. Macrophage mediated release of proinflammatory cytokines such as IL-1α and -β is critical for bacterial control as demonstrated by mouse knockout (KO) experiments (15). High levels of necrosis has also been noted in these mice, indicating that IL-1 has a role in regulating controlled cell death in Mtb infection

(16). Increased IL-1 levels support IL-17 release which, although dispensable for control of the lab strain of Mtb H37Rv, is required for protection against virulent clinical isolates (17). IL-17 in turn acts through the IL-17 receptor to induce the chemokine CXCL-13, which is required for correct T cell localisation in the lung (17). Finally, while IL-22 has the function of maintaining IL-17, IL-23 is considered most important for long-term persistence of IL-17 in the lung (18).

To establish a cellular response, innate release of IL-12p40 occurs from dendritic cells in large quantities following TLR2 ligation, inducing a migratory phenotype upon immature dendritic cells, important for T cell priming (19). In addition, IL-12p70, which is not highly expressed in the lung, seems to be required for an optimal IFN-γ response (20). A similar role is ascribed to IL-6, which not only promotes an optimal T cell response but has also been shown to be protective against high doses of aerosol mycobacteria in animal studies (21, 22). IFN-γ is well documented and critical for protective immunity via its main role of early macrophage and DC maturation, mediating phagosome and lysosome fusion to kill Mtb (23, 24). Conversely, type 1 IFN release results in greater Mtb susceptibility (25), and is a correlate of exacerbated disease (26). In a study involving transcript signatures from latent and active TB patients, neutrophil driven type 1 IFN production was exacerbated in active TB patients and a subset of latent patients (26). The authors therefore suggest type 1 IFN is a marker of patients at risk of developing active disease.

Once innate immunity has been triggered, an ongoing adaptive immune response is vital for long-term bacterial control and potential clearance. Central to this are macrophages and dendritic cells, which drive T cell recruitment and their polarisation. Monocyte chemoattractant proteins are secreted by macrophages and DC upon infection such as CCL2 7, 8, 12, 13, and 16 which draw NKs, monocytes, DCs and memory T cells to sites of infection (27). A major cytokine involved in regulating chemokine release is TNF-α, which is responsible for early granuloma formation (28). For example, in TNF-/- mice, there was significant delay in chemo-attractants which led to a reduction in cell recruitment early in infection and therefore increased bacterial growth compared to wild type mice (28). Opposing the effects of TNF-α however is IL-10, which acts as a negative regulator of granuloma formation. Once T cells are present in the infected area,

infected macrophages are less capable of inducing a Th1 response due to upregulation of IL-10 production which in turn diminishes IL-12 release (29). Infected DC on the other hand were unaffected by IL-10 production because of copious and early release of IL-12, promoting a Th1 polarised T cell response (29).

It is clear therefore, that during Mtb infection a myriad of cytokines and chemokines are released to deal with the ensuing infection. Although the role of individual cytokines has been established, there is little appreciation of the effects of the global cytokine micro-environment. This is more technically difficult to investigate but the balance of each cytokine will likely dictate infection outcome as opposed to levels of any single effector molecule. Furthermore, it may be that either a deficiency or excess of individual cytokines is deleterious, leading to a balance between protection and excessive immunopathology.

1.3 Modelling Mtb infection

A number of *in vitro* cultured models of Mtb infection have been developed; however new anti-TB drugs are still required to be tested in animal models. Thus, developing animal models that can accurately recapitulate human disease while generating a well-rounded immune response has been primarily linked to progress in the study of Mtb.

Several animal models of TB currently exist, with mouse as the most widely used. Mice are genetically tractable, have a large number of available reagents and are easily housed and manipulated making them a very useful model. Indeed, many *in vivo* studies have taken place in mice, evaluating efficacy of experimental drugs and more recently showing that humanized mice are useful for recapitulating human disease (30, 31). However in general, mice models are limited due to the lack of the latency seen in humans and the consistent development of disease unless chemotherapy is administered (32). In addition, there is a lack of granuloma structure seen in mouse lungs, as well as no evidence of caseation, a hallmark of advanced human Mtb infection. Thus, investigators are forced to use granulomatous necrosis as a surrogate for cavitation in mouse models (33). Critically, mice lack group 1 CD1 molecules and

although humanized CD1 transgenic mice have been generated, the T cell response has not been formally evaluated (34).

Historically, other animal models have been used such as guinea pigs and rabbits and although these more faithfully represent human TB, they have a limited choice of reagents and guinea pigs succumb rapidly to Mtb infection, thereby making them unsuitable for many studies. Their benefits and limitations as animal models of Mtb infection are summarised in table 1. More recently, other animal models have been employed including zebrafish infected with *Mycobacterium marinum*. They are cheap, optically transparent and genetically tractable. For these reasons zebrafish have contributed greatly to our knowledge of TB pathology (35, 36).

Characteristics	**Mice**	**Guinea pig**	**Rabbit**	**Monkeys**
Cell-mediated Immunity (CMI)	Good	Poor	Good	Poor
Caseation	Little	Large	Moderate	Large
Spread of disease	Confluent granulomas	Haematogenous spread, continual caseous necrosis	Disease heals, except for cavity formation and bronchial dissemination	Haematogenous spread, continual caseous necrosis

Table 1.1: Mtb pathology in 4 animal species

Summary of the features of pathology in mice, guinea pigs, rabbits and monkeys animal models used to study Mtb infection Adapted from Gupta et al (2005) (37).

The model that most accurately recapitulates human TB however, are the non-human primates (NHPs). They have been used extensively over the last 50 years to study multiple infectious diseases, predominantly HIV. Their use in TB declined in the 60's and 70's, but is now growing again due to the increasing threat of TB. In addition, their presentation of disease pathology, immunological events and general anatomy is remarkably similar to humans (38, 39). Similarly to mice, NHP have a good set of reagents available but express the variety of solid, caseous, necrotic and cavitary granulomas, even in the same monkey (32). Furthermore, NHPs are an excellent model

to study the interaction of SIV with Mtb infection, as SIV has already been extensively studied in these animals (40). Critically, NHPs express all CD1 isotypes and some human clones restricted to human group 1 CD1 have been shown to cross-react with macaque CD1, highlighting sequence conservation between these species (35, 41). As NHPs are the penultimate animal model of vaccination, they are very useful to study CD1 restricted immune responses in Mtb infection.

1.4 An Overview of CD1

1.4.1 CD1 structure and evolution

CD1 molecules were first identified in 1979 through antibody staining on the surface of human thymocytes (42). There are five isotypes that are grouped based on sequence similarity which have evolved different antigen binding capacities and intracellular trafficking routes, suggesting different functions. Group 1 includes CD1a, CD1b and CD1c and group 2 contains CD1d. Their restricted T cell repertoires is discussed at length below. CD1 isotypes are most similar to MHC class I molecules, as they comprise a heavy chain containing α1, α2 and α3 domains, with α3 domain being the most homologous between CD1 isotypes (43). Similar to MHC, CD1 molecules require non-covalent association with beta-2-microglobulin (β_2M) for surface expression. While group 1 and 2 molecules are relatively similar in sequence, CD1e has less homology to group 1 and 2 and is unique in as far as it is always expressed in a soluble form and never expressed on the cell surface. Its role therefore is not to act as an antigen presenting molecule, but to aid the processing of complex glycolipids and to bind and assist loading of lipids to other CD1 molecules (44). Group 1 CD1 molecules are expressed only on the surface of professional antigen presenting cells such as Langerhans cells (predominantly CD1a), dendritic cells (DCs) and macrophages (CD1b and CD1c) (45, 46). However, CD1d can be found on the surface of haematopoietic cells as well as a number of tissues in the epithelia, vascular smooth muscle and parenchymal cells (47-49). Most mammals express all five isotypes of CD1 with the exception of mice and rats which express only CD1d (50).

Interestingly, chickens were shown to be the first non-mammalian species to possess CD1 encoding genes (51). Divergence of CD1 from the classical antigen presenting molecules has raised questions about its evolution, but now has been shown to go back as far as the first common ancestor of birds and mammals, around 300 million years ago (figure 1.1). Despite such a long period of evolution, CD1 isotypes have not developed any of the polymorphism seen in MHC. Studies that have found polymorphisms in CD1 isotypes from unrelated donors are very rare and are most frequently silent nucleotide substitutions. Most amino acid changes in the antigen-binding groove occurred in CD1e, which does not function to present antigen (52, 53).

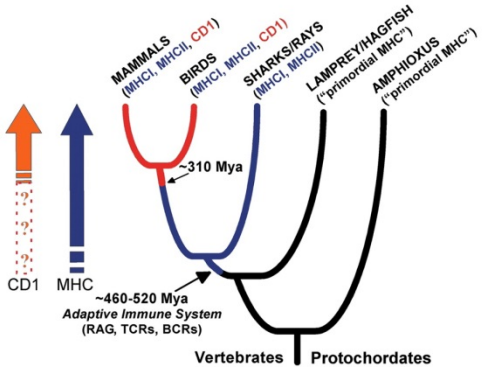

Figure 1.1: CD1 Evolution

Evolution of CD1. First appearance of somatic recombination which leads to diverse TCR and B cell receptors (BCRs) and defines adaptive immunity occurred around 460-520 million years ago. CD1 molecules first appeared after this around 310 million years ago in birds (54).

1.4.2 CD1 trafficking

CD1b is principally localised in the late endocytic system of monocyte derived dendritic cells (moDCs), particularly in endosomal and lysosomal compartments. It contains a nine amino acid sequence in its cytoplasmic tail critical for endosomal targeting. CD1b mutants which lack this motif are expressed normally but are unable to present antigenic lipids exogenously or from intracellular pathogens (55). Likewise, other CD1

molecules have a tyrosine based motif in their short cytoplasmic tail corresponding the sequence YXXω = tyrosine and X =any AA, ω = AA with bulky hydrophobic side chain). The interaction of this tyrosine based motif with cytosolic adaptor protein (AP) forms complexes that dictate route of the molecules and their localization. For example, CD1d was shown in mice to move from its origin in the ER to the late endosomes/lysosomes. The route of CD1d differs from MHC class II molecules in that it goes to the surface immediately after biosynthesis. It then recycles from the cell surface into MHC class II compartments (MIIC) whereas MHCII moves straight from the ER to the MIIC (56).

Elegant experiments using chimeras of CD1a combined with the tyrosine based motif of CD1b showed an inability to present the endogenous lipid sulfatide, which in wild-type, co-localises with CD1a in the early endocytic system (57). Whilst the chimera maintained the same antigen binding capacity as wildtype, differential trafficking meant it failed to present sulfatide efficiently (58). CD1c, despite containing a similar tyrosine based motif in its cytoplasmic tail, acts uniquely in that it surveys the entire endocytic system including recycling endosomes and late endocytic compartments. Also in contrast to CD1b, it does not require lower pH to function or aid lipid binding (59). Differential trafficking suggests each CD1 isotype has adopted its own unique sampling pathway to access diverse lipid repertoires.

Finally, CD1e is a soluble molecule and never expressed on the cell surface, therefore has no role in presenting lipids to T cells. Its localization within dendritic cells depends on the maturation stage, ranging from the trans-golgi network (TGN) in immature DCs to the endosomes and lysosomes in mature DCs. Enzymatic cleavage is required to activate the molecule. With regard to its function, little is known. However, experiments have shown that it can up-regulate or down-regulate surface expression of other CD1 molecules. In a panel of T cells restricted to either CD1b or CD1c, the presence or absence of CD1e caused a differential T cell response, suggesting it can regulate lipid antigen loading or processing. This was highlighted in type 1 and type 2 iNKT clones which differed in their response to APCs with or without CD1e. Its mechanism of action was linked to how the molecule affects the kinetics of CD1d antigen complex formation and duration (44). Furthermore, CD1e has been absolutely required to form the lipid

immunogenic form of the Mtb lipids hexamannosylated PIM_6 for presentation by CD1b. Indeed, it also has a role as a lipid transfer protein, influencing lipid immunoediting and membrane transfer of PIM lipids (60).

As well as having a unique selection of intracellular compartments to sample, each CD1 isotype also contains different shaped antigen binding sites to present a unique repertoire of lipids (Figure 1.2). This affects their lipid binding properties and the specific T cell subsets they restrict. The subject of this project will focus on the antigen binding of CD1b and CD1d and their respective T cell responses.

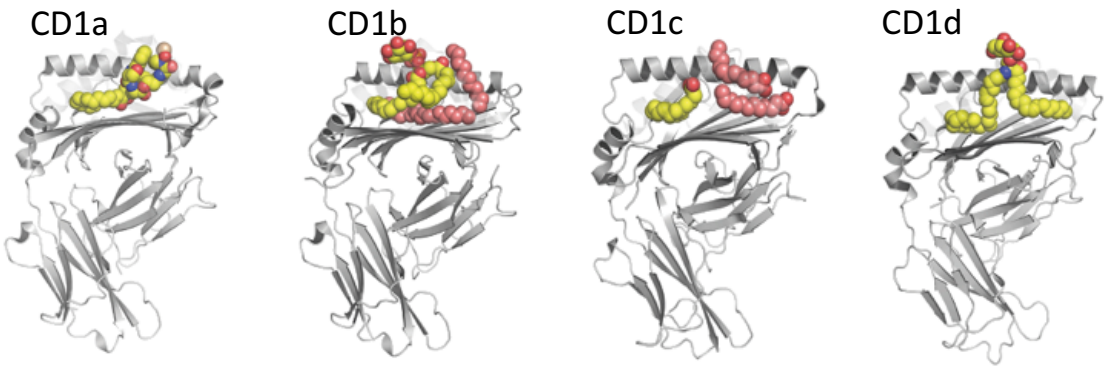

Figure 1.2: Comparison of lipid binding pockets of CD1 isotypes

CD1a, b, c and d each contain unique antigen binding pockets which are formed by their α1 and α2 helices enabling them to bind diverse lipid classes. In this figure, a ribbon representation of each CD1 molecule with antigen presentation function is shown. (Left to right) CD1a is bound to dideoxymycobactin, a lipopeptide belonging to a family of mycobacterial siderophores (49). CD1b is bound to phosphatidyl inositol and two scaffold lipids able to fill the A'T'F' superchannel and the C' channel (61). CD1c contains spacer ligands filling the entire A' and F' channels (62). Finally, CD1d is bound to the prototypic iNKT agonist αGC, this ligand has optimal length sphingosine and acyl chains to fill the entire A' and F' channels with the glucose moiety protruding from the top of the molecule where the TCR interacts (63).

1.5 CD1b structure and antigen presentation

Group 1 CD1 molecules present an array of lipids, glycolipids and lipopeptides that are presented to antigen specific T cells. CD1a, CD1b and CD1c molecules differ in their

structure and localisation dictating the lipid repertoire they are exposed to and subsequently bind (64). Although all cell surface expressed group 1 CD1 molecules have been shown to present lipids from Mtb, CD1b presents lipids almost exclusively from Mtb including: free mycolic acids, glycosylated mycolic acids and PI containing lipoglycans such as LAM and PIM (65). Indeed, it has also been shown that self-lipids are presented by CD1b including gangliosides such as GM1, which may be a cause of harmful T cell autoreactivity in diseases such as multiple sclerosis (66). The most immunodominant CD1b autoantigen is phosphatidylglycerol, which is in low concentration in the membranes carrying CD1b, but relatively high in bacteria and mitochondria (67). Furthermore, upon biosynthesis of CD1b in the cell, structural integrity of the lipid binding cavities is maintained by immediately binding phosphatidylcholine (PC) and other spacer ligands of 40-41 carbons in length (68). Therefore, CD1b is capable of binding many different ligands, with enough space to accommodate multiple shorter lipids, many of which are yet to be identified.

The structure of CD1 molecules is the main factor that dictates antigen binding. Each CD1 isotype has its own unique binding pocket that allows for a limited repertoire of antigens to bind. CD1b, is suggested to have specifically adapted to present the long alkyl chains contained within lipids derived from Mtb due to the volume of its hydrophobic pocket and its exclusive expression in professional APCs. It contains four channels designated channel A', C', F' and T'. Figure 1.3 depicts their layout, showing channels A', C' and F' as those surface exposed, with A' and F' connecting via T'. This unique interlinked channel structure is responsible for the binding of long alkyl chains forming the largest volume binding groove of all CD1 isotypes. In addition, a comparison between CD1d and CD1b suggests a tailored conformation that can be achieved to allow binding of specific ligands in CD1b (69). Furthermore, professional APCs are the only cells equipped to deal with the antigen processing required for MA presentation. This has been demonstrated experimentally by Moody et al., who show rapid internalisation of long MA (C_{80}) but a slow presentation on the cell surface due to the extensive processing leading to their delivery to endosomal pathways in DCs. Conversely, nonprofessional APCs are unable to present these long hydrophobic chains because of the lack of CD1b and an active endosomal pathway (70).

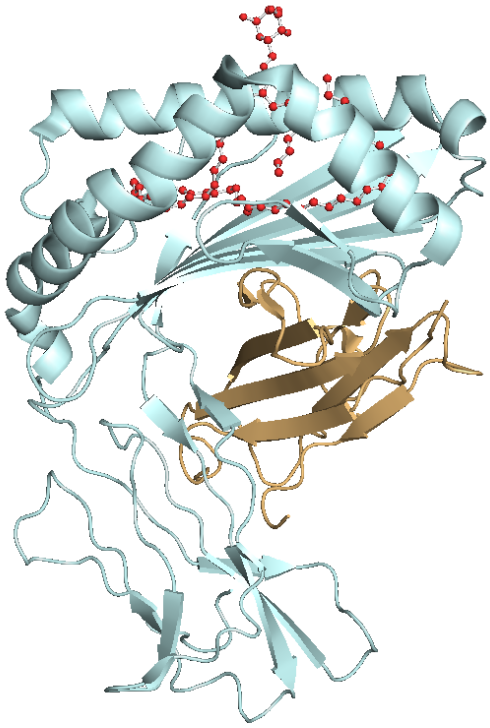

Figure 1.3: Structure of CD1b with bound mycobacterial lipid

Ribbon representation of CD1b containing a GMM. The A', T' and F' channels are interlinked in one super-channel through the protein while C' channel protrudes from the front surface of CD1b. The sugar moiety of the embedded mycolic acid (red) is exposed at the CD1b/TCR interface and contributes towards their interaction. Adapted from Butuwangala et. al. (2004) (61).

Until now, there has only been a limited number of lipids studied in depth that are presented by CD1b. One such lipid, glucose monomycolate (GMM), is a single glucopyranoside residue esterified at its sixth carbon to mycolic acid, a lipid expressed on the cell wall of Mtb and presented by CD1b to induce a specific T cell response (71). GMM was identified as an antigen presented by CD1b to a specific T cell clone, LDN5, taken from the skin lesion of a patient infected with *Mycobacterium leprae* (72). Since then, many studies have defined the specific lipid moieties responsible for enabling lipid binding to CD1b and those that mediate the interaction with the TCR, which are discussed later (65).

1.6 The CD1d/iNKT system

CD1d is so far the best documented of all the CD1 isotypes. Unlike CD1b, it has only two pockets that bind short alkyl chains (73). Figure 2 shows the crystal structure of CD1d highlighting the lipid binding channels A' and F', which can bind a maximum lipid alkyl chain length of 26 and 18 carbons respectively (63). Many foreign and self-lipids are presented by CD1d. Of note, the prototypic glycolipid α-galactosylceramide (αGC) binds CD1d optimally because of its carbon chains that are the perfect length to fit into the binding grooves. The alpha refers to the glycosidic linkage between the carbohydrate and the lipid backbone, not yet formally identified in mammals, despite evidence for their production (74, 75). The α-glycosidic linkage leaves the galactose head group at an orientation such that there is little induced fit required from the TCR. Therefore, αGC binds the iNKT TCR with the highest known affinity of any CD1d ligand, strongly activating iNKTs. This is contrary to β-linked lipids where the head group is flattened into an orientation similar to αGC, to induce binding. Other CD1d ligands, such as the αGC analogue OCH, have shorter sphingosine chains and therefore a shorter half-life in association with CD1d. This supports the notion that ligands with an optimum chain length have a greater binding potential with CD1d and therefore more robustly stimulate CD1d restricted T cells or iNKTs (figure 1.4).

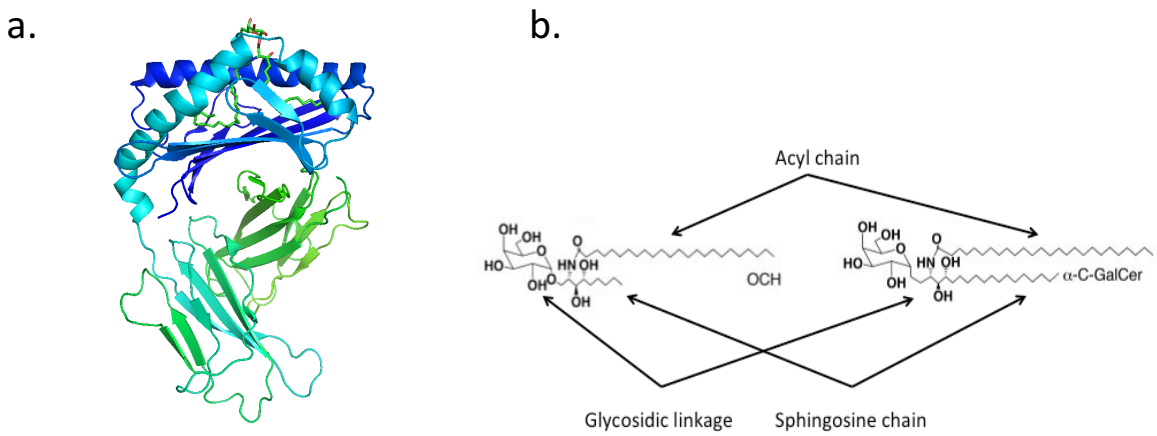

Figure 1.4: Structure of CD1d and its ligands

(a) Crystal structure of CD1d as a ribbon cartoon showing bound α-GC in orange and yellow. The two alkyl chains are inserted into pockets A' and F' with the hydrophilic galactose moiety exposed at the surface. Adapted from Koch et al (2005) (63); (b) The structure of the iNKT superantigen α-GC (right) next to its analogue OCH (Left). Adapted from O'Konek et al. (2011) (76).

iNKTs are an invariant population of T cells restricted to CD1d. They constitutively express surface markers such as CD25, CD69 and CD122 as well as NK1.1 and CD161 that are characteristic of effector cells and natural killer (NK) cells (77). However, they can be definitively identified using CD1d tetramers loaded with αGC. iNKTs are found in the peripheral blood of humans at a frequency of 0.1-0.2% of T cells, however there are large inter-individual differences with some having as high as 5% iNKTs (74). On recognition of self or foreign stimulatory antigens that are presented by CD1d, iNKTs produce numerous effector functions. Functions that are described include bacterial and viral infection control, and modulation of the immune response in many autoimmune conditions leading to either a protective or pathological response.

iNKTs are so called because of their expression of the invariant TCR on their cell surface. The TCR is formed by Vα24Jα18 and Vβ11 chains that are found in both human and macaque, the Vα14Jα18 alpha chain is paired with a more diverse but still limited number of beta chains in mice (78). Also, 'type 2' or diverse NKT cells (dNKT) have been

described that bind to CD1d secreting pro- and anti-inflammatory cytokines, suggesting a redundancy and flexibility of the CD1d restricted arm of the immune system (79). Current models of iNKT activation implicate 3 main pathways: 1) direct TCR interaction with foreign microbial lipid presented by CD1d, 2) iNKT-TCR engagement with weak endogenous self-lipid/CD1d and/or 3) iNKT activation via cytokines such as IL-12, independent of TCR engagement (80). For example, during *S. pneumonia* infection, bacteria are engulfed by APCs leading to presentation of antigenic lipids presented by CD1d, which are recognised by the iNKT TCR (81). This model of T cell activation is more familiar, typically seen in conventional T cell activation.

On the other hand, bacterial recognition by Toll-like receptors (TLRs) leads to the secretion of iNKT stimulatory endogenous lipids, such as β-D-glucopyranosylceramide (β-GlcCer), a self-lipid iNKT agonist, which is then presented by CD1d (82). This so-called type 2 activation in the absence of a foreign ligand is usually less stimulatory but has been found as the dominant pathway for iNKT activation (83). These responses, called direct activation, can be blocked using an anti-TCR antibody, demonstrating a CD1d and iNKT-TCR specific cognate response. Cytokine driven responses have also been shown to activate iNKTs, termed indirect activation, and usually but not always occurs in conjunction with innate CD1d/antigen recognition. IL-12 is the predominant cytokine implicated in this mode of activation, mainly secreted by APCs in response to pattern recognition receptor (PRR) mediated recognition of innate danger signals. High expression of IL-12 receptor on the surface of iNKTs induces a response via signal transducer and activator of transcription 4 (STAT4) activation (83). Indirect activation leads to a lower quantity secretion of IFN-γ than TCR mediated activation (80). iNKT mobilisation via these pathways leads to an array of functions that orchestrates the immune response.

There are many lipid antigens that bind CD1d and activate iNKTs, broadly categorised into two groups: ceramide based glycolipids, glycosphingolipids and glycerol based lipids such as phospholipids. Foreign bacterial lipids and the marine sponge derived αGC, a member of the ceramide glycolipid family and the prototypic iNKT agonist, have all been shown to activate iNKTs. Other α-linked lipids that activate iNKTs, not present in humans, have been found in *Sphingomonas spp*., *Borrelia burgdoferi* and *Streptococcus*

pneumonia, Heliobacter pylori, Leishmania donovani and Entamoeba histolytica (81, 84-88). Also as mentioned previously, iNKTs can be activated potently by CD1d bound host lipids. There is an array of CD1d presented self-lipids identified, including: phosphatidylethanolamine, phosphatidyl inositol (PI), PC, phosphatidylglycerol, glycosylphosphatidylinositol, cardiolipin, sphingomyelin, lysophospholipids, plasmalogens, and gangliosides (89). Initially, the β-linked glycoshpingolipid isoglobotrihexosylceramide (iGb3) was suggested to be the sole self-antigen that promotes iNKT self-reactivity and their thymic selection recognized in both the mouse and human systems (90). However, the gene in humans for the iGb3 synthase appears to be a pseudogene, and there is no functional protein (91). This suggests that iGb3 does not have a role in human iNKT autoreactivity (92).

Once activated, iNKTs can produce a large variety of different Th1 and Th2 cytokines, however their precise *in vivo* functional responses are not always predictable. Broadly, iNKTs are able to secrete: IL-2, -3, -4, -5, -6, -9, -10, -13, -17 and -21, IFN-γ, TNF-α, granulocyte monocyte-colony stimulating factor (GM-CSF), RANTES, MIP-1a and MIP-1b (93, 94). Their function *in vivo* during host infection is associated predominantly with the potent release of IFN-γ and TNF-α or IL-4, IL-10 and IL-13 respectively. The particular repertoire of cytokines released is seemingly specific to particular subsets of iNKTs or those obtained from different organs. In addition, the response is dependent on their mode of activation, cytokine environment, duration of activation and other factors. However, no one has yet identified the exact reasons for the differences in their functional responses, that are likely to be due to a combination of reasons (77). Hence, to fully understand the role of the iNKT repertoire in infection control, they should to be studied under different environmental scenarios to understand how the manipulation of their responses can shape future therapies.

1.7 Mtb evades MHC responses but not CD1

Mtb employs a number of tactics to evade an innate immune response. The most well described strategy is the prevention of phagosome maturation and acidification which allows Mtb to reside and replicate uninterrupted within the cell (95). Mtb is also able to resist the bactericidal effects of oxidative and nitrosative stress via ROIs and reactive nitrogen intermediates (RNIs) (96). It does this not only through prevention of macrophage maturation and low permeability of its cell envelope, but also through counter defence mechanisms mediated by production of molecules able to detoxify ROIs and RNIs (96).

More importantly for its long-term establishment, Mtb is able to evade a robust peptide specific T cell response at the early stages of infection. Firstly, Mtb resides within the phagosomes and does not enter the cytosol, completely avoiding the MHC class I presentation pathway. Secondly, Mtb interferes with cysteine protease cathepsins which cleave the invariant chain (Ii) before MHC is fully assembled subsequently preventing correct trafficking and loading of MHC II molecules and therefore a $CD4^+$ T cell response (95). Antigen specific T cell responses have also been shown to be delayed in virulent Mtb compared to BCG. This is perhaps due to reduced macrophage and DC trafficking to local lymph nodes and/or low antigen availability due to slow mycobacterial division, although definitive experiments are lacking (95). In addition, Mtb prevents controlled cell death which can release peptide antigens for uptake, via release of superoxide dismutase (SodA) which blocks ROI production. Simultaneously enhanced $CD8^+$ T cell priming occurs with reductions of SodA (95). Finally, Mtb directly prevents a T cell response through downregulation of CD3 zeta but not epsilon expression on T cells isolated from the granuloma (97). In addition, ZAP-70 phosphorylation, which is essential for T cell activation, was also greatly reduced in the presence of Mtb lipids LAM and PIM. (98). These features of Mtb suggest an inherent drive to prevent peptide specific T cell responses.

Further to its direct prevention of T cell responses, Mtb may employ a decoy tactic. For example, there are a few immunodominant antigens secreted by Mtb shortly after infection, as in the case of antigen 85 (Ag85) which is not essential for bacterial survival.

This may underline an attempt to mask less dominant antigens that are more relevant for survival of the pathogen (99). Once infection has been established Ag85 production is then switched off. In addition, many of the non-secreted Mtb antigens fail to induce an immune response, another possible attempt to evade direct recognition (99). Furthermore, Mtb is able to delay an adaptive immune response, chiefly due to prevention of migration of dendritic cells to local lymph nodes. Experimental evidence also demonstrates a slower T cell response from aerosol infection compared to intravenous, indicating specific immune evasion from pulmonary infection (99).

With regard to lipid specific T cell responses, very little evidence even describes how CD1b/lipid antigens are presented to T cells in the local granuloma environment. Experiments have not yet demonstratively identified macrophages, the principle cell infected with Mtb, to express CD1b. However, DCs which express CD1b normally have high migratory potential and impaired peptide antigen presentation function when infected, therefore potentially serve to prime lipid specific T cells (5). In addition, Mtb cannot avoid presentation via the 'detour pathway', whereby apoptotic blebs and vesicles shed from infected APCs, contain lipid antigens which upon uptake via nearby DCs are presented on the cell surface (100). This mechanism of cross priming allows lipid antigens to be presented by CD1, not necessarily present on macrophages. CD1b also has an advantage, as it avoids downregulation, which occurs in MHC, principally from ESAT-6 and LAM (100). Finally, CD1b has the highest recycling rate of any antigen presenting molecule, thus allowing it to constantly survey the endocytic vacuoles for new Mtb antigens (57).

1.8 Kinetics of Innate and Adaptive Immune responses

Typically, upon pathogen invasion, the host will generate a non-specific local inflammation mediated by recognition of pathogen associated molecular patterns (PAMPs) (101). The cells involved include: neutrophils, monocytes, macrophages, dendritic cells and natural killer cells. They are activated within hours of pathogen recognition and upregulate co-stimulatory receptors required for correct T cell

activation (102). Conventional T cells then specifically recognise presented antigen and begin clonal expansion, which can take up to a few weeks to complete. These T cells then migrate to the site of infection through upregulation of chemokine receptors and adhesion molecules on the cell surface (103). iNKTs however, display more of an innate-like phenotype, in as much as they release cytokine rapidly upon TCR engagement. For example, iNKTs from mice contained >1000-fold more IL-4 mRNA and 200-fold more IFN-γ mRNA transcripts than naïve conventional T cells, and even more than NK cells (104). Transcription of cytokine genes occurs early in development within the thymus compared to conventional T cells where it occurs only when activated (105). While the kinetics of GEM T cell activation has not been studied, they may generate responses similar to those of conventional T cells. Due to their unusual specificity toward foreign ligand and their similar frequency to conventional peptide specific T cells, it is likely that they are one example of an extremely public TCR (106). Which is logical given their restriction toward a non-polymorphic antigen presenting molecule. Also, CD1b/MA responses have been investigated leading to the conclusion this population has features of conventional T cells such a low number of naïve cells and recall expansion implying memory (107). Although this doesn't apply necessarily to GEMs, it suggests they are similar to conventional T cells.

1.9 A role for T cells in Mtb

Granulomas provide an opportunity for T cells to accumulate at the site of infection to elicit important effector functions for long term containment of Mtb. Human immunodeficiency virus (HIV) co-infection with Mtb is the most powerful known risk factor predisposing for active disease and is predominantly associated with the loss of $CD4^+$ T cells (108). Within the granuloma, T cells account for 10-50% of leukocytes and around 60-70% of those are $CD4^+$, the majority of the remaining are $CD8^+$ with other minor populations present such as invariant natural killer T cells (iNKTs) and gamma/delta T cells (14). Investigation into the T cell repertoire within the granuloma has been performed in mice and although this poorly reflects pathology in humans, it is still a popular choice of animal model. T cells from homogenised granulomas stained

with a panel of anti-TCR β-chain antibodies, revealed no one TCR chain was over-represented within the population and a diverse T cell repertoire was present. This suggested that although there was no strong selection for a particular T cell clonal population where expansion had occurred on antigen recognition, there was limited T cell recruitment (109). Recently in contrast, investigation of the $CD8^+$ T cell repertoire discovered limited T cell diversity, and clonal expansion toward immunodominant antigens (110).

The role of both $CD4^+$ and $CD8^+$ T cells in the host defence against Mtb is sometimes controversial, an idea partly exacerbated by use of different infection models. In 5CC7/recombinase-activating gene 2 deficient (RAG2-/-) mice, a single $CD4^+$ clonal T cell population was sufficient to control bacteria and adequately form granulomas (109). Furthermore, absence of MHC class II in mice resulted in survival times reduced by more than half, mice were less able to control bacterial growth and had an increased burden in lungs, liver and spleen, suggesting $CD4^+$ T cells controlled Mtb infection. In addition, CD4 negative mice showed a delayed ability to form granulomas (111). With regard to the Mtb antigen specific repertoire, intravital microscopy revealed little difference in cytokine production and motility between antigen specific and non-specific T cells within the granuloma, with both demonstrating little retention and high T cell turnover. In addition, recruitment to the granuloma which occurred independently of antigen presentation suggests limited or masked antigen presentation. This study however, focused only on peptide specific T cells in mouse hepatic granuloma (112).

As well as their role in generating protective immunity towards Mtb, $CD4^+$ T cells are required for the development of a $CD8^+$ T cell response (113). $CD8^+$ T cells elicit a number of functions to participate in the Mtb immune response. Mycobacteria specific $CD8^+$ T cells recognise Mtb infected macrophages and produce granulysin, perforin and also kill via the FAS ligand (FasL) pathway (114). Indeed, activation of Fas receptors on the surface of macrophages has also been implicated in macrophage activation of subsequent bacterial control (115, 116). Furthermore, β2m knockout mice that fail to develop functional $CD8^+$ T cells, demonstrated a markedly reduced lifespan post challenge compared to wildtype. Granulomas present in both control and knockout mice contained greater numbers of bacilli in knockout strains as well as caseation not seen in

control mice. This suggests that $CD8^+$ T cells are necessary for bacterial control in Mtb infection (117).

In the periphery, Mtb specific T cells are also found. Various studies have correlated multifunctional T cells that are able to simultaneously secrete IFN-γ, TNF-α and IL-2 (118) with protection while others have found such T cells and their responses correlate with active Mtb, suggesting their presence can be used in diagnostics (119). In mice, multifunctional T cells have been shown to correlate with protection. However, in macaque, they correlate with antigen burden rather than protection (119-122). Contrasting responses are likely due to differences in the animal model, techniques, disease stage, prior exposure to environmental mycobacteria and different populations studied. However, it highlights how peripheral T cell behaviour in Mtb infection is still unclear.

1.10 Lipid Specific T cells in Mtb

In addition to the classical T cells which have been extensively studied, lipid specific T cells likely play a critical role in TB pathogenesis due to the complex lipid-rich cell wall of Mtb. Over the last 10-15 years there has been a burgeoning number of lipid specific T cells identified, recognising both self and foreign lipids when presented by CD1 isotypes. A total of eight Mycobacterial lipids have been identified as group 1 CD1 presented antigens which form the bulk of all foreign lipids studied when presented by CD1 group 1 (123). Most recently, development of CD1a (124), CD1b (125) and CD1c (126) tetramers bound to mycobacterial ligands, has allowed the efficient capture and analysis of CD1 restricted T cell clones.

1.10.1 CD1a lipid Specific T cells

Many endogenous lipid antigens bind CD1a including: sphingolipids, triacylglyceride (TAG) and phosphatidic acid containing compounds such as phosphatidylglycerol,

phosphatidylethanolamine and phosphatidylserine (127). In addition, apolar autoantigens have been identified for CD1a including: squalene, wax esters, TAG and fatty acids (127). Interestingly, bee and wasp venom was demonstrated to 'hijack' the CD1a system and cleave the polar head group from these skin resident antigens to initiate an autoreactive inflammatory response (128). T cells specific for these autoantigens are diverse, so far demonstrating no TCR conservation and represent up to 0.4% of the memory T cells in the blood (129).

The first CD1a/mycobacteria specific line was $CD8^+$ and demonstrated cytotoxicity and strong Th1 responses (130). Using TCRs derived from this line, the mycobacterial antigen didehydroxymycobactin was identified and is responsible for the CD1a restricted T cell response of the TCR CD8-2 (131). The mechanism of lipopeptide presentation was subsequently elucidated (49). The lipopeptide is an essential intermediate in the mycobactin synthesis pathway, a molecule necessary for mycobacterial iron capture (131). TCR interaction is entirely dependent on peptide-peptide specific interaction, as modification of the peptide head group completely ablates recognition (49).

1.10.2 CD1b Lipid Specific T cells

Many TB cell wall lipids are likely to be presented by CD1b because of its extensive antigen binding site that can adapt to different ligand sizes. Therefore, the anti-mycobacterial potential of CD1b restricted T cells have been better characterised than CD1a or CD1c. For example, in a humanized RAG-/- transgenic mouse model expressing the MA specific TCR DN1 and group 1 CD1, MA specific T cells demonstrated faster kinetics compared to Ag85B specific $CD4^+$ T cells after aerosol infection (132). Furthermore, the potential to target these cells via vaccination is highlighted as they accumulated in the lung granuloma, exhibited polyfunctional characteristics and ultimately protected against Mtb infection (132). Moreover, in humans, PPD positive subjects elicited a robust T cell response toward CD1b presenting GMM, an immunodominant antigen (133-135). These responses can be blocked by CD1b specific antibodies and revealed the majority of cells are $CD4^+$ (133). Furthermore, GMM specific

responses were at a frequency comparable to that of the well characterised peptide antigens CFP-10 and ESAT-6, with a frequency of between 0.05-0.1% (133).

In addition, CD1b/MA-specific T cells are found in unexposed humans in the periphery and are in higher numbers in patients infected with Mtb (133, 136). These T cells have little functional correlation to peptide specific T cells, however, more closely follow levels of pathogen burden when measured longitudinally in patients receiving anti-Mtb chemotherapy (135). In particular, MA specific T cell responses peaked at diagnosis and declined sharply with treatment, suggesting they were clonally expanded during infection. Furthermore, PBMCs exposed to MA up to 27 months post curative treatment led to 12-16 fold expansion in responding T cells suggestive of a memory response (107).

There is also a growing base of evidence suggesting that CD1b restricted T cells are able to secrete protective Th1 cytokines as well as respond in a cytotoxic manner (136, 137). Demonstration of efficient secretion of IFN-γ (132) and TNF-α (134, 135) has been shown in multiple isolated clones and lines from several donors. In addition, bronchoalveolar lavage samples taken from donors latently infected with Mtb were identified to limit Mtb growth more efficiently than samples taken from patients who developed active disease (138). Critically, they demonstrated that LAM was the immunodominant antigen and inhibition via CD1b blocking antibodies increased Mtb cell growth over 55% (138). Finally, the CD1b specific T cells were shown to be $CD8^+$ and polycytotoxic releasing: granulysin, granzyme B and perforin, all anti-mycobacterial effector molecules (138). Therefore, CD1b restricted T cells clearly have a role in immunity to Mtb, however this is still poorly understood. Better understanding the T cell response in Mtb infection may identify them as targets for future TB therapeutics.

1.10.3 CD1c Lipid Specific T cells

First evidence of mycobacterial antigens presentation by CD1c were demonstrated by the T cell lines DN6 and BDN2e which were restricted to phosphomycoketides (PMs) and *M.leprae* derived lipoarabinomannans (LAMs) respectively (126, 139). Later a specific

line CD8-1 was generated, this $CD8^+$ positive T cell line was responsive towards CD1c/lipid. Isoprenoid glycolipids present in both *Mycobacterium tuberculosis* and *Mycobacterium avium* were responsible for the T cell activity (140). Specifically mannosyl-B1-phosphomycoketide (MPM) was identified and synthetic lipid structures that more closely resembled the natural branched MPM were most antigenic (141). In addition, the mechanism of binding of CD1c to the mycobacterial antigen mannosyl-B1-phosphomycoketide (MPM) was elucidated in 2010 with a crystal structure which highlighted an open F' groove structure indicating a CD1c unique feature which enables the binding of dodecameric lipopeptides (142). Using soluble CD1c monomers loaded with MPM and MP, evidence of lipid processing was shown as MPM did not activate DN6, instead the mannosyl head group was cleaved leaving the active MP antigen available for DN6 activation (126). Functionally this CD1c lipid complex provided a platform for TCR docking and a T cell response able to kill macrophages infected with mycobacteria (130). Finally, in 2016, cholesterol esters were found to bind to CD1c and crystallisation revealed a closed CD1c conformation state able to bind the self-reactive TCR NM4 (62). These self-reactive T cells may well be involved in Mtb immunity, as it is well known that Mtb perturbs the cholesterol synthesis pathway. Hence, Mtb induced changes in cholesterol metabolism may induce CD1c restricted immunity in the host.

Sequencing of Mtb*'s* genome revealed >250 distinct genes encoding enzymes involved in fatty acid synthesis and the catabolism of an array of lipophilic molecules. This is compared to *E.coli* which has a mere 50 genes devoted to fatty acid metabolism. Thus, fatty acid metabolism is important for Mtb and may well induce a CD1 restricted T cell response. In terms of the co-evolution of CD1 alongside this ancient pathogen, Shinkai et. al. suggested it was unlikely CD1 was specifically selected to confront Mtb or *M. leprae*. This is primarily because of the age of the two organisms where Mtb is suggested to have adapted as a human pathogen only 60,000 years ago but also because mice who are inherently more resistant to Mtb than humans have no group 1 CD1 expression compared to guinea pigs who have all CD1 expression, and are very susceptible to infection (143). However, it does raise the question as to why Mtb has evolved such a unique repertoire of lipid antigens able to bind CD1 molecules, many that cause a T cell response.

1.11 MAIT cells in Mtb infection

Mucosal associated Invariant T cells (MAITs) are an unconventional T cell subset that recognizes vitamin B derivatives when presented by the non-classical MHC class I like molecule MR1 (144). They contain an invariant TRAV1-2 chain, are $CD161^+$ and are predominantly $CD8^+$ in humans (145). As an invariant T cell they provide a rapid immune response at mucosal barriers, activated by bacilli containing a riboflavin biosynthetic pathway, with no need for prior antigen exposure (146). Their conserved docking mode suggests the MAIT TCR acts more as a pattern recognition receptor than a conventional TCR (144). Their role in Mtb infection has not been widely investigated, however there have been a few critical observations made. Firstly, in mice lacking MR1, lung control of *M. bovis* and BCG was decreased suggestive of a protective role (147). In humans, $TRAV1\text{-}2^+$ T cells represent up to 20% of all $CD8^+$ T cells in bronchoalveolar lavage (BAL), which are further enriched in Mtb infection (147). Simultaneously, MAIT cells contribute up to 10% of T cells in the blood which is reduced in Mtb infection, suggesting they home to site of infection (146). Finally, MAIT cells are capable of producing IFN-γ, TNF-α and IL-17a upon bacterial infection in the lungs (145). Therefore, it stands to reason that MAIT cells would have a significant role to play in the early immune response toward Mtb.

1.12 γ/δ T cells in Mtb infection

Unlike MAITs, there has been greater investigation into the role of γ/δ T cells in Mtb infection. However, these T cells that express a TCR composed of both a γ-chain and a δ-chain are less well characterised in general. The first observations were in mice, where γ/δ T cells were higher in number in the peripheral blood after mycobacterial infection (148). The predominant γ/δ subset in humans that respond to mycobacterial antigens is the Vγ9/Vδ2 subset, which originate from the blood, suggesting a strong homing response from these cells (149). Responding γ/δ cells produce high levels of IFN-γ and can recognise both peptide and non-peptide antigens, like phosphoantigens such as isopentenyl pyrophosphate (IPPP) and related prenyl pyrophosphates, derived from the

isoprenoid pathway (148). Subsets of γ/δ T cells are also polyfunctional, and are able to release IFN-γ, TNF-α and IL-2 (150). In addition, γ/δ T cells can elicit cytotoxic activity against mycobacterial antigens which can be blocked by anti-γ/δ TCR antibodies (151). A separate study also found that direct expansion of γ/δ T cells in response to mycobacterial antigens is dependent on exogenous IL-2 (152). Finally, in a study investigating the protective role of γ/δ T cells in TB, the authors found far higher numbers in patients that controlled infection compared to those with ineffective immunity, suggesting their significant contribution to protection against Mtb (153).

1.13 Development of Classical and non-classical T cells

Classical T cells develop from haematopoietic stem cells located in the thymus, where signals from non-haematopoietic cells initiate their development. The central tenet of T cell development involves two main stages of positive and negative selection to ensure a healthy T cell repertoire.

T cells begin as double negative progenitor cells that enter the thymus at the cortico-medullary junction and pass through three phases defined by $CD44^+/CD25^-$, $CD44^+/CD25^-$ and $CD44^-/CD25^+$ expression called DN1, DN2 and DN3 (154). TCR rearrangement then occurs after pre-TCR activation, which causes re-expression of RAG genes and likely α/β or γ/δ TCR expression, at which stage the cells are double positive for CD4 and CD8 (154). However, despite high RAG recombinase activity it is unlikely a functional MHC restricted TCR is produced due to the large probability of improper gene recombination. Productive TCR rearrangement needs to occur within 3-4 days or the cells will move into apoptosis (155). Upon MHC restricted TCR expression, the cell engages its target and remains bound while RAG recombinase activity is reduced, and long term survival signals are upregulated (156). This model suggests that thymocytes expressing TCRs with no or very low affinity for peptide–MHC complexes die by neglect. Commitment into a $CD4^+$ or $CD8^+$ lineage only takes place when an intermediate affinity interaction occurs, to ensure only T cells with correct restriction are generated.

On the other hand, clonal deletion occurs if the affinity of the TCR interaction with its MHC target is of high affinity within the thymus. This is called negative selection which functions to prevent self-reactive T cells from entering the periphery and causing inappropriate autoimmune responses. This process likely requires a second co-receptor signal as CD28 deficient mice are resistant to anti-CD3 or peptide induced apoptosis (157). Once correct T cell selection has occurred, there is attenuation of their response toward intermediate affinity self-peptides. These T cells lose their sensitivity toward self antigens altogether, while responses toward agonist peptides stays the same or increases (158). Several mechanisms have been suggested to account for this including: increased TCR levels (159), reduction in Lck association with the TCR (160), and upregulation of inhibitory receptors CD2 and CD5 (158).

Although iNKTs develop from the same precursor, their development is different from classical T cells, owing to their inherent autoreactivity and hybrid expression of an $\alpha\beta$ TCR as well as the inhibitory MHC specific NK receptors (161). Thymocyte progression to DP status appears similar between classical and iNKT cells, and generation of the invariant iNKT TCR seems to be random, where no preferential joining of the Vα14 to Jα18 occurs in mice (162). However, CD4 and CD8 expression is particularly low at this stage (163). Therefore, there is no evidence to suggest pre-commitment for the iNKT lineage. However, double positive cells expressing the iNKT TCR are then positively selected for by CD1d presenting endogenous ligand, expressed on other haematopoietically derived thymocytes rather than thymic epithelial cells like mainstream T cells (164). DP cells then downregulate CD8 and upregulate CD4 in humans and mice as well as undergo massive expansion. At which time, negative selection occurs, at an earlier stage to conventional T cells, as delayed addition of the superagonist αGC failed to delete iNKTs, where conventional T cells otherwise would have been deleted (165). Finally, 70% of iNKTs released from the thymus are NK1.1$^-$ and therefore it is likely a late stage development of iNKTs occurs in the periphery, compared to conventional T cells whose release is tightly regulated to ensure only mature T cells are circulating.

1.14 TCR Recombination

T cell receptors enable the highly specific detection of an enormous number of peptide and lipid antigens derived from self and foreign organisms. Therefore, an equally large number of TCRs need to be available to recognise these antigens. Individual humans have around $x10^{12}$ circulating T cells, however not all express a unique TCR, and there are approximately $0.5\text{-}5x10^{6}$ unique β-chain sequences per individual (166). The theoretical maximum number of β-chain sequences has been estimated at both $5x10^{11}$ or $3.5x10^{23}$ and the number of α/β combinations at $x10^{15}$, highlighting the potential number of recognisable antigens (167).

After pre-TCR activation during T cell development, RAG genes are active and begin V(D)J recombination; the process which occurs in a stochastic manner and leads to TCR diversity (168). In mammals, there are 4 TCR antigen receptor loci, the α, β, γ and δ. Each locus is a linear array of gene segments containing variable (V), diversity (D) and joining (J) gene fragments that require recombination to generate functional genes. However only the β and δ loci contain the diversity elements. Gene segments are typically flanked by conserved nonamer and heptamer sequences separated by either 12 or 23 base pairs (bp) of non-conserved DNA called a spacer (168). These so called recombination signal sequences (RSS) are the sites for RAG1 and RAG2 activity, two enzymes which are required to cut the DNA (168). The RSS are essential for DNA recombination as correct 12/23 pairing ensures functional output. Importantly, TCR diversity is also generated through inclusion of N-nucleotide sequences at the junctions of gene segments. Coding joints frequently generate non-templated and templated nucleotide insertions, which can be up to 15 bp long (168). This also means in many cases the reading frame is shifted or stop codons are introduced rendering the rearrangement non-functional.

1.15 iNKTs in Mtb infection

There has been an expanding body of work over the last few years regarding the specific role of iNKTs in Mtb infection, with the majority being conducted in mice. Basic observations have been made regarding iNKT frequency in the peripheral blood. In patients with active TB disease, iNKT numbers are reduced and are hypothesised to home quickly to the site of infection within the lung (169). In addition, the few iNKTs that are found in the periphery show more of an activated phenotype, as measured by increased CD38, CD69, HLA-DR and a much higher expression of CD25 (169).

Studies comparing lung pathology and bacterial burden in iNKT knockout (KO) mice with wild type mice post infection found little difference in disease development or capacity of the immune system to control infection (170). A second group independently corroborated this effect at a similar time, however they were able to show that administration of 100μg αGC/Kg *in vivo* to Mtb susceptible mice resulted in a clear protective effect. Bacterial burden was reduced in the lung whilst also almost doubling the mean survival time of the mice (171). This suggests that although they are not required for a protective immune response, iNKTs can exhibit features that will enhance immunity against Mtb infection. iNKTs may therefore be an ideal target when developing vaccines or new treatments.

Further to their role in modulating immune responses to infection including Mtb, iNKTs have also been shown to have direct anti-mycobacterial activity. Adoptive transfer of iNKTs into mice prevented mycobacterial replication, even without activation by αGC and at limiting dilution (172). Furthermore, *in vitro* co-culture of Mtb infected macrophages with αGC activated iNKTs improved control of bacterial replication. This was verified in *in vivo* mouse models where systemic application of αGC prevented the death of even the most susceptible mouse strains against Mtb (173).

Experiments evaluating the role of iNKTs in Mtb infection invariably generate data based on the release of Th1 cytokines such as IFN-γ and TNF-α. Indeed IFN-γ has been shown to be protective both *in vitro* and *in vivo* in mouse models, which is released in a CD1d dependant manner (172). These pro-inflammatory cytokines have traditionally been shown in many different settings to be protective in humans and in mice, including the

observation that mice deficient in IFN-γ production are more susceptible to disease (2). In addition, bacterial protection could be driven largely by GM-CSF. In a study looking to describe specific mechanisms of iNKT control in Mtb infection, the suppressive effect was independent of IFN-γ, TNF-α and any cytolytic activity and surprisingly shown to be the result of a CD1d-dependant release of GM-CSF. Moreover, GM-CSF alone is sufficient to inhibit growth of Mtb in human and mouse infected macrophages (174).

Granulysin is known for its ability to kill bacteria directly and had been implicated in protection in Mtb infection (175). Convincing *in vitro* data showed that release of granulysin has a role in directly killing Mtb. Two double negative iNKT clones that secreted granulysin on exposure to infected macrophages were treated with strontium to initiate reversible degranulation, in turn it reduced granulysin production. This completely inhibited their ability to control the growth of Mtb (176). The effect was enhanced by addition of *α*GC into cultures, suggesting the CD1d dependant release of granulysin. This is similar to group 1 CD1-restricted T cells that also produced granulysin in response to CD1/antigen complexes (177). Furthermore, the same group showed the presence of CD1d on the surface of antigen presenting cells within the granuloma, suggesting that *in vivo* activation of iNKTs and antimicrobial responses can be initiated (176). Thus, there is a growing body of work to suggest an important role for iNKTs in Mtb infection, and the relative role of diverse secreted molecules such as granulysin and GM-CSF are increasingly understood.

1.16 iNKTs in Macaques

Although some mammals do not express group 1 CD1 molecules, nearly all express the group 2 CD1, CD1d. The CD1d antigen presenting system is highly conserved between humans and macaques. Early studies describing this system showed αGC presented by human CD1d is recognised by macaque iNKTs where they expand on recognition of dendritic cell CD1d/αGC (178). Genetic analysis of the macaque CD1D gene revealed 22bp changes causing 11 amino acid changes in the α1 and α2 domains. These substitutions did contribute toward the formation of the antigen binding pockets (178).

Despite few amino acid substitutions there is no commercially available macaque cross-reactive antibody toward CD1d, and therefore it is not possible to clearly define the extent of CD1d expression using standard flow cytometry. Sequence analysis of the macaque iNKT TCR revealed that the Vα24 chain has a 93% sequence identity with the human chain with only one amino acid change in the V-J region leading to a substitution of the human arginine to the rhesus lysine. This is not proposed to alter binding to CD1d/antigen (178)

To identify iNKTs in humans, anti-Vβ11 and anti-Vα24 antibodies are commonly used, binding the invariant TCR found on human iNKTs. It has been suggested that anti-human Vβ11 cross-reacts with the iNKT beta chain in 4% of macaque iNKTs, however many other studies have not demonstrated this cross-reactivity (179). It is likely that macaque iNKTs express the Vβ11 chain but contain amino acid substitutions that affect the anti-human antibody binding site, although it cannot be ruled out that macaque iNKTs use a distinct VβTCR chain (178). *Ex vivo* iNKT frequencies are reported between <0.01%-0.4% in the peripheral blood of rhesus macaque, 0.19% in pigtailed macaque, <0.01% in sooty mangabey and >0.1% in Cynomolgus (180, 181). However, there is a clear disparity between studies in reagents used to identify and enumerate iNKT cells by flow cytometry. Commonly used reagents are anti-CD3 and anti-Vα24 antibodies, or a combination of anti-Vα24 and 6B11 antibodies, where 6B11 recognises the joining region of the iNKT alpha chain (182). More recently CD1d tetramers have been used with either αGC or analogues such as PBS-57 (178, 179, 181, 183, 184). The use of different reagents may affect specificity of binding and therefore either do not identify the few non-invariant iNKTs that have been described, or may identify classical T cells expressing the Vα24 chain.

Phenotypically, iNKTs in macaques are slightly different to those in humans, and surface expression can depend on tissue location. Whereas in humans iNKTs are more commonly $CD4^+$ in the periphery, Rhesus and Cynomolgus macaque are more commonly $CD8^+$ in peripheral blood, with a major population of double positive and $CD4^+$ in the spleen (184). Other phonotypical differences are shown by iNKTs in macaque spleen, for example they generally express more CD56 as well as release far more IL-4 than

peripheral blood iNKTs, suggesting they are a phenotypically and functionally distinct population (184). Functionally, iNKTs from macaque spleen have also been shown to be semi-anergic under normal culture conditions, and they exhibited weak proliferation despite frequent stimulation with immature αGC pulsed moDCs (179). Rhesus macaque spleen derived iNKTs showed a central memory phenotype, with strong expression of CD11a and CCR7, and were negative for CD69, CD62L, CD28 and CD45RA. CD45 was present in all iNKTs analysed however its expression varied (179). This was in contrast to an effector memory phenotype in long term cultured iNKTs. Thus, not only can iNKTs differ between human and macaque, but they can differ depending on anatomical location within macaques.

As macaques are the ideal penultimate animal models for many diseases, they have been widely studied investigating the effects of iNKTs stimulation for therapeutic benefits. Many studies have focused on simian immunodeficiency virus (SIV) infection. Since the effects of *in vivo* administration of αGC are considered to modulate iNKTs in mice, the effects of subcutaneous delivery, intravenous delivery and administration of αGC pulsed moDC were investigated and compared in pig-tailed Macaques (185, 186). iNKTs almost disappeared from the periphery but numbers slowly recovered 2-3 days after αGC pulsed moDC administration, with iNKT depression most pronounced in doses over 10μg by all modes of delivery (183). This is either as a result of their homing and relocation or because they became unidentifiable due to internalisation of the TCR after activation (180, 187). Initial work performed on the role of iNKTs in anti-viral immunity showed simultaneous delivery of αGC with live attenuated influenza virus identified no enhancement of overall immunity. In addition, administration of αGC two days prior to SIV infection resulted in no differences in $CD4^+$ T cell counts or extent of viraemia (183). This suggests that although *in vivo* delivery of αGC modulates iNKTs, it has no clinical impact on macaque anti-viral immunity.

1.17 Mtb cell wall and mycolic acid structures

The cell walls of species found in the genus *Mycobacterium* are truly unique, elegantly constructed from exotic lipids many of which are found only within this genus. The insoluble matrix, found beyond the mycobacterium cell membrane (outer membrane), consists of cross-linked peptidoglycan (PG) covalently bound to arabinogalactan (AG) with mycolic acids attached at the distal end via esterified links (figure 1.5). This complex is termed the cell wall core or the mycolyl arabinogalactan-peptidoglycan (mAGP) complex (188). The inner membrane is then hydrophobically associated with other lipids such as triacylglycerols, glycolipids and complex waxes forming the outer leaflet. Indeed, other common lipids such as lypoglycans, LAM, lipomannan and glycophospholipids can also be found within the cell wall (189).

Currently, Mtb is suggested to infect around 30% of the global population. The highly complex cell wall structure is widely documented as a requirement for antibiotic resistance, cell viability, growth and virulence, allowing it to become one of history's most successful infectious disease. The unique structure and biosynthesis of the cell wall has been intensely studied since the late 1950s with particular research into its fluidity and permeability to antimicrobials in the early 90s (190-193).

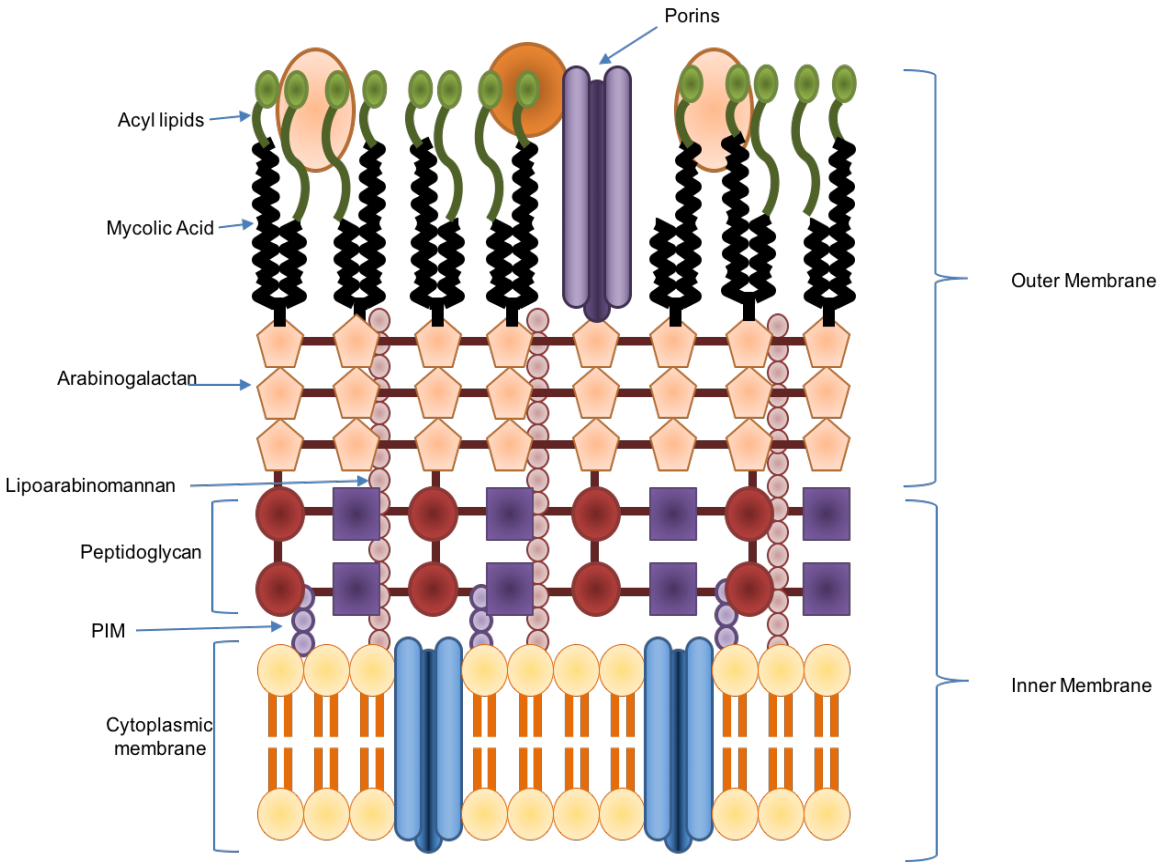

Figure 1.5: Mycobacterium tuberculosis cell wall

Cartoon representation of the highly impenetrable barrier of mycobacterium also known as the mAGP. The outer membrane contains mycolic acids and other unique Mtb lipids that form the bulk of the wall. They are tightly packed and highly hydrophobic with low fluidity. They are arranged perpendicular to the cytoplasmic membrane. The inner membrane contains a typical bacterial cytoplasmic membrane. (Adapted from Kaiser et al. 2008)

Antibacterial drugs are unable to penetrate the cell wall due to its low permeability. Furthermore, the few porin molecules that traverse the cell wall are low in number and extremely slow at transporting hydrophilic molecules (194). In studies investigating thermal transitioning of the cell wall, a strong correlation was observed between the composition and structure of mycolic acids present and the highest transition temperatures measured. These fatty acid lipids of an unusual structure were therefore put forward as being responsible for providing many of the unique functions of the

mycobacterium cell wall (195-197). In nature, there are a huge variety of MAs, and Mtb itself can contain up to 80 different species all differing in structure (198).

When considering the T cell responses towards lipids that bind CD1 molecules, it is vital to understand the molecular interaction between the lipid ligands and CD1 molecules. This has been shown most clearly by studies on CD1d binding of αGC and OCH (199). Mycolic acid binding to CD1b is purely a hydrophobic interaction where the long meromycolate chains sit in the CD1b groove and the polar head group is exposed at the TCR interface (61). To this end, it is important to understand the structural variety and repertoire of mycolic acids found in Mtb. Mycolic acids can be found bound to sugar moieties such as trehalose or glycosylated mono- and dimycolates as well as glycerol monomycolates and free mycolates with no sugar head groups (figure 1.6).

All free mycolic acids share common features containing a meromycolate chain, the main source of functional diversity, and a mycolic motif which can accommodate different head groups (figure 1.6b). The meromycolate chain usually contains two functional groups, one distal to the carboxylic acid and one proximal. These functional groups are commonly cyclopropanes but can also be a methoxyl group, double bond, epoxy group, carbonyl group, carboxyl group or methyl group (figure 1.6c). Based on these functionalities MAs can be assigned to three broad groups: the α-, keto- and methoxy- mycolates. Other functional groups exist such as epoxy-, alkene- and diene-MAs (figure 1.6c). Within each group, MAs can be further described based on their stereochemistry around the functional groups, in a cis- or trans- conformation. There is strong evidence from multiple studies showing these different mycolate structures are responsible for providing Mtb with different levels of virulence and confer individual folding structures (200-202).

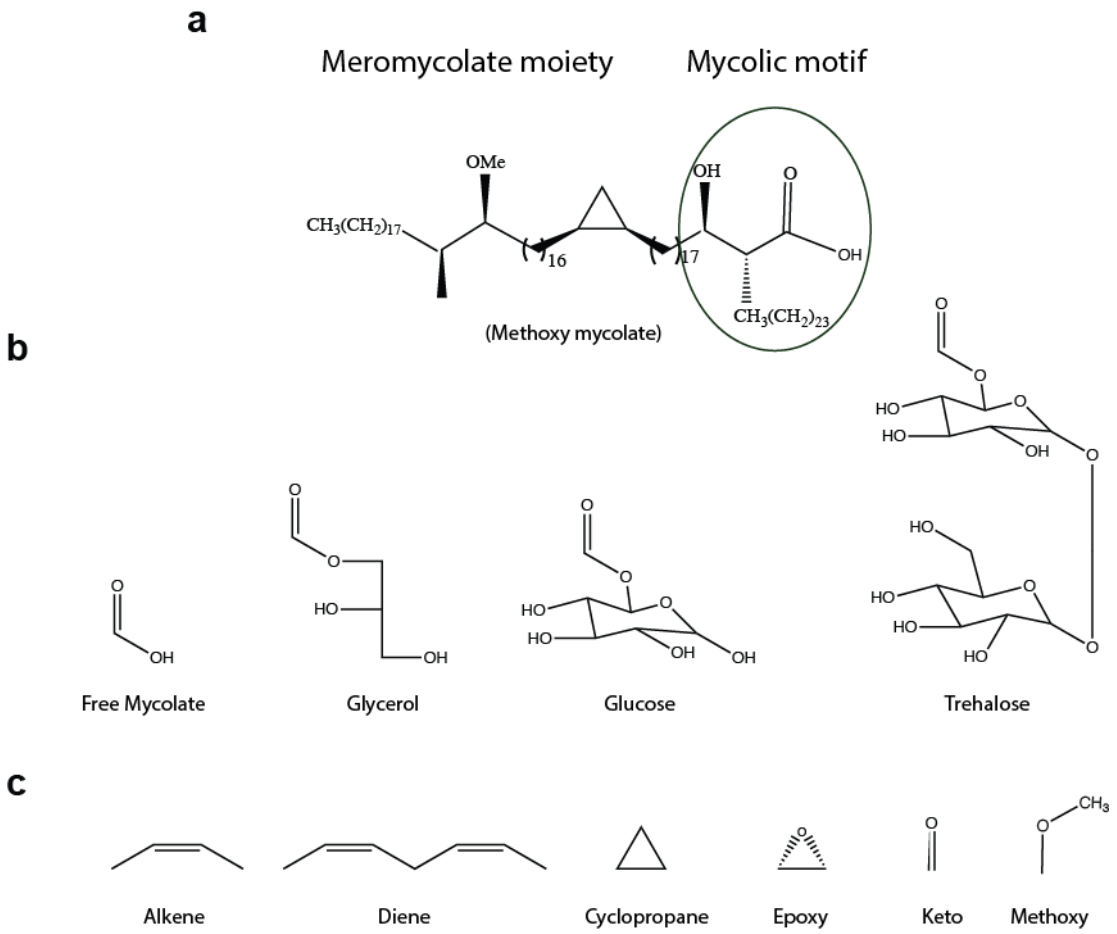

Figure 1.6: Mycolic acid: General Structure

Mycolic acid structure; a) Methoxy mycolic acid, circled area contains mycolic motif β-hydroxy head group which can also contain a glycerol (Gro-MM), glucose (GMM) or a trehalose (TMM) with structures outlined in (b). The meromycolate moiety consists of the long hydrocarbon chain containing various functional groups, proximal and distal to the mycolic motif, shown in (c). Numbers next to brackets along meromycolate chain indicate number of carbons.

One critical aspect of mycolates is that inherent structural properties can be used to predict their conformational behavior (Figure 1.7). As shown previously by a series of papers from Villeneuve et al., slow growing mycobacteria synthesise energetically more stable forms of MAs in folded conformations where the four chain segments are aligned parallel in a so called W-formation (203, 204). This indicates that functional groups have significant impact on mycolate macrostructure. This is especially true of the keto-MAs in trans, which favor the W-conformations, compared to the α-MAs that have the

capability of accessing the widest range of conformations such as W, U and Z folds (205). Condensed chain structures are achieved at low temperatures and pressures, while increasing these parameters in α- and MeO-MAs tend to take a stretched conformation in which the distal functional group leaves the hydroxyl group (206). The folded conformations have already been shown to confer profound effects on the biological and biophysical properties of the Mycobacterium cell wall. Presumably, the folding structures could determine ligand orientation within CD1b and therefore its stability.

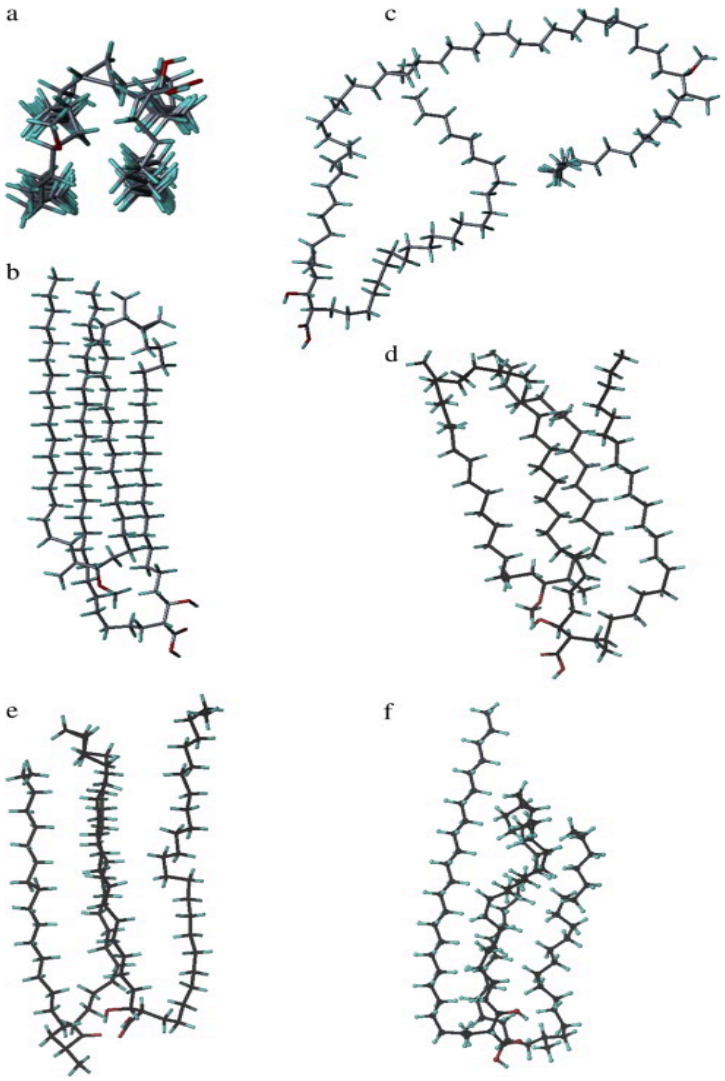

Figure 1.7: Mycolic acid: Folding Structure

(a and b) Molecular dynamics (MD) of conformational folding of MA. MeO-MA molecules viewed from top and bottom; (c) Stretched structure of MeO-MA after 20ps MD; (d) Retention of W structure of MeO-MA after 20ps MD; (e and f) keto-MA and deoxo-MA structural conformation. Adapted from Villeneuve et al. (2013) (206).

1.18 Interactions involving CD1b, mycolic acid and T cell receptors

A limited number of glycosylated – MA and free – MA reactive T cell clones have been identified which have been used to provide evidence for MA structural requirements for CD1b presentation and TCR recognition. Using GMM isolated from three independent sources, Moody et al. determined the carbohydrate moiety was responsible for LDN5 TCR recognition and variation in the acyl chain did not change the strength of TCR interaction (72). GMM has been isolated from *Mycobacterium bovis* BCG, *M. fortuitum, M. smegmatis* and *M. pheli*, which are species that differ in mycolic acid composition. Recovered GMMs differed in acyl chain length, R (side chain) group substitution, double bonds and cyclopropane rings, but all contained an esterified glucose. LDN5 responded to each of these GMMs at equivalent doses, indicating that the hydrophobic tails are not important for recognition by this TCR (72). Also, synthetic GMM lacking in long chain length and functional groups still conferred LDN5 recognition. Furthermore, lipids lacking the distinctive features of a mycolic acid (α-branched, β-hydroxy structure) were not recognized. The meromycolate chain therefore is not required for LDN5 TCR recognition. This also supported the view that CD1b binds lipids non-specifically via the alkyl chain leaving the polar head group exposed for highly specific interaction with the TCR, a hypothesis that was confirmed later by structural analysis of the lipid/CD1b complex.

Crystal structures of CD1b with bound lipid antigens unequivocally show the lipid position within the antigen binding pockets. The first crystal structure revealed by Gadola et al. showed CD1b has the capacity to contain the entire acyl chain from MAs up to 60 carbons in the A', T' and F' superchannel (69). Subsequent crystal structures of CD1b bound to GMM show the entire meromycolate chain is contained within the A', T' and F' channels as well as a protrusion from the F' channel, leading to the TCR recognition surface. Since knowledge of mycolate-CD1b T cell recognition is based on data from a small number of T cell clones and mainly the LDN5 TCR, it is not unreasonable to hypothesise some TCRs may discriminate bound MAs of differing meromycolate chain structures. However, such a TCR has not yet been isolated. Figure 1.8 shows the hydrophobic binding channels of CD1b with bound GMM (61).

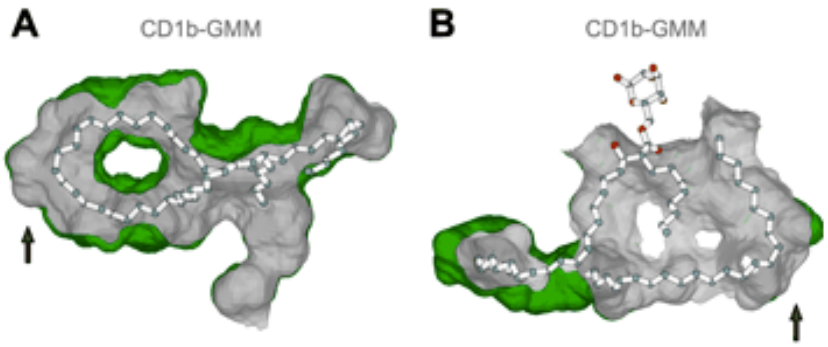

Figure 1.8: CD1b/MA Binding

Grey/green colours depict the van der waals surface of the CD1b binding groove. (A) View from top of protein looking down, arrow indicates A'-T' channel junction. (B) Side on view of protein. Arrow indicates F'-T' channel junction. Adapted from Butuwangala et al. (2004) (61).

Modelling MAs that bear differing functional groups indicate plasticity of CD1b and the ability for acyl chain accommodation. Channel volume varies locally immediately surrounding the minor functional group changes, with little change in the overall size of the super-channel or the TCR interface surface (61). These structural data provide little suggestion that functional groups may affect TCR recognition and T cell activation.

Furthermore, mutational analyses of CD1b revealed key residues in the A' and F' pockets responsible for GMM binding. Thirty-six alanine substitutions of CD1b corresponding to the residues lining the A' and F' channels of mouse CD1d antigen binding groove were generated and subsequent binding of a naturally occurring GMM and a synthetic GMM (sGMM) with acyl chain lengths of C54-C62 and C22-C24 respectively were then studied (207). Eight residues were critical for the binding of both GMM and sGMM in the A' and F' channels. Four residues in the distal region of the A' channel were important for GMM presentation only. Conversely, nine residues in the F' pocket were critical for sGMM binding only (207). CD1b therefore confers specific stabilizing interactions with its ligand that may affect binding strength and therefore T cell interactions.

The first suggestion however, that various mycolate hydrocarbon chains structures could affect T cell activation was offered by Ethan et al. as they observed differences in DN1 T cell activation to crude fractions of α-, keto- and methoxy- mycolates (208). While the group did not discount the possibility the differences were mediated by differential mycolate processing, it was largely dismissed as there are no known enzymes to mediate hydrocarbon chain processing.

1.19 CD1b/MA restricted TCR repertoire and binding requirements

The first modeling data describing the TCR of the T cell clone DN1 suggest similar TCR/CD1b interaction requirements to that of TCR/MHC, with the CDR3 loop positioned above the antigen binding site. This orientation would allow basic residues in the CDR3 loops to directly interact with the exposed antigen (209). Further characterisation of the CD1b/TCR interaction using five known CD1b reactive TCRs showed a cluster of functionally important amino acids in the center of each helix on the CD1b surface, revealing a diagonal orientation of each TCR with respect to the membrane distal aspects of the α1 and α2 helices, distinct from that of the MHC/TCR interaction (210). Finally, mutations of the beta chain CDR3 loop from the DN1 TCR show even conservative alterations (arginine to lysine) of polar residues within this side chain completely abrogates TCR/lipid/CD1b binding. These results unequivocally demonstrate the critical interaction of the CDR3 loop with the CD1b/MA complex. Mutations of the CDR1 loop also reduce recognition of CD1b α1 helix, and thus reduce overall affinity of the interaction, revealing the importance of TCR binding to both the CD1 molecule as well as the presented antigen (208).

Mycolic acids can exist as free, glycosylated, glycerol or trehalose bound molecules. The different hydrophillic structures do not dictate lipid binding to CD1b, however they do confer highly specific interactions with TCRs (61, 72, 208). The polar moieties found on GMM and glycerol monomycolate (Gro-MM) specifically bind TCRs from LDN5 and Z5B71 respectively. However, the TCRs from DN1 T cells are reactive toward free non-

glycosylated mycolates (65, 130, 211, 212). Methylation or esterification of the carboxylic acid group of free MAs abrogates binding of DN1 (208). Likewise, removal of the carbohydrate moiety completely abrogates the binding of TCRs specific for either Gro-MM or GMM. Furthermore, glycosylated MA cannot be bound by the C18 GEM or DN1 TCRs, highlighting the specificity of CD1b restricted TCRs. Whilst the mechanism of TCR binding to peptide antigens bound to MHC are better defined, mechanisms dictating the TCR interactions with CD1 lipid antigens are lacking.

To date our knowledge of the CD1 restricted TCR repertoire is dominated by assumptions based on the highly diverse pattern of TCRs responsible for binding the polymorphic MHC molecules. However, given the non-polymorphic nature of CD1 molecules, this pattern does not logically fit with regard to the CD1 restricted TCR repertoire. Studies have been conducted on only a handful of clones each with diverse receptor usage. In 2013, the first study using CD1b/GMM tetramers to capture multiple restricted clones found a major population of T cells with limited receptor usage that arose through distinct rearrangement events in individual donors. These high affinity CD1b/GMM and CD1b/MA specific T cells were termed Germline-encoded mycolyl specific T cells (GEMs) (134). The GEM population is only the third invariant T cell population discovered after iNKTs and MAITs.

1.20 GEMs

GEM T cells are defined by their conserved receptor usage and expression of CD4. The GEM TCR confers tetramer high staining, revealing a high affinity interaction. It is important to note the difference between MA and GMM specific GEM T cells however, whose binding specificity is dictated by subtle changes in both the alpha and beta chain usage (Figure 1.9). Through the generation of chimeric GEM TCRs, it was clearly demonstrated that TRBV4-1/TRBJ2-1 beta chain of clone 18 confers binding to CD1b/MA, while removing CD1b/GMM specificity. In contrast, clones 1, 21 and 42 specificity for GMM is abrogated by TRAV1-2/TRAJ9 alpha chain displacement (134). This suggests that the GEM/CD1b/GMM interaction is more stringent than that of

GEM/CD1b/MA, requiring both the native alpha and beta chains. Clone 18 α-chain differs from clones 1, 21 and 42 in positions 107/108, 107/108 and 107 respectively within the CDR3α sequence of the α chain. Clone 42 however demonstrates an arginine in place of leucine is crucial for determining GMM recognition. Solving the crystal structure revealed how the arginine residue packs the CDR3α loop against the CDR3β loop, reducing its mobility, defining a mechanism for the finely tuned TCR specificity (134). Thus, it was clearly shown that TCR usage toward CD1b/lipid complex is not diverse but in fact based on an invariant TCR alpha sequence with biased β-chain usage.

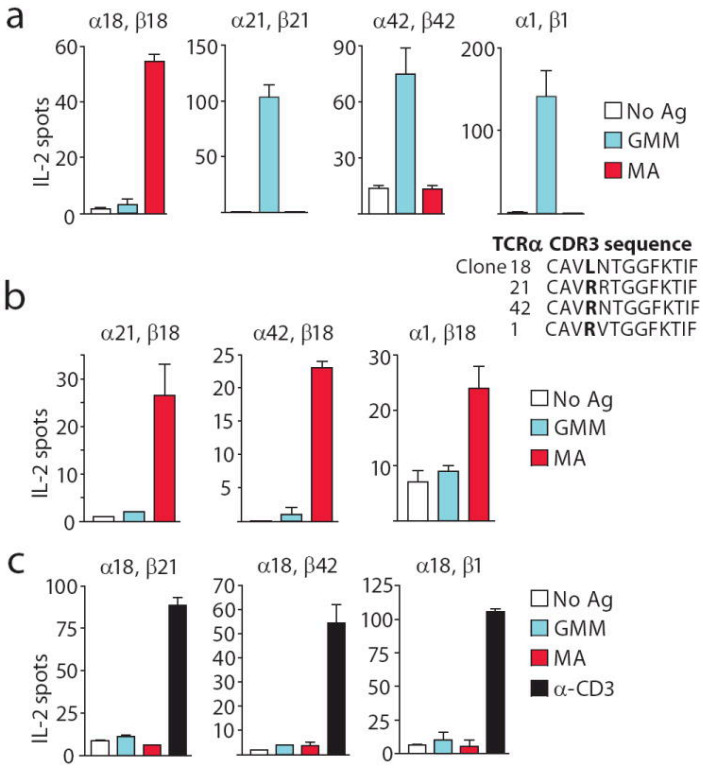

Figure 1.9: GEM TCR Specificity

Specificity of GEM clones restricted towards MA (clone 18) or GMM (clones 1, 21 and 42) (134). (a) Native specificity of GEM TCRs; (b) GMM specific TCRs with beta chain replaced by MA specific clone 18 which abrogates GMM specificity and supports MA binding; (c) GMM specific TCRs with alpha chain replaced with clone 18 alpha chain abrogates binding to both MA and GMM. Adapted from Ildiko van Rhijn et al. (2013) (134).

Furthermore, LDN5 and other tetramer intermediate T cell clones (called LDN5-like T cells), also showed a conserved pattern of TCR usage. The conservation of CDR3α loop sequences are not as stringent as that seen in GEM TCRs, but they share some common features. TRAV17 usage was shown in five of eight clones analysed as well as by LDN5, which was isolated many years earlier. In addition, all but one of the clones expressed TRVB1-4, which is expressed by LDN5 (213). Thus, recent evidence from multiple T cell clones isolated using the same CD1 glycolipid tetramer revealed a more conserved T cell population than previously appreciated. It allowed understanding of the fine specificity of the TCR and its ability to discern between lipid antigens. Furthermore, it revealed a pattern of TCR usage that may be extended to CD1a and CD1c antigen presenting molecules, given their similar non-polymorphic state.

Whilst in humans, research into group 1 CD1 mediated T cell immunity has progressed in the last 20 years, the NHP model has been relatively understudied. However, there have been a number of key observations that are of interest. Investigation into the cross reactivity of Rhesus macaque CD1 molecules with known human TCRs showed that LDN5, specific for GMM/CD1b complex, was the only cross reactive TCR in a panel of three, one for each CD1 isotype (41). This was the first demonstration of human TCR crossreactivity with NHPs. Sequence alignment of group 1 CD1 molecules reveal a high degree of homology: 85.6% for CD1a, 94.6% for CD1b and 90.4% for CD1c. It is therefore not surprising that a CD1b restricted TCR was the only one capable of binding NHP CD1b (41). Indeed, it is also important to note sequences critical for the early endosomal and lysosomal trafficking of CD1b and CD1c molecules are identical between the two species. (214, 215). In addition, the cysteine residues forming intrachain disulphide bonds between the α1 and α2 domains are totally conserved. Furthermore, a molecular model of Rhesus macaque CD1b showed nearly identical intramolecular antigen binding pockets of the A', C', F' and connecting T' tunnels. The critical amino acid residues lining the binding sites such as E80 and D83 in the α1 domain and T157 and T165 in the α2 domain are also conserved between the two species, suggesting a stable interaction between MAs and macaque CD1b (41).

Further investigation into Rhesus macaque T cell populations reactive to GMM presented by autologous APC populations showed how GMM-specific T cell responses were elicited after BCG vaccination (216). Surprisingly, CD1c was clearly shown as the antigen presenting molecule, which was not consistent with the presentation of GMM by CD1b in human. T cells responsive toward GMM/CD1c were shown not only to be able to expand *in vivo*, but were able to extravasate to the site of BCG inoculation in the skin (216). A possible explanation as to how NHP CD1c is able to bind such long meromycolate chains without the interconnecting T' tunnel found in CD1b is the availability of two portals (D' and E') which the chain may be able to exit and enter back in immediately using the A' and F' channels to accommodate these long lipids. However, this hypothesis is based on observations of human CD1c, as the macaque CD1c crystal structure has not yet been elucidated.

1.21 Comparison of iNKT and GEM T cell interaction with CD1 molecules

The iNKT TCR is able to recognise diverse lipid structures when bound to CD1d. It does this through the germline encoded regions CDR3α, CDR1α and CDR2β, whose binding mechanism did not change toward CD1d with different bound α-linked glycolipids (217). This is in comparison to GMM specific TCRs which have high specificity for the glucose component of the lipid (134). Other basic comparisons can be made, such as the orthogonal vs parallel binding modes of the GEM and iNKT TCR respectively with respect to the antigen binding cleft (Figure 1.10a and b). Both different to the typical diagonal orientation of typical class I pMHC restricted TCRs (218). In addition, the GEM TCR is centrally located, directly over the glucose and interacts using the CDR3α and CDR3β loops as tweezers that grip the glucose head group of GMM (219). This differs to the iNKT TCR which sits over the F' pocket in a more acute docking mode (220).

Interestingly, the buried surface area of the iNKT TCR, typical pMHC TCRs and the GMM specific GEM TCR is 900Å, 1,200-1,400Å and 1,600Å respectively. The iNKT footprint is dramatically reduced and yet confers equivalent affinity, which is due to the structural and energetic overlap of germline encoded residues in the iNKT TCR (217). However, in

the GMM specific TCR, the germline encoded residues are responsible for mediating a capstone interaction (Figure 1.10d) over the glucose head group. Removal of the conserved Arg107α completely abrogates binding, and is a molecular interpretation for its specificity (219). Furthermore, both the iNKT TCR and the GEM TCR interactions with their respective targets are relatively rigid, compared to pMHC TCR interactions, suggesting both contained fixed recognition determinants (219, 220).

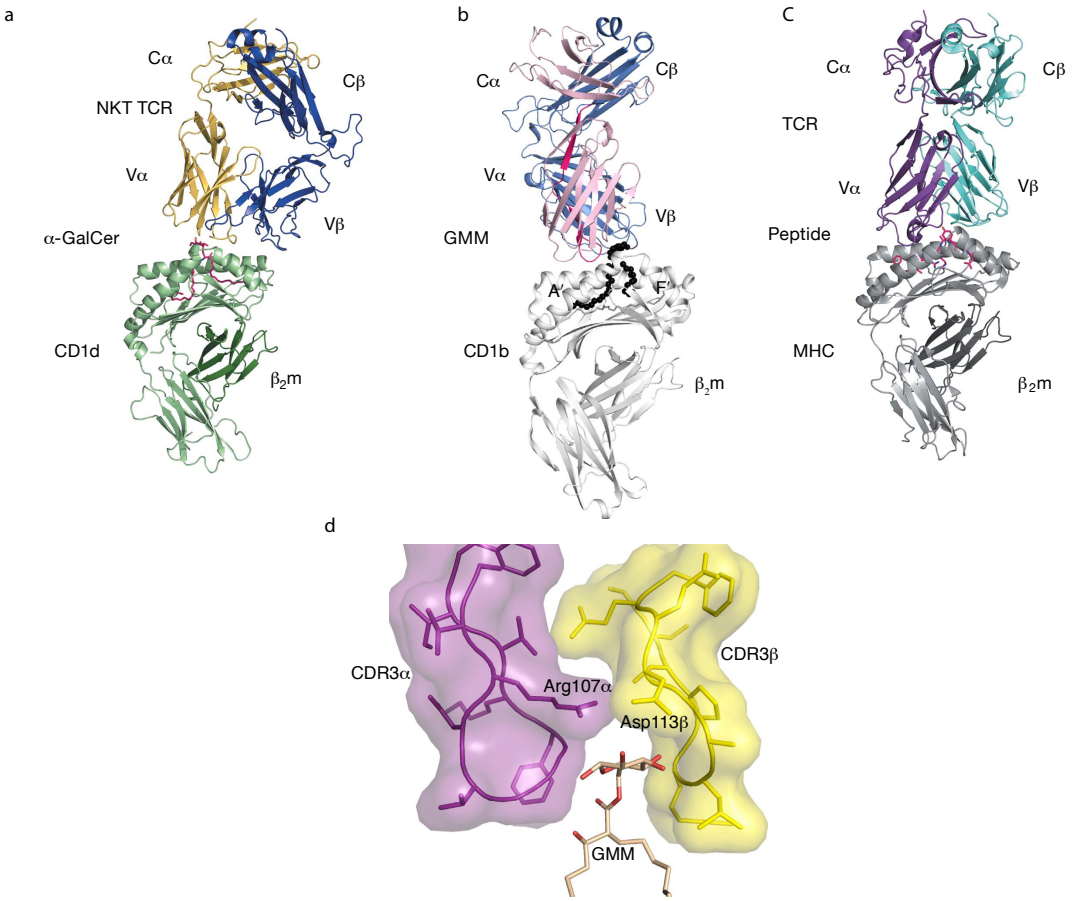

Figure 1.10: Crystal structures of CD1d, CD1b and MHC complexes bound to their respective TCRs

Co-crystal ribbon representation of: a) an iNKT TCR bound to CD1d/α-GC, b) Clone 42 GMM specific GEM TCR bound to CD1b presenting C32 GMM, c) LC13 TCR bound to HLA-B8 presenting a peptide derived from Epstein-Barr virus. The structures demonstrate different TCR binding orientations. d) Shows CDR3α and CDR3β loops of the GMM specific GEM TCR, their tweezer-like interaction with the glucose head group and the salt bridge described as a capstone which is essential for TCR binding. Adapted from Gras. S. et. al. (2016) (219).

1.22 Summary

Mycobacterium tuberculosis is a pathogen of huge global concern killing millions of people every year and is becoming increasingly difficult to eradicate due to the appearance of drug resistant strains. In addition, the diagnostic strategies widely employed and the only vaccine available has done little to prevent spread of the organism. Huge efforts have been made to understand immunology toward Mtb. However, there still remains a poorly defined T cell response in humans and despite evidence suggesting cytokines such as IFN-γ, GM-CSF and TNF-α are required for controlling infection they are not sufficient. Therefore, animal models such as macaques that accurately recapitulate human disease pathology need to be further understood and the humoral and cellular immune responses need to be considered on a more holistic level to aid development of further strategies for Mtb elimination. Crucially our understanding of the role of unconventional CD1 restricted T cells in Mtb is lacking. Due to the lipid rich cell wall of Mtb, it is likely these T cells have a dominant role in producing and coordinating an immune response, although it is not known whether this is protective or drives pathology. Better understanding of these T cells and their function may lead to effective immune therapies to treat Mtb, vaccine candidates that target activation of germline encoded T cells as well as more novel and rapid diagnostic strategies.

1.23 Hypothesis

In this study we hypothesise that lipid-dependent T cell immune responses are important in TB and specifically:

- Quantitative and qualitative iNKT repertoire differences may associate with disease susceptibility and outcome in macaque tuberculosis infection
- Lipid tails of mycolic acid contain different functional groups that may determine CD1b presentation and GEM T cell activation

Chapter 2: Materials and Methods

2.1 Experimental animals

The animals used in this study were Rhesus macaques of Indian origin, Chinese cynomolgus macaques, Mauritian cynomolgus macaques or Indonesian cynomolgus macaques obtained from established breeding colonies in the United Kingdom (MCM, ICM, RM) and China (CCM). All healthy animals were between 4 and 10 years old at the time of sample collection and were naïve in terms of prior exposure to mycobacterial antigens (*M. tuberculosis* infection or environmental mycobacteria), as demonstrated by a negative tuberculin test while in their original breeding colony and by the gamma interferon (IFN-γ)-based Primagam test kit (Biocor; CSL) or screening using an ex-vivo IFN-γ ELISPOT (MabTech) to measure responses to mycobacterial antigens: PPD (Statens Serum Institut (SSI)), and pooled 15-mer peptides of ESAT6 and CFP10 (Peptide Protein Research) just prior to the start of the study.

Animals were housed in compatible social groups, in accordance with the Home Office (UK) Code of Practice for the Housing and Care of Animals Used in Scientific Procedures (1989), and the National Committee for Refinement, Reduction and Replacement (NC3Rs), Guidelines on Primate Accommodation, Care and Use, August 2006 (NC3Rs, 2006). Animals were sedated by intramuscular (IM) injection of ketamine hydrochloride (Ketaset, 100mg/ml, Fort Dodge Animal Health Ltd; 10mg/kg) for procedures requiring removal from their housing. None of the animals had been used previously for experimental procedures and each socially compatible group was randomly assigned to a particular study treatment. All animal procedures and study design were approved by the Public Health England, Porton Down Ethical Review Committee, and authorized under an appropriate UK Home Office project license.

Animal vaccination and infection: All animal vaccination and infection procedures were performed at Public Health England in studies previously carried in accordance with appropriate home office code of practice. BCG vaccine, Danish strain 1331 (SSI) was used for all vaccinations and administered intradermally. The Erdman K01 stock (HPA-2001) was used for all challenge studies and prepared from stock of the Mtb Erdman

strain K 01 (BEI Resources). Challenge was delivered via aerosol to the nares of each sedated primate.

2.2 Protein production

Generation of macaque and human CD1d: Sequences encoding the extracellular domains of macaque or human CD1d and human β2m were separately cloned into the prokaryotic expression vector pET23d (Novagen), and recombinant proteins were generated separately as inclusion bodies in *E. coli* Rosetta strain (Novagen). Inclusion bodies were thoroughly washed and fully denatured and reduced in 6 M guanidine-HCL and 20 mM DTT prior to *in vitro* refolding. Refolding of CD1d/β2m complexes was carried out by oxidative *in vitro* refolding as previously described (80, 221-223), in the presence of specific ligand; αGC (Avanti). In brief, completely denatured and reduced protein was refolded at 4°C in the presence of agarose gel coated with protein chaperone molecules, GroEL, protein disulphide isomerase (DsbA) and peptidyl-prolyl *cis-trans* isomerase (PPI) in Tris buffer (pH 7.5). Correctly folded proteins were purified by repeated FPLC (Pharmacia) size-exclusion chromatography using preparatory grade SD75 26/60 and analytical grade SD75 GL 10/300 gel filtration columns (GE Healthcare).

Soluble GEM 18 TCR: Extracellular region of clone 18 GEM TCR chains were synthesised by GeneArt and optimised for expression in bacterial cells. Optimised sequences were then sub-cloned into the following pGMT7 vectors: α-chain/pEX956 and β-chain/pEX651 (Immunocore). Rosetta (DE3) PlysS bacterial cells (Millipore) were transformed with plasmid DNA, plated and grown overnight on agar plates containing 100ug/ml ampicillin. Cultures were grown in 1 L TYP medium (containing 16 g yeast, 16 g tryptone, 5 g NaCl, 1% glucose and 1.25 g K_2HPO_4) with overnight shaking at 240 revolutions per minute (rpm) at 37°C. In the morning 50 μg/ml ampicillin was added to the cultures as well as 0.4mM IPTG to induce protein production and left for a further 3 hours. Bacterial cells were then centrifuged for 10 minutes at 10,000 g and sonicated for half an hour on ice. Protein inclusion bodies were harvested by repeated centrifugation at 10,000 g for 10 minutes and washed with buffer containing: 50 mM Tris pH7.5, 100 mM NaCl, 1 mM

DTT, 1mM EDTA, 0.5% Triton X and 0.1% NaN_3. Finally, protein was resuspended in 8M urea before running on a 12% acrylamide SDS-PAGE gel to assess purity.

TCR refolding: TCR refolding and purification was performed by our collaborator; Dr Nikolai Lissin (Immunocore). Briefly, the extracellular domains of TCR alpha and beta chain inclusion bodies were denatured then combined at a ratio of 4α:1β. Inclusion bodies were added to one litre-refolding buffer containing 1 M Urea, 400 mM L-Arginine, 100 mM Tris pH 8.1, 3.7 mM Cystamine Dichloride, and 6.5 mM Cysteamine chloride. Refolding mixture was dialysed against water for 18 hours and subsequently dialysed against Tris pH 8.1 for another 18 hours at 4 °C. After dialysis, the protein mixture was purified by anion exchange chromatography before further purification by size exclusion chromatography. Purified protein peaks were subjected to reducing and non-reducing SDS-PAGE gel analyses to confirm the presence of properly refolded TCR αβ heterodimer. Once confirmed, up to 1 mg refolded TCR is biotinylated to generate C18 TCR tetramers and dextramers.

2.3 Cell purification

Macaque PBMC: Macaque blood samples were received in 20 ml universal tubes with heparin. PBMCs from Cynomolgus blood were isolated using accuspin tubes (Sigma-Aldrich) and 60% Percoll (Sigma-Aldrich). 20 ml 1:1 blood diluted with phosphate buffered saline (PBS) was poured onto the frit and centrifuged at 800 relative centrifugal force (rcf) for 15 minutes with the brake off at room temperature; the buffy coat was then removed and washed three times in PBS (Lonza). Rhesus macaque blood was layered directly onto Ficoll-Paque (GE Healthcare) after 1:1 dilution with PBS and centrifuged at 480 rcf for half an hour with brake and acceleration turned off at room temperature. PBMC fraction was extracted and all macaque PBMCs were then resuspended in red blood cell lysis buffer (Life Technologies) for five minutes before one further wash in cold PBS.

Human PBMC: Blood was obtained from asymptomatic tuberculin-positive donors clinically assessed to have latent tuberculosis with no evidence of active disease. Density

gradient centrifugation was used to isolate PBMCs from each sample by layering 1:1 PBS diluted blood onto 15 ml Ficoll-Paque (GE Healthcare) in a 50 ml falcon (Corning), where cells were spun for 30 minutes, 480 rcf at room temperature with the brake off. PBMC fractions were carefully extracted before washing twice with cold PBS to remove residual Ficoll-Paque. For moDC generation; cells were counted and monocytes removed by positive $CD14^+$ selection by magnetic activated cell sorting (MACS) (Miltenyi Biotec). The enriched T cell fraction was frozen immediately for later use.

moDC preparation: Monocytes were separated by anti-CD14 beads (Miltenyi Biotec) using MACS technology (Miltenyi Biotec). $3x10^5$ purified $CD14^+$ monocytes were seeded into 24 well plates and differentiated into moDCs by incubating in RPMI 1640 supplemented with 100 IU Penicillin, 100 μg/ml Streptomycin and 10% fetal calf serum (FCS) (complete media) and 25 ng/ml GM-CSF and 20 ng/ml IL-4 (both from Immunotools) for 6 days. Media was replenished every 2 days. On day 6 the moDCs were harvested and either stained for FACS analysis or frozen for later use.

2.4 Flow cytometry

CD1d and GEM TCR tetramers: Refolded CD1d and TCR complexes were biotinylated via an engineered BirA motif at the C-terminus (223) using a biotinylation kit (Avidity). Biotinylated proteins were purified by size exclusion chromatography, and used to generate fluorescent-labelled CD1d and TCR tetramers (224) by conjugation to phycoerythrin (PE)-streptavidin (Sigma-Aldrich).

iNKT staining: *Ex vivo* frequency was determined by washing $2x10^6$ PBMCs with PBS at 4°C, followed by addition of 3 μl of 8 nM tetramer in PBS and were stained on ice in FACS tubes (BD Biosciences). After 30 minutes the following antibodies were added at concentrations dictated by titration: anti-Vα24-FITC (Beckman Coulter), anti-CD3-APC (SP34-2-BD Biosciences). Following a further 20 minutes incubation, cells were washed twice with cold PBS and resuspended in PBS containing 500 nM propidium iodide (PI) before acquisition on the FACScalibur. Cells were phenotyped post expansion by flow cytometry via staining of $5x10^5$ cultured cells on ice in 50 μl PBS for 45 minutes using

PECy7 anti-CD8 (Clone SK1, Biolegend) and PerCPCy5.5 anti CD4 (Clone OKT4, Biolegend), as well as CD1d-αGC, anti-Vα24 and anti-CD3. Following all stains, PI (Sigma-Aldrich) was added before acquisition on either a FACSCalibur or a FACS Aria II (BD Biosciences).

Monocyte and moDC staining: $2x10^5$ cells were washed in cold PBS and antibodies added at concentrations dictated by titration in FACS tubes (BD Biosciences). The following antibodies were crossreactive in macaque: anti-CD14-APC (TUK4; Miltenyi Biotec.), anti-CD1b-Purified (SN13; K5-1B8 Abcam), anti-CD1b-APC (MT-101; Serotec), anti-CD11c-FITC (BU15; Immunotools), anti-CD86-PE (IT2.2; Biolegend), anti-HLA-DR-PE (L243; Biolegend). After addition of 2.5 μl of each antibody, cells were washed twice before addition of 500 nM PI and acquisition on a FACSCalibur.

Intracellular cytokine staining (ICS): $5x10^5$ purified T cells were added to $5x10^4$ MA pulsed autologous moDC for 6 hours of stimulation (see 2.10). Cells were then transferred to FACS tubes and stained with the following: Fixable live/Dead-Violet 450 (Zombie Violet), anti-CD3-APC-Cy7 (UCHT3), anti-CD4-PerCPCy5.5 (OKT4), anti-CD161-APC (HP-3G10), anti-IFN-γ PeCy7 (BS.4S), anti-IL-2-PE (JES6-5H4) and anti-TNF-α–Violet-510 (MP6-XT22) (all Biolegend). After washing samples with PBS containing 2 mM EDTA, surface markers were labelled first for 45 minutes on ice with live/dead stain. Samples were then fixed and permeablised for 20 minutes in the dark (BD Cytofix/cytoperm Kit) on ice before addition of intracellular markers. Finally, cells were washed twice in PBS before suspension in PBS and acquisition on the FACS Aria (BD Biosciences). Data was analysed using FloJo software (version 9.7.6).

Dextramer preparation and staining: Soluble TCR and CD1b monomers were dextramerised using PE-conjugated dextramer backbone (Immudex) to give 20 monomers/dextramer. Briefly, 20 μg of biotinylated monomer was added to 66 μl dextramer backbone for half an hour at room temperature before addition of TRIS-HCL buffer containing 0.1% BSA and 0.1% NaN_3. 10 μl of the final preparation was then used to stain up to $5x10^5$ cells on ice, in the dark for 45 minutes. Cells were then washed twice with cold PBS before acquisition on a FACSCalibur (BD Biosciences).

2.5 iNKT Expansion

Twenty four well plates were seeded with $4x10^6$ PBMCs in T cell media made up of RPMI 1640 (Lonza) containing 1% penicillin/streptomycin (Lonza), 1% glutamine (Thermofisher Scientific), 10% fetal bovine serum (FBS-Lonza), 1% essential amino acids, 1% non-essential amino acids, 1% sodium pyruvate (Sigma-Aldrich) supplemented with 5 μg/ml Plasmocin (InvivoGen), 2% human AB serum (Sigma-Aldrich) and 200 μg/ml of αGC (Avanti). On day 14 iNKT cultures were stained again to determine fold expansion. Fold expansion is the ratio of *in vitro* iNKT percentage on day 14 / *ex vivo* iNKT frequency on day 0. All iNKT frequency data is shown as the percentage of live, $CD3^+$, CD1d-tet^+, $Vα24^+$ lymphocytes.

2.6 Cloning

Human and Macaque CD1b: Monocytes from freshly prepared human and macaque PBMCs were MACS sorted using $CD14^+$ beads (Miltenyi Biotec). Monocytes were then differentiated into moDC and trizol (Invitrogen) was used to lyse cells and precipitate RNA from $1x10^6$ cells. cDNA was synthesised using superscript III first strand synthesis system using random primers (Invitrogen). For PCR of the CD1b sequences, we designed primers to anneal to both the human and macaque CD1b with the following sequences: Forward primer 5'-GCGCGCTAGCCGCCACCATGCTGCTGCTGCCATTTCAACTGTTAGC-'3, reverse primer 5'-GCGCGTCGACTCATGGGATATTCTGATATGACC-'3. Primers introduced NheI and SalI restriction sites respectively for cloning into PJet easy cloning vector (Thermofisher Scientific). CD1b sequence was digested and cloned into the mammalian expression lentivector pELNS (University of Pennsylvania).

TCR cloning for mammalian cell expression: The publically available clone 18 GEM TCR chain sequences (GenBank Accession numbers JQ778258.1-JQ778257.1) were synthesised by GeneArt (Germany) and sub-cloned into the lentivector pELNS for virus production. Clone 1 GEM TCR was also generated by GeneArt, the Vβ20 chain (Genbank accession JQ778264.1) was synthesised and cloned into the GEM C18 cassette; replacing the C18 Vβ13.2 sequence. We subsequently performed site-directed mutagenesis on the

alpha chain to yield a complete GEM C1 sequence, using the following: forward primer 5'-GCCGTGCGGGTCACCGGCGGCT-3', reverse primer 5'AGCCGCCGGTGACCCGCACGGC-3'. LDN5 TCR was previously cloned by Dr Salah Mansour (225).

Cloning of soluble TCR: α- and β-chain cassettes of the GEM C18 TCR were engineered separately for expression in vectors pEX956 and pEX651 respectively (Immunocore). Leader sequences were removed and the restriction site NdeI was introduced at the 3' end. The following reverse primers were used to remove the constant region and introduce the restriction site SalI and BglII in the α- and β- sequences respectively at the 5' end: alpha chain reverse primer 5'-ttgtcagtcgacttagagtctctcagctggtacacg-3', beta chain reverse primer 5'-ggtgtgggagatctctgcttctgatggctcaaa-3'. The remaining sequence encoded the soluble portion of the α- and β- TCR chains. pEX651 contained an engineered BirA tag site for subsequent biotinylation.

2.7 Virus Production

Virus production for cell line transduction: Endotoxin free plasmid DNA was prepared from E-coli via the Maxiprep protocol (Qaigen). 2 x10^6 HEK 293T cells (Sigma-Aldrich) were seeded in a 10 cm dish (Corning) in a total of 7 ml complete DMEM (Lonza). Plasmid transfection media was prepared the following day combining 10 μg total DNA with 60 μl Superfect (Qaigen). The following Pol/Gag (3 μg), pRSV.REV (3 μg), pVSV-G (1.5 μg) and engineered CD1b pELNS plasmids (2.5 μg) were added together in FBS free DMEM to a total of 300 μl. 60 μl Superfect reagent was then added and incubated at room temperature for 5-10 minutes. During this incubation, HEK293TN cells were washed once with 4 ml PBS, 3 ml complete DMEM was added to the plasmid reaction mix and then pipetted in a dropwise manner onto the cells. Three hours later supernatant was removed, cells were washed with 4 ml PBS and 6ml fresh complete DMEM was added to the cells. Virus was harvested on day 3 and day 4 with media replenished in between virus collection. Virus was spun at 2000 rpm for 5 minutes twice to remove debris and stored at 4°C if used within 7 days and -20°C if in storage for longer. Generally, freshly extracted virus was used directly for transduction.

Virus production for primary T cell transduction: The protocol was used as above with the following changes. $1x10^7$ HEK 293TN cells were seeded in a T150 flask to achieve 50% confluence in 20 ml complete Dulbecco's Modified Eagle Medium (DMEM). The next day plasmid transfection media was prepared by combining 57 μg total DNA with 117 μl Superfect reagent. Pol/Gag (18 μg), pRSV.REV (18 μg), pVSV-G (7 μg) and engineered pELNS TCR plasmids (15 μg) were added to FBS free DMEM to a total of 3 ml. After addition of reaction mix to 20 ml fresh complete DMEM media, it was added to washed cells. Cultures were left for two days before harvesting 20 ml supernatant. Virus was then concentrated by centrifugation for 12 hours at 20,000 rcf, 4°C and re-suspended in 4 ml fresh complete IMDM media.

2.8 CD1b and GEM TCR cell transduction

Transduction of cell lines: Cells including T2 lymphoblasts or human Jurkat T cell lines were seeded in a 6 well dish at both $5x10^5$ and $1x10^6$ in a total of 1.5 ml. 1.5 ml of fresh neat virus was added to the culture wells and the plates were spun for 90 minutes at 37°C at 2200 rpm. Cells were left at 37°C at 5% CO_2 and expanded in complete RPMI. After one week $2x10^5$ cells were stained to check expression of either CD1b or GEM TCRs. Positively expressing cells were then sorted into a line using the FACSAria and then expanded and maintained in complete RPMI. LDN5 TCR expressing Jurkats were previously generated (225).

Transduction of primary T cells: $1x10^6$ CD14 depleted PBMCs were seeded in a 24 well plate overnight in 1 ml of complete Iscove's Modified Dulbecco's Media (IMDM-Thermofisher Scientific) supplemented with 100 IU penicillin, 100 μg/ml streptomycin and 10% FBS (complete IMDM-Lonza) 100 IU/ml IL-2 and $5x10^5$ CD3/CD28 conjugated Dynabeads (Thermofisher Scientific). The following day, 1 ml of concentrated virus was added to the activated T cells, 7 days later the Dynabeads were removed by magnetic separation. Cells were then left for an additional 1 week replacing media every two days before staining with relevant anti-TCR specific antibodies and co-stained with anti-CD3, anti-CD8 and PI. Cells were acquired on a FACScalibur (BD Biosciences).

2.9 Preparation of Lipid antigens

Mycolic Acids: All dried chemically synthesised mycolic acids were provided by Mark Baird, University of Bangor. They were resuspended at 1 mg/ml in 9:1 chloroform/methanol, aliquoted, dried and then frozen at -20°C for future use. When required, the aliquots were resuspended in appropriate media and sonicated for 30 minutes at 80°C before addition to cultures.

α-galactosylceramide: Lyophilized αGC (Avanti) were solubilised in vehicle (150 mM NaCl, 0.5% Tween 20 (Biorad)) to 200 μg/ml using repeated 1-minute pulses of sonication for a total of 15 minutes and heating to 40°C.

2.10 Cell stimulation assays

Stimulation of Jurkats with MA: $2x10^5$ CD1b-T2 cell line were seeded in a 96 well plate and pulsed for 18-20 hours overnight with either 0.1 μg/ml, 1 μg/ml, 10 μg/ml or 20 μg/ml of lipid antigen. Total volume for lipid pulse was 50 μl. The following day Jurkat T cells were washed in fresh media and added in a 1:1 ratio for a final volume of 200 μl. The co-culture was left for 16-18 hours before harvesting for FACS or luminescence assay. All wells were performed in duplicate. In all cases negative controls consisted of TCR negative Jurkats, unpulsed T2s or CD1b negative T2s. Positive control consisted of $2x10^5$ TCR expressing Jurkats cultured with 50 ng/ml PMA and 500 ng/ml Ionomycin (both from Sigma-Aldrich).

Measuring Jurkat T cell activation: Activation of J.RT3.5 Jurkats was assessed via flow cytometry by measuring the expression of the T cell activation marker CD69. Activation of NFAT-GLuc Jurkats was measured using Gaussia luciferase kit (New England Biolabs) as per manufacturer's instructions. In brief, GLuc assay solution was made containing 100x diluted Biolux GLuc substrate (containing coelenterazine) in Biolux GLuc assay buffer immediately before performing the assay. 25 μl of GLuc assay solution was added to 10 μl of Jurkat/antigen culture supernatant in a half area 96 well plate (Corning) and

luminescence was read using a luminometer plate reader (Glomax discover – Promega) with 1 second delay.

Stimulation of ex vivo T cells with MA: $5x10^4$ autologous moDC were seeded into a 96 well dish in a total volume of 50 μl complete medium containing 1 μg of purified synthetic mycolate and left for 18 hours at 37°C, 5% CO_2 to facilitate lipid loading. On the same day CD14- T cell fractions were defrosted rapidly in a heated water bath and left to recover overnight in complete medium at 37°C with 5% CO_2. The next day T cells were washed, counted and added to unwashed moDC in a ratio of 1:10 in T cell media containing 10% human serum and 2.5 mg/ml plasmocin (Invivogen), 2.5 μg/ml purified anti-CD28 (Biolegend), 1x Brefeldin-A (Biolegend) and 1x monensin (Biolegend). Co-cultures were left at 37°C for 6 hours. Cells were then immediately transferred to FACS tubes prepared for intracellular cytokine staining assay.

Transduced primary T cell stimulation: Transduced T cells were thawed rapidly and recovered in complete media for 4 hours. T2 lymphoblasts were pulsed at 10 mg/ml, a concentration found to be in excess of the minimal concentration required to activate transduced T cells. Cells were then washed and added to pulsed APCs in a ratio of 1:2 for 24 hours in a total volume of 200 μl. After activation, half of the supernatant was removed for cytokine analysis using luminex and cell viability was directly assessed using Cytotox-glo cytotoxicity assay (Promega).

2.11 Cytokine release by Luminex assay

Concentrations of cytokine (R & D Systems) were determined using a Bioplex 200 platform (Bio-Rad) according to the manufacturer's protocol. In brief, 50 μl of culture supernatant was incubated for two hours at room temperature after three minutes shaking with microparticle cocktail conjugated to the following anti-cytokine antibodies; IL-2, TNF-α, IFN-γ, IL12p70, IL-17a, IL-6, IL-8, GM-CSF, IL-4 and IL-10. Samples were then washed three times in 50x diluted wash buffer (kit provided) before addition of biotin conjugated antibody cocktail (kit provided) for one hour at room temperature shaking at 50 rpm. Following three further washes, streptavidin-PE (kit provided) was added to all

wells for 30 minutes at room temperature shaking at 50 rpm. Following three further washes, microparticles were resuspended in 100 μl PBS (Lonza) and immediately analysed.

2.12 Immunohistochemistry

Paraffin-embedded human healthy or Mtb infected lung tissues were obtained from the histology archive at University Hospital Southampton in accordance with the ethical approval for this study. Sections (4 μm thick) were taken in the histochemistry research unit and mounted onto APS coated glass slides and allowed to dry for at least 48 hours in 40^{o}C incubator. Sections were dewaxed stepwise for 5 minutes each time in two different vessels of clearene and then rehydrated through graded alcohol to 70%. Freshly made 0.5% of 30% hydrogen peroxide in methanol was used to block endogenous peroxidase for 10 minutes. Sections were washed 3 X 2 minutes in TBS buffer, pH 7.2-7.6. (10x concentrate TBS prepared by mixing 80 g NaCl and 6.053 g Tris base in 1 L of distilled water). Heat induced-epitope retrieval was performed by: boiling the slides in 1 mM EDTA (pH 8.0) in distilled water for 25 minutes for CD1b, and boiling slides in citrate buffer for CD68 and CD11c in microwave at 50% power.

All subsequent steps required three consecutive washes between each step. Dulbecco's modified eagle medium supplemented with 10% FCS and 2% BSA was incubated on each sample for 20 minutes at room temperature to block slides. The following primary antibodies were applied to appropriate sections at indicated dilutions overnight at 4°C : anti-CD1b mouse monoclonal (SN13;K5 1B8-Abcam) 1:50, anti-CD11c rabbit polyclonal (polyclonal-LSBio) 1:100 and CD68 mouse monoclonal 1:200. Secondary antibody for CD1b and CD68 was a Vector goat anti-mouse used at 1:800, and a Vector goat anti-rabbit at 1:800 was used for CD11c. After a second 3 X 5 minutes TBS wash steps, sections were incubated for 30 minutes in streptavidin biotin-peroxidase complexes to amplify signal detection (Elite vectastain ABC kit, Vector laboratories), containing 1:1:75 parts of reagent A, reagent B and TBS respectively. Sections were washed and incubated in freshly prepared DAB (2-component DAB pack, BioGenex) substrate for 5 minutes

followed by a wash in TBS and 5 minutes wash under running tap water. For approximately 1 ml of DAB, 32 µl of DAB chromogen and 50 µl of 15% sodium azide were added to 1 ml of stable DAB substrate buffer. Counter staining was performed in Mayer's haematoxylin for 20 seconds after which sections held under running tap water for 5 minutes. Slides were dehydrated for 1 minute in each of 3 graded alcohols to clearene, followed by mounting in pertex. Sections were allowed to dry before imaging on an Olympus BX51, CC12 (dotSlide). CD11c and CD68 staining was carried out by Jenny Norman, as part of an immunohistochemistry service, University Hospital Southampton.

2.13 Molecular Dynamics

All MD simulations were carried out by Dr. Chris Cave-Ayland, University of Southampton.

A crystal structure of CD1b in complex with a GMM is available (PDB code: 1UQS), however the poor resolution (3.1 Å) prevented its direct use as a simulation starting structure. A higher resolution structure (PDB code: 1GZQ) containing CD1b in complex with a phophatidylinositol was therefore used to provide the initial geometry of the CD1b and $ß_2$-microglobulin chains.

Molecular Dynamics simulations were performed using the Amber 14 software package (ref2) with the ff99SB forcefield. The protein ligand complex was solvated in a box of 91x84x68 Å using the TIP3P water model and neutralized through the addition of 7 Na+ ions. Bond lengths were constrained using the SHAKE algorithm (ref3), allowing use of a 2 fs time step. Simulations were conducted at 300 K using a Langevin thermostat (ref4) with a collision frequency of 3 ps^{-1}. Where relevant below, pressure was regulated using a Monte Carlo barostat (ref5) with volume moves attempted every 100 time steps. All systems were initially equilibrated with protein and ligand heavy atom restraints to preserve secondary structure elements. All systems were gradually heated from 100 to 300 K over 0.5 ns. The system volume was then allowed to equilibrate for 2 ns under NPT dynamics. The system was then cooled over 0.1 ns, and the previous process

repeated with restraints on protein backbone heavy atoms only. Protein backbone restraints were then removed and the system equilibrated for a further 2 ns at 300 K.

2.14 3D Immunoaugmentation

Mtb culture: All Mtb was cultured by Dr Liku Tezera (University of Southampton). *M. tuberculosis* H37Rv was cultured in Middlebrook 7H9 medium (supplemented with 10% OADC, 0.2% glycerol and 0.05% Tween 80) (BD Biosciences, Oxford) and bioluminescent *M. tuberculosis* H37Rv (226), GFP or mCherry expressing *M. tuberculosis* H37Rv (227) were cultured with Kanamycin 25 mg/ml and Hygromycin 50 mg/ml, respectively. Cultures at 1x 10^8 colony forming unit/ml (cfu/ml) Mtb (OD= 0.6) was used for all experiments at multiplicity of infection (M.O.I) of 0.1.

Cell encapsulation: Microspheres were generated with an electrostatic generator (Nisco, Zurich, Switzerland) as described previously (228). For cellular encapsulation, PBMCs were infected with Mtb overnight and mixed with transduced T cells to give 1% C18 TCR expressing cells the next day. This was then mixed with 1.5% sterile alginate (Pronova UP MVG alginate, Nova Matrix, Norway) or alginate with human collagen (VitroCol, Advanced BioMatrix) at a final concentration of 5 x 10^6 cells/ml. The cell-alginate suspension was injected into the bead generator at 10 mL/hour via a Harvard syringe driver through a 0.7 mm external diameter nozzle. Microspheres formed in an ionotropic gelling bath of 100 mM $CaCl_2$. After washing twice with HBSS, microspheres were transferred in RPMI 1640 medium containing 10% of human AB serum and incubated at 37^{o}C. Supernatant was harvested at defined time points and Mtb growth monitored by luminescence (GloMax® 20/20 Luminometer, Promega). For flow cytometry, microspheres were dissolved in 55mM Sodium Citrate and 10mM EDTA with 1% Saponin in HBSS.

2.15 Cell Viability

Cell viability was measured using Cytotox-glo cytotoxicity assay (Promega) after five days of microsphere culture in a 96 well plate following manufacturer's instructions. In brief, Cytotoxicity assay reagent was generated by adding provided assay buffer to AAF-Glo substrate. 50 µl of the assay reagent was added to 100 µl of suspended microspheres and luminescence was measured using Glo-Max discover after 15 minutes of shaking. 50 µl of assay reagent containing 30 µg/ml digitonin was then added to the wells prior to another 15 minutes shaking and reading of luminescence.

2.16 Statistical Analysis

GraphPad Prism version 5.01 (GraphPad Software Inc., La Jolla, California, USA) was used for statistical analysis, and p values ≤0.05 were considered statistically significant. Statistical analysis of iNKT subset proportion between animal groups were measured using chi-Squared test with post hoc analysis using bonnferoni in the R software package. Spearman's rank correlation coefficient test was used for all correlations. Mann-whitney U test was used to show statistical significance comparing iNKT frequency and proliferation between animal groups and differences between cell stimulation with different MA compounds. Heat map was generated in R software package using euclidean correlation metric to calculate distances and clustered using complete linkage. Cytokine levels were $\log_2$ transformed and normalised by median cytokine level across all lipids and cytokines. Heat map generation and chi-squared analysis were performed in R by Dr Akul Singhania (University of Southampton/The Crick Institute, London).

Chapter 3: Results

3.1 CD1d-K7 tetramer staining of human and macaque iNKTs

Numerous studies indicate that iNKT cells may have a protective role in mouse and human TB infection (171, 172, 174, 229-231). Additionally, our preliminary data generated by Joe Fenn using human CD1d tetramers in the macaque, suggested that iNKT frequency correlated with resistance to Mtb infection in macaque species. Therefore, we wanted to investigate iNKTs further in the macaque model of Mtb infection, in samples taken from vaccination and challenge studies. To date the most sensitive method to identify and characterise circulating iNKTs in human and mouse PBMCs is using CD1d-αGC tetramers that specifically bind the iNKT-TCR (78). Therefore, we sought to develop working macaque CD1d-αGC tetramers for this same purpose. In order to achieve this, macaque CD1d was expressed as inclusion bodies in a bacterial protein expression system (see methods section 2.2). We refolded denatured macaque CD1d and β_2M inclusion bodies with the strong iNKT agonist, αGC. The refolded protein was purified (Figure 3.1) via gel filtration chromatography.

CD1d is a heterodimer consisting of a CD1d (48 kDa) heavy chain, and a light chain represented by β_2M (12 kDa) (63). The stability of our refolded macaque CD1d protein monomers were assessed by SDS-PAGE gel analysis (Figure 3.2). Our results indicated that the refolded macaque CD1d-αGC protein complexes had the correct stoichiometry of heavy to light chain protein fragments (1:1) and it behaved in a similar way to control human CD1d protein complexes (Figure 3.2).

a b

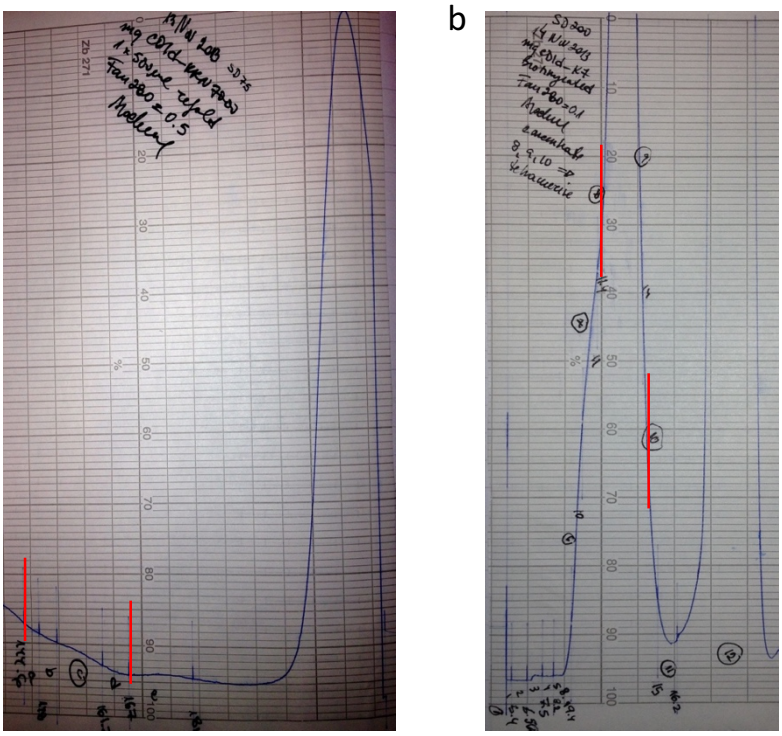

Figure 3.1: Purification of macaque CD1d-αGC complexes

Gel filtration (size exclusion) chromatograph of refolded macaque CD1d-αGC protein. (a) The protein elution volume via SD75 preparation column was between 144.6 and 157ml (red line). (b) After elution, biotinylated protein was run through SD75 analytical column to remove protein aggregate and biotinylation reaction impurities. Protein was eluted between 10.3 and 12.2 ml.

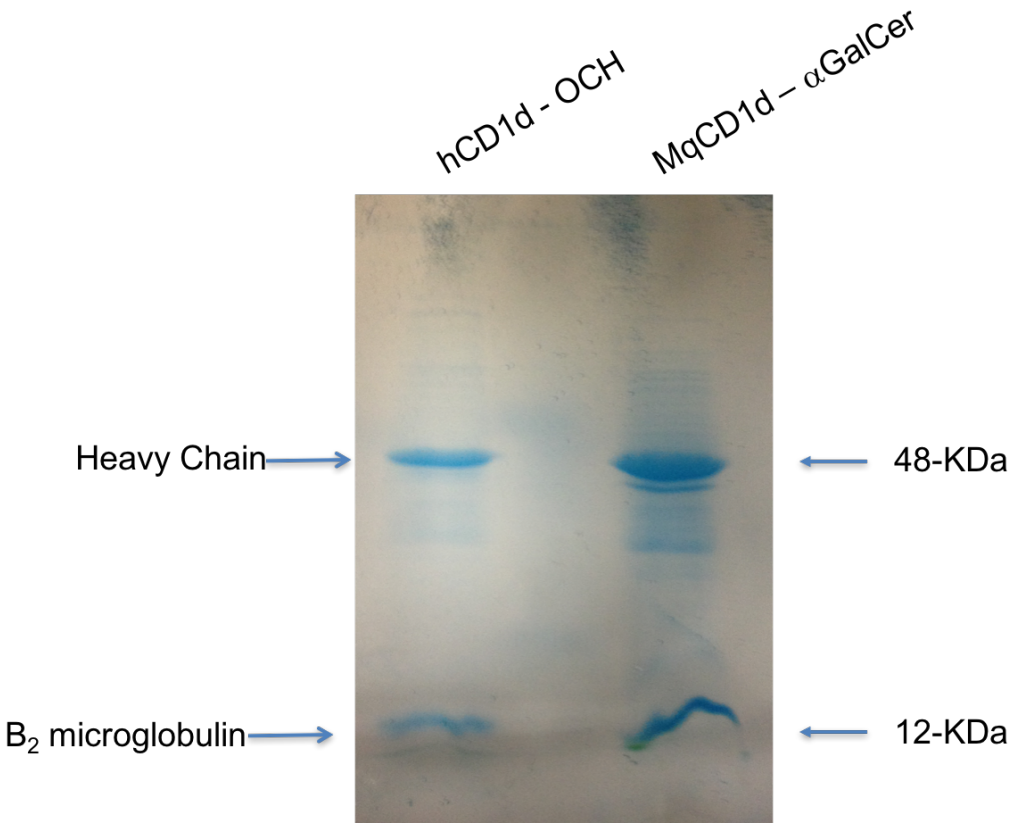

Figure 3.2: SDS-PAGE analysis of refolded macaque CD1d

Reduced SDS-PAGE gel electrophoresis of refolded macaque CD1d-αGC monomers, showing heavy chain macaque CD1d fragment (48 kDa) and beta-2-microglobulin fragment (12 kDa). Refolded macaque CD1d protein behaves similarly to a previously validated control human CD1d, indicating correct heavy to light chain stoichiometry.

To investigate the functional stability of our newly refolded macaque CD1d, we produced macaque CD1d-αGC tetramers and then stained two human iNKT clones that were previously isolated using human CD1d-αGC tetramers (232). In addition, tetramer staining of human iNKT clones has previously been used as a surrogate of affinity measurement (232). Our results demonstrated that macaque CD1d tetramers could bind human iNKT clones (Figure 3.3). However, they bound with lower mean fluorescence intensity (MFI=1774) when compared to human CD1d-αGC tetramer (MFI=3146). Furthermore, macaque CD1d tetramer staining was specific, as blocking by addition of

anti-iNKT TCR alpha and beta (anti-Vα24 and anti-Vβ11) antibodies 30 minutes prior to staining with tetramers abolished tetramer binding (Figure 3.3). Our results demonstrate the specific interaction between newly generated macaque CD1d and the iNKT-TCR, indicating that newly generated macaque proteins are functional and are therefore a valid tool for studying iNKT cells.

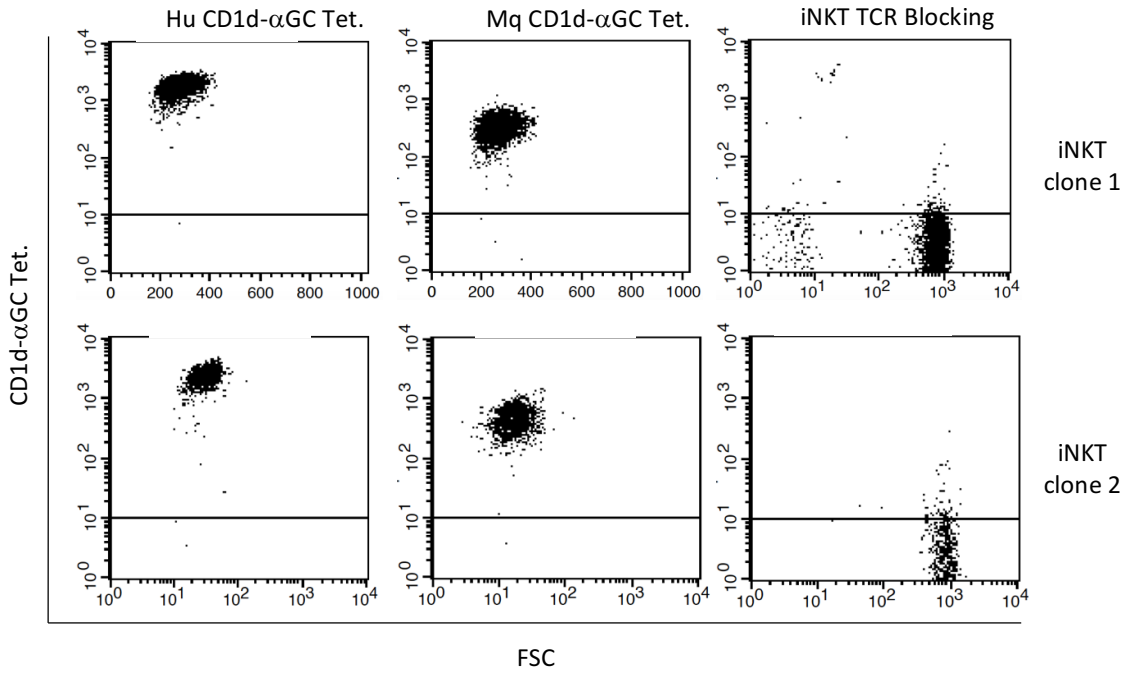

Figure 3.3: Macaque CD1d tetramer staining of human iNKT clones

Dot plots showing staining of human iNKT clones with both macaque and human CD1d-αGC tetramer. Macaque CD1d-αGC tetramer stains human iNKT clones (middle panels) with relatively less MFI than control human CD1d-αGC tetramers (left panels). Macaque CD1d-αGC tetramer staining is specifically blocked by anti-iNKT TCR blocking antibodies (anti-Vα24 and anti-Vβ11) (right panel).

To further characterise the macaque CD1d-αGC tetramers, we performed titration experiments with human iNKT clones. We found that at very high tetramer concentrations, macaque CD1d tetramers did not reach the level of staining shown by human CD1d tetramers (Figure 3.4). Our results revealed that even at a maximum

tetramer concentration of 5µl, macaque tetramers (MFI)=1422) bound iNKTs with reduced affinity compared to human (MFI=3121) (Figure 3.4). This could either indicate a reduced concentration of tetramer due to the presence of improperly refolded protein or perhaps be due to a reduced binding affinity of macaque CD1d protein to human iNKT-TCRs.

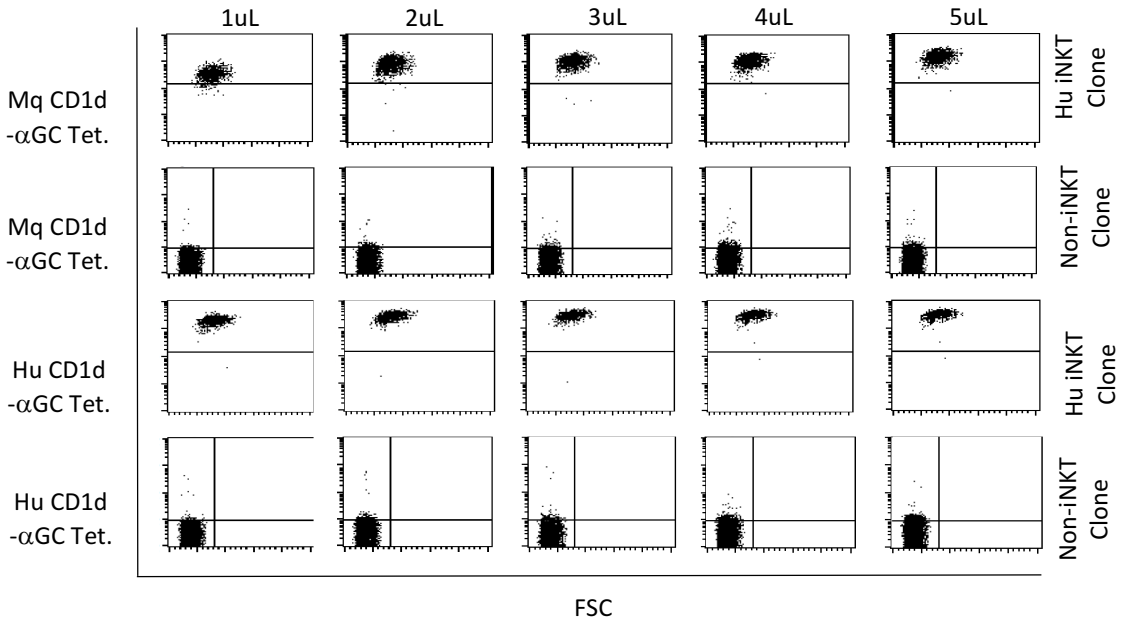

Figure 3.4: Macaque and human CD1d-αGC tetramer titrations

A clonal population of iNKTs were stained with different concentrations of macaque (top two rows) and human (bottom two rows) CD1d-αGC tetramers to ascertain differences in MFI. Tetramers concentrations increase from left to right where 1-5 µl were added for staining. The same human iNKT clone was used and shows human CD1d-αGC tetramer works better at all concentrations. Negative control consists of sequential staining of a non-iNKT clone demonstrating tetramer specificity.

In line with the above functional validation of macaque CD1d tetramers with human iNKT clones, we sought to characterise the binding of these tetramers to human iNKT cells *ex vivo*. Our staining of human *ex vivo* iNKTs were consistent with clone staining data, which demonstrated that macaque CD1d tetramers stained human iNKT cells with

much lower binding affinities relative to human CD1d tetramers (Figure 3.5). Furthermore, we found that macaque CD1d tetramers identified less iNKTs relative to human CD1d tetramers (macaque CD1d: 0.7% vs. human CD1d: 0.9%). These results suggested that macaque CD1d tetramers may fail to bind some iNKT cells due to a lower binding affinity.

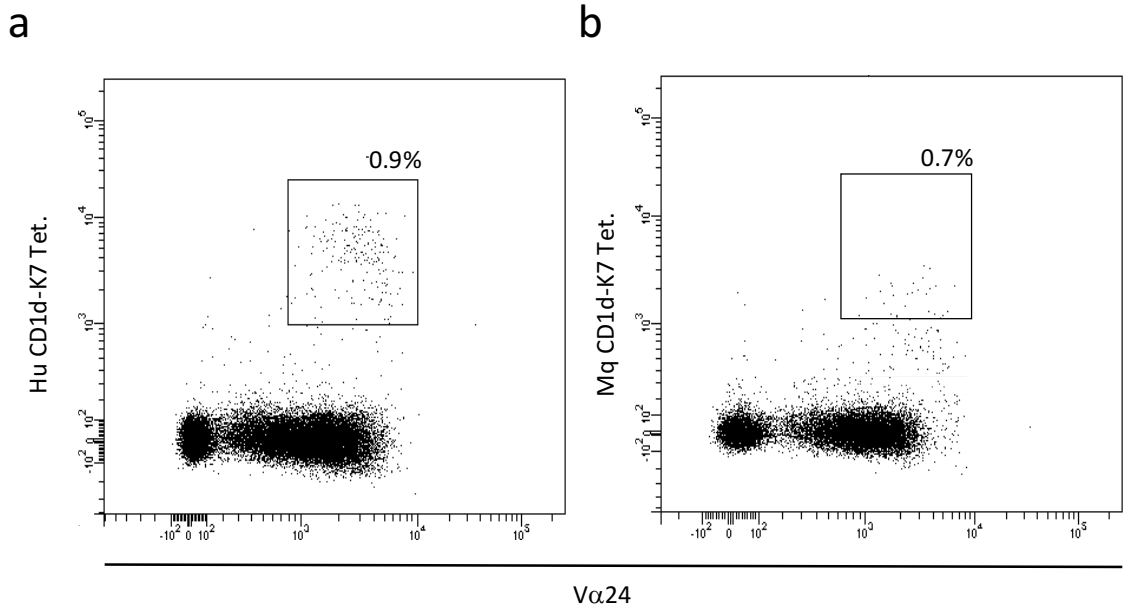

Figure 3.5: Macaque CD1d-αGC tetramer staining of human PBMCs

FACS dot plots showing staining of *ex vivo* live $CD3^+$ iNKT ($CD1d\text{-}tetrmer^+$, $V\alpha24^+$ iNKTs showed in boxed areas) populations from a single human donor. (a) Human CD1d-αGC tetramer staining is compared to macaque CD1d-αGC tetramer staining (b) of the same population of PBMCs. Numbers indicate the percentage of iNKTs identified with each tetramer. Macaque CD1d-αGC tetramer stains human iNKT with lower fluorescence intensity, identifying a lower number of iNKTs.

We next wanted to compare the binding of macaque and human CD1d tetramers to macaque iNKTs. For this purpose, we stained iNKT cells from macaque PBMCs (Figure 3.6). Our staining of a small cohort of mycobacteria-naive rhesus macaques demonstrated reduced binding of macaque CD1d tetramers relative to human CD1d (Figure 3.5). The population of iNKTs identified with the human tetramer had on average a higher MFI (mean MFI=78) than iNKTs stained with macaque tetramers (mean MFI=31)

which was significantly different, suggestive of reduced binding affinity. In addition, there were equal or increased numbers of iNKTs identified with the human tetramer compared to macaque, that was consistent with our human iNKT staining data. In conclusion, our data suggests that the human CD1d-αGC tetramer is more efficient at enumerating iNKT frequencies in macaques. Therefore, human CD1d-αGC tetramers were used to study iNKTs in all further studies.

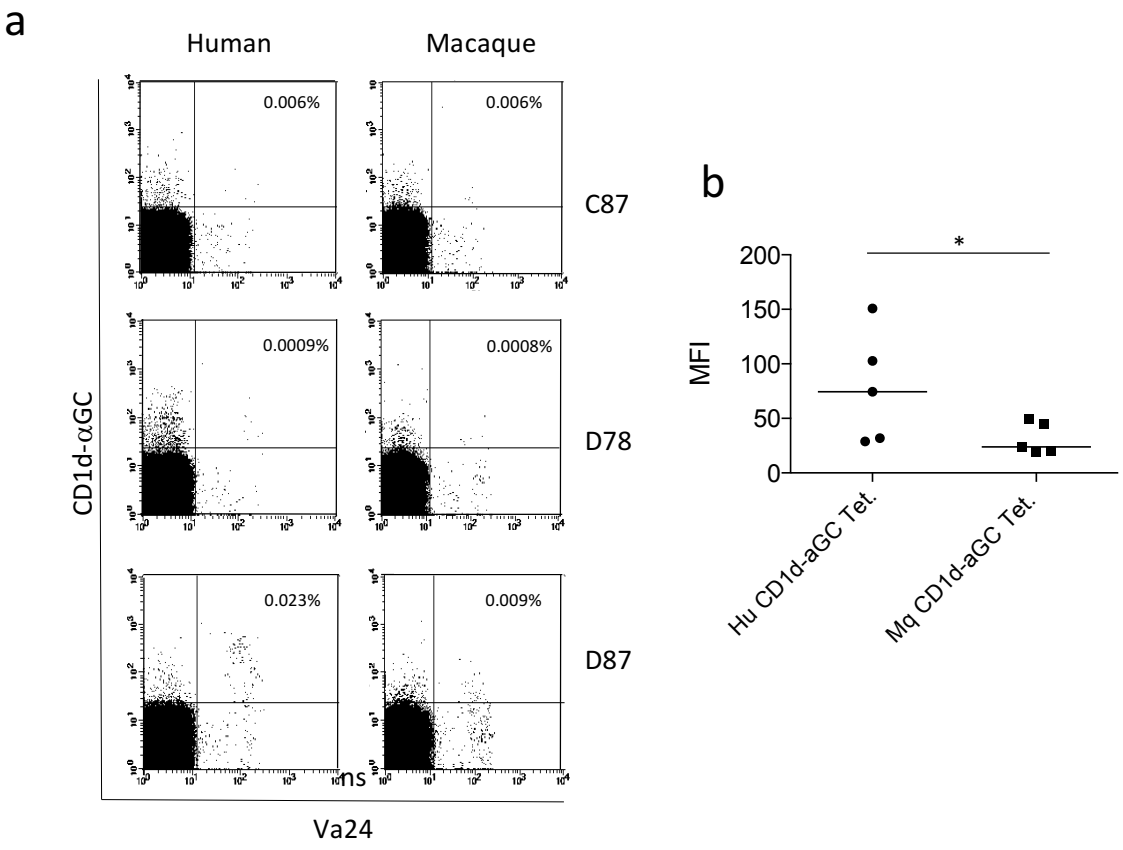

Figure 3.6: Macaque CD1d-αGC tetramer staining of macaque PBMCs

FACS dot plots showing staining of *ex vivo* live $CD3^+$ iNKT (CD1d-$tetrmer^+$ $V\alpha24^+$) populations from three macaque individuals with the following identification: C87, D78 and D87. (a) Dot plots comparing human CD1d-αGC tetramer staining (left) and macaque CD1d-αGC tetramer staining (right) of the same population of macaque PBMCs. Percentage in top right hand quadrant of each plot indicates percentage of iNKTs identified. Equal or more iNKTs are identified using the human tetramer. (b) Scatter dot plot of representative MFIs with both

macaque and human CD1d-αGC tetramer stained macaque PBMCs indicates human CD1d-αGC tetramers bind iNKT cells with significantly increased MFI.

3.2 *Ex vivo* iNKT frequency associates with protection in macaque model of Mtb infection

Published data suggest that a higher peripheral blood iNKT cell frequency is associated with protection in Mtb infection in mice (170, 171). In addition, published data on macaque Mtb resistance, as well as our own unpublished observations (table 3.1) demonstrate a similar observation within genetically distinct macaque groups (35, 38, 233). To investigate this further and to find other iNKT specific correlates responsible for underlying protection in macaque Mtb infection, we set out to determine the frequency and function of the iNKT repertoire in four macaque groups within the rhesus and Cynomolgus species. Each group differing in their inherent ability to control Mtb infection.

Macaque Species	Resistance* upon Mtb challenge	iNKT Frequency***	Resistance** post BCG Vaccination
Chinese Cynomolgus	Most resistant	Unknown	Almost complete resistance
Indonesian Cynomolgus	Very resistant	0.008 - 0.6% Mean = 0.1%	Almost complete resistance
Indian Rhesus	Very susceptible	0 - 0.04% Mean = 0.003%	Confers little resistance
Mauritian Cynomolgus	Most susceptible	0.001-0.62%Mean = 0.096%	Data not available

Table 3.1: Macaque susceptibility to Mtb

Table of observed resistance of macaque species based on multiple clinical observations. *Observations at Porton down; (234) ** Jan A. M. Langermans, 2001; ***Namita Rout, 2012.

Our NHP cohort contains naive outbred populations of macaque with restricted gene pools derived from macaques from the following groups: Chinese cynomolgus, Indonesian cynomolgus, Mauritian cynomolgus and rhesus macaque. Although we stained a large number of PBMCs ($2x10^6$) to determine an iNKT frequency, our initial staining did not yield any positive cells using anti-Vα24 and CD1d-αGC tetramer. We were unsure whether this result was due to a complete lack of iNKTs or simultaneous blocking of tetramer staining by anti-Vα24. To address this, we used MACS to enrich iNKTs from $1x10^8$ PBMCs from macaque peripheral blood. In rhesus and Mauritian cynomolgus samples, each with an initial *ex vivo* frequency of 0% we were able to enrich iNKTs to 0.07% and 0.45% of the population respectively (Figure 3.7). This process,

although highly specific, still resulted in a very low yield of iNKTs. Therefore, it is unlikely there is concurrent blocking of tetramer staining with anti-Vα24 antibody. The observed lack of iNKT staining is likely due to an extremely low number of iNKTs present in some macaques.

iNKTs are critical for an effective immune response in infectious disease and comprise between <0.01% - 1% of T cells in the periphery in humans (235). To investigate the relationship between iNKTs and disease outcome, we first determined peripheral blood *ex vivo* iNKT cell frequencies of mycobacteria-naive macaques (234, 236). We therefore employed our validation method for specifically detecting iNKTs by flow cytometry (Figure 3.8). Staining of live $CD3^+$, CD1d-αGC tet^+, V$\alpha24^+$ iNKTs revealed wide inter-individual differences in iNKT frequencies within each animal group ranging between <0.001% - >0.1%. We sequentially studied a total of 123 animals and *ex vivo* iNKT numbers were significantly higher in the Cynomolgus macaque of Chinese origin (CCM, median=0.0143%), which are most highly resistant to TB infection, compared to those of Indonesian origin (ICM, median=0.0011%, *p=0.0001*), rhesus macaque (IRM, median=0.0023%, *p=0.0006*) and Mauritian cynomolgus (MCM, median=0.0012%, *p<0.0001* (Figure 3.8)). These results indicated that a greater peripheral blood iNKT frequency associate with increased Mtb resistance in macaques.

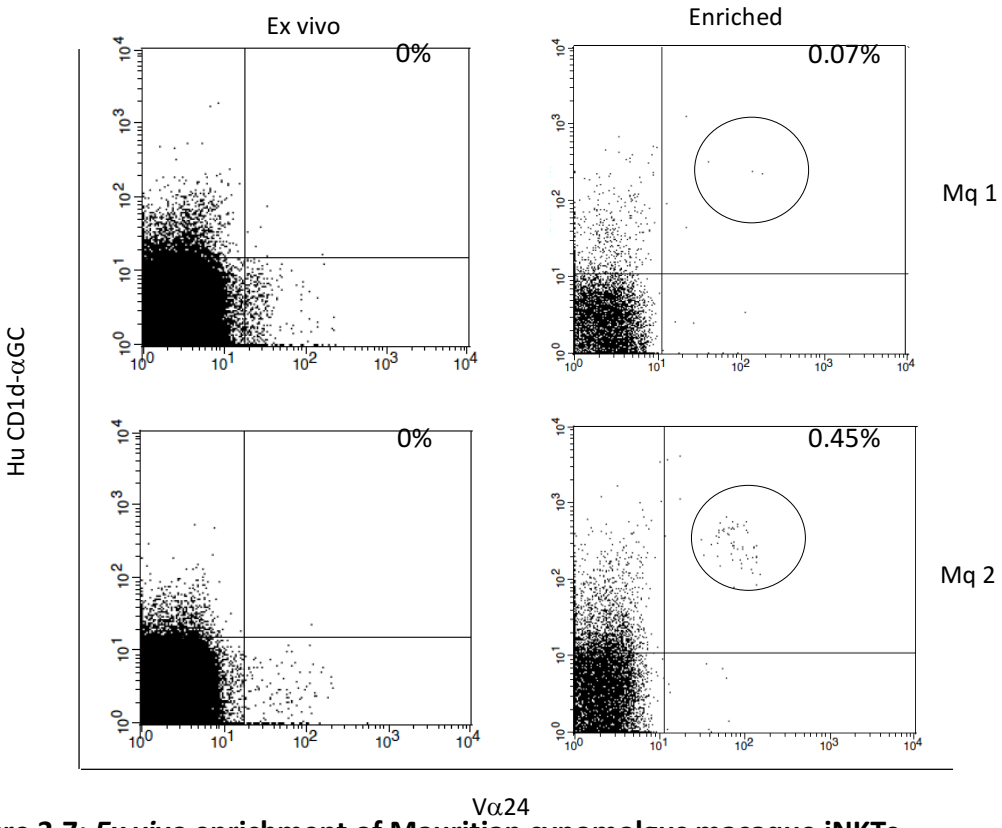

Figure 3.7: *Ex vivo* enrichment of Mauritian cynomolgus macaque iNKTs

Plots showing *ex vivo* iNKT staining of enriched PBMC fractions from two Mauritian cynomolgus macaques. iNKTs were enriched using MACS sorting by staining with CD1d-αGC tetramers to positively select for iNKTs from $1x10^8$ PBMCs with anti-PE microbeads. $2x10^6$ cells from the enriched iNKT fraction were then stained for iNKTs pre-gating on live, $CD3^+$ cells. iNKTs are displayed in top right hand quadrants as double positive for CD1d-tetramer and Vα24, and are only visible post enrichment (right). Black circle highlights iNKT population and numbers indicate percentage of iNKTs identified.

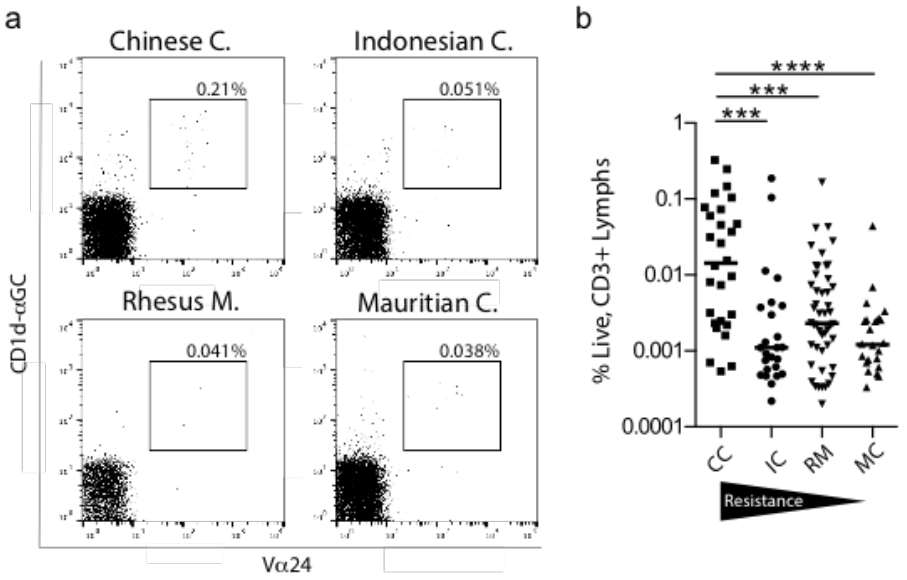

Figure 3.8: TB-resistant Chinese cynomolgus macaque have significantly increased peripheral blood iNKT frequencies relative to other macaques

(a) Representative *ex vivo* flow cytometry dot plots of live $CD3^+$ iNKT cells (CD1d-αGC $tetramer^{+,}$ $Vα24^+$) from PBMCs of four genetically distinct groups of macaque. (b) Cumulative iNKT staining data from Chinese cynomolgus (CCM, n=28), Indonesian cynomolgus (ICM, n=25), Indian rhesus (IRM, n=48) and Mauritian cynomolgus (MCM, n=24); horizontal lines are median values. Significant differences in iNKT frequency are observed between CCM compared to ICM, IRM and MCM. Relative susceptibility to Mtb within each group is shown as a resistance bar below the x-axis (234). *Ex vivo* iNKT frequency is higher in more resistant groups.

3.3 Optimisation of iNKT culture and proliferation

Once activated, iNKTs are potent immune cells with many effector and regulatory roles in infection, cancer and autoimmune disease (237). Dysfunction in the iNKT cell subset may lead to inefficient control of Mtb infection, or conversely, a highly potent response that may cause detrimental pathology. One measure of iNKT function is the lymphoproliferative response to the superantigen α-GC when presented in the context

of CD1d by APCs (220). We have previously used human monocytes that are efficient CD1d expressing APCs, to stimulate human iNKT cell expansion (47). To initiate *in vitro* macaque iNKT cell expansion, we first used purified α-GC pulsed $CD14^+$ monocytes from macaque PBMCs and returned them to autologous $CD14^+$ negative T cell fractions in a ratio of 1:10 (APC: T cell). Despite frequent stimulation with α-GC pulsed monocytes, we observed no iNKT expansion in these experiments.

Other studies used moDC as CD1d APCs (179, 238). We therefore decided to use moDC as APC for the specific stimulation and expansion of macaque iNKT cells. In order to achieve this, we sought to functionally verify and characterise macaque moDC. To differentiate macaque monocytes into moDC, we used a similar protocol used in generating human moDC, using recombinant human IL-4 and GM-CSF cytokines (239). After 6 days *in vitro* macaque monocyte differentiation, the morphology of the cells, which was observed under light microscopy, changed from small, round cells to larger cells with multiple membrane extensions, typical of moDC morphology (239). To confirm their correct differentiation into moDC, we compared cell surface markers of macaque and human moDC via antibody staining (Figure 3.9 & 3.10). We identified those antibodies which bind epitopes common to multiple species of human and NHP. These include anti-CD86, anti-HLA-DR, anti-CD11c, anti-CD1c and anti-CD1b that collectively define moDC phenotype (240).

We first characterised the phenotype of macaque monocytes (Figure 3.9), CD14 is a defining marker of monocytes and our staining revealed high expression of this marker in both macaque and human monocytes (Figure 3.9). Furthermore, macaque and human monocytes both express similar levels of the macaque equivalent MHC class II molecule HLA-DR and the co-stimulatory receptor CD86 (Figure 3.9). We did not observe CD1 group 1 expression on monocytes as these are normally present only in professional antigen presenting cells (1). In addition, although we observed expression of CD1d on human monocytes, there is no macaque reactive anti-CD1d antibody commercially available to characterise expression on macaque monocytes.

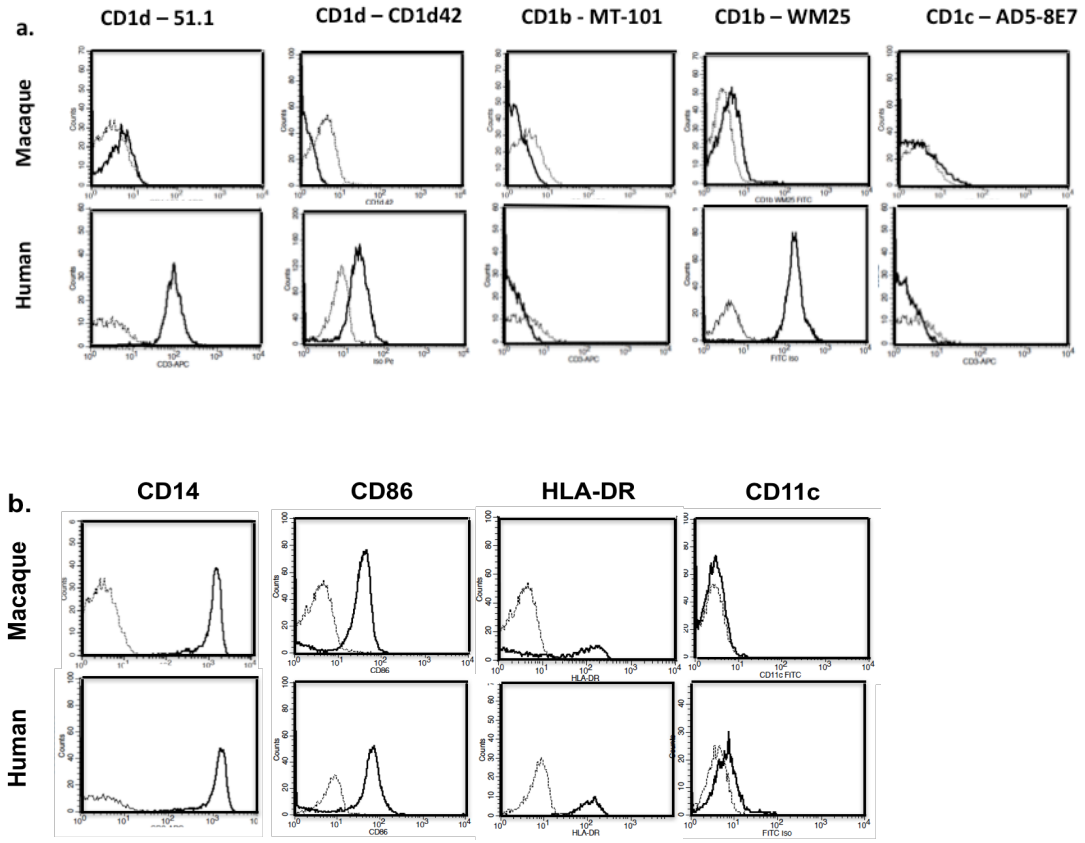

Figure 3.9: Phenotypic analysis of macaque monocytes

Phenotypic analysis of monocytes from macaque (upper panel) and human (lower panel) using; (a) CD1 markers; (b) other markers key in defining monocytes and moDC in human and macaque. Broken line depicts isotype control staining and solid line represents antibody marker. Macaque monocytes expressed no CD11c, CD1c or CD1b but expressed high levels of CD14, a typical marker for monocytes.

After six days of monocyte differentiation *in vitro*, we analysed the newly generated moDC with the same markers. We found that HLA-DR had increased on human moDC and marginally decreased on macaque, while CD14 had been retained in macaque moDC and reduced slightly on human moDC, a feature documented previously (240-242). CD11c had significantly increased on macaque moDC compared to monocytes and only marginally increased on human moDC (Figure 3.10). The major defining markers of newly generated moDC are the group 1 CD1 molecules (243) and moDC from both

macaque and human expressed CD1b and CD1c (Figure 3.10). There was no increase in CD1b expression on macaque moDC with antibody clone WM25, suggesting that this is likely not cross-reactive. Previous work demonstrated that CD1c and CD11c can be used in combination to identify all subsets of NHP moDC (241). Importantly, our results indicated that our macaque moDC expressed both these markers suggesting their full functional differentiation into moDC.

Following successful iNKT expansion in previous published reports using moDC mediated iNKT expansion (179), we attempted to use these cells to expand iNKTs in our cultures. However, we did not observe iNKT expansion using moDC as APC. We found that optimal macaque iNKT expansion was achieved through direct addition of lipid antigen into freshly purified PBMCs (Figure 3.11). On day 14 after the start of *in vitro* cultures, we stained with CD1d-αGC tetramers to identify iNKT cell numbers in order to measure their proliferative response.

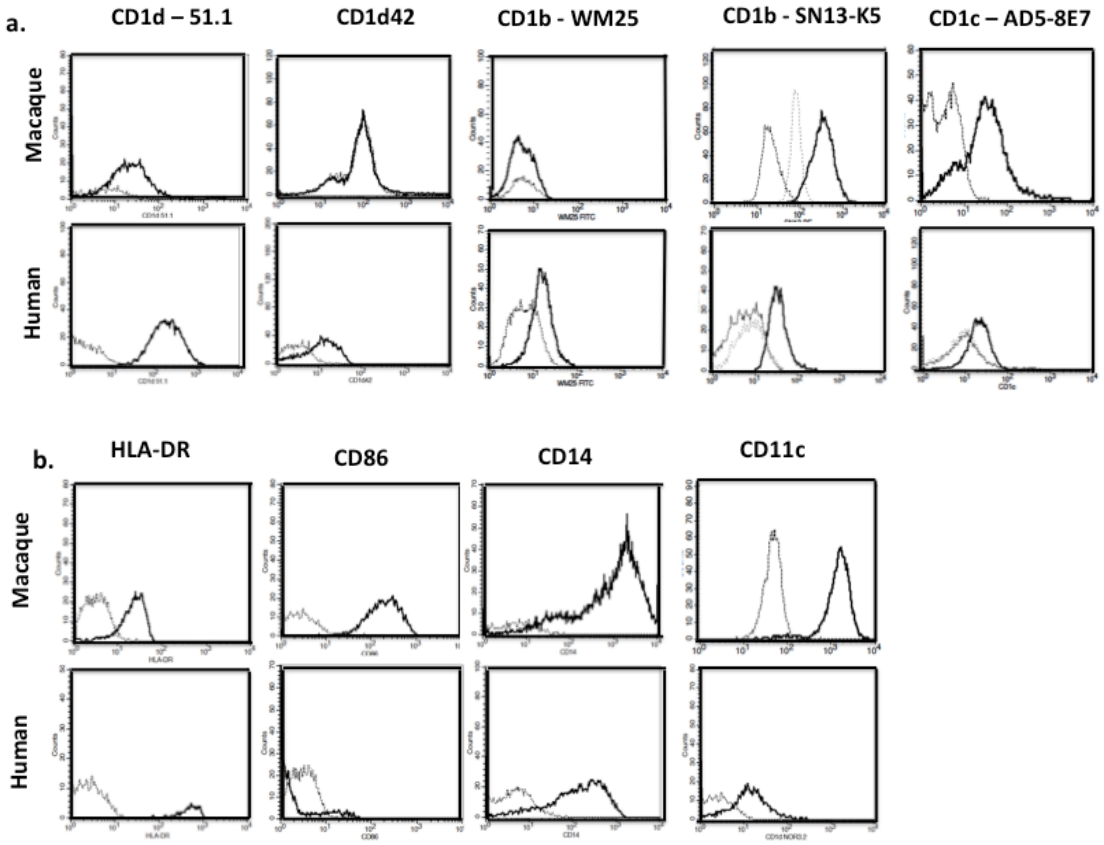

Figure 3.10: Phenotypic analysis of macaque moDC

Surface marker expression on moDCs after 6 days of monocyte-differentiation. Antibodies used are common to macaque and human after 6 days of differentiation; a) CD1 markers; b) other markers common to all species of moDC. Broken line depicts isotype control staining, solid line represents antibody marker and dotted line represents secondary antibody alone. Macaque moDC expressed typical markers such as CD11c, CD1c, CD14 and CD86.

3.4 Skewed iNKT subset ratios associate with *Mtb* susceptibility in macaques

After assessing total iNKT cell numbers in the peripheral blood of macaques, we next investigated iNKT cell function by antigen-specific *in vitro* expansion. We determined the proliferative capacity of iNKTs from animals within each macaque group by *in vitro* expansion with the potent iNKT agonist αGC (Figure 3.11a). We found large inter-individual differences in iNKT expansion between animals of the same genetic background, ranging between <10 - >1000-fold expansion in Indonesian cynomolgus, rhesus macaque and Mauritian cynomolgus, with Chinese cynomolgus displaying the

greatest variance ranging between <1 - >10000-fold expansion. We did not observe significant differences in the fold expansion of total iNKTs between the macaque groups (CC median=8.26, IC median=22.25, RM median=16.94, MC median=15.43, *p=0.25*), although Chinese cynomolgus showed a trend towards a weaker iNKT expansion overall (Figure 3.11b). In contrast, stratification of expanded iNKTs according to CD4 and CD8 co-receptor expression revealed statistically significant differences in the percentages of iNKT subsets (Figure 3.11c). Chinese cynomolgus had a significantly greater percentage of $CD8^+$ iNKTs than Mauritian cynomolgus (*p=0.02*). Likewise, rhesus macaque had a significantly higher percentage of $CD8^+$ iNKTs compared to Mauritian cynomolgus (*p=0.006*) (Figure 3.11c). Furthermore, analysis of iNKT proportions of $CD4^+$, $CD8^+$, double positive (DP) and double negative (DN) subsets revealed statistically significant differences between Chinese cynomolgus vs. Mauritian cynomolgus (Pearson's Chi-squared, *p=0.0002*), Indonesian cynomolgus vs. Mauritian cynomolgus (*p=0.0004*) and Indonesian cynomolgus vs. rhesus macaque (*p=0.027*) (Figure 3.11d). In addition, analysis of $CD4^+/CD8^+$ subset ratios revealed a more skewed iNKT subset ratio in TB susceptible animals (compare resistant CC=0.61 and IC=0.71 to susceptible RM=0.27 and MC=1.57). Taken together, our data suggest that a skewed $CD4^+/CD8^+$ iNKT subset ratio following antigen-specific expansion associates with disease susceptibility and therefore we investigated this observation further in challenge and vaccination studies.

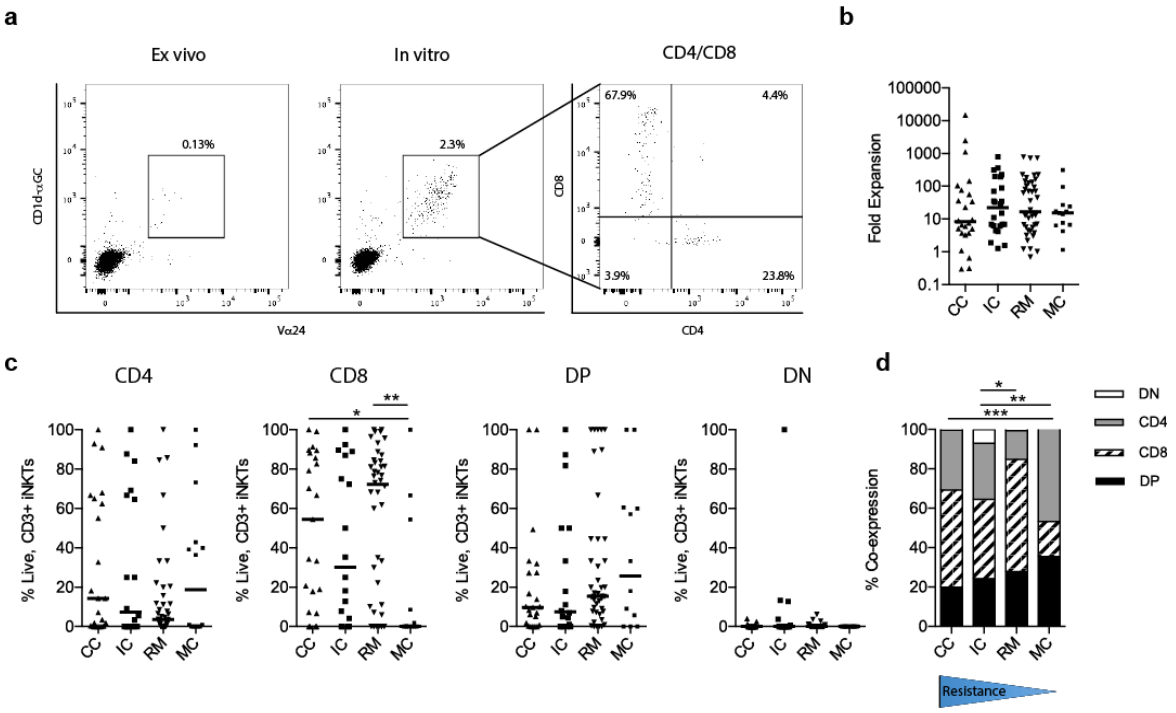

Figure 3.11: *In vitro* antigen-induced iNKT proliferative response reveals divergent expansion of subsets

a) Representative flow cytometry staining of iNKTs two weeks pre- (*ex vivo*) and two weeks post- (*in vitro*) αGC mediated expansion. Expanded cells were also stained and gated on CD4 and CD8 to determine subset proportion. Number displayed in each quadrant indicates percentage of iNKT subset within expanded iNKT population. (b) Cumulative data of fold expansion (ratio of *in vitro* expanded iNKT/*ex vivo* frequency) of iNKTs which is similar between macaque groups; Mauritian cynomolgus (n=13), Indonesian cynomolgus (n=24) Chinese cynomolgus (n=24) and rhesus macaque (n=42); median values are shown. c) iNKT subsets within expanded iNKTs in (b) are shown. Macaque groups exhibit significant differences in their percentage of *in vitro* $CD4^+/CD8^-$, $CD4^-/CD8^+$, $CD4^+/CD8^+$ and $CD4^-/CD8^-$ subsets. Median values are shown. d) Analysis of iNKT subset proportions using chi squared test with post hoc analysis after αGC mediated expansion in macaque groups revealed a skewed iNKT subset proportion in less resistant macaque groups.

3.5 Increased $CD8^+$ iNKTs associate with better disease outcome in macaques

Having found that increased peripheral blood iNKTs and a balanced iNKT subset ratio post antigen expansion correlated with TB resistance in mycobacteria naive macaques, we investigated whether BCG vaccination conferred an iNKT phenotype that may correlate with protection to Mtb. We first studied a cohort of six Chinese cynomolgus macaques, reasoning that since vaccination in this group rendered a high ability to control infection for 26 weeks after exposure to high dose aerosol challenge (manuscript in preparation), we may uncover an iNKT correlate. No consistent pattern of change was observed in iNKT frequency or expansion post BCG administration (Figure 3.12a). In addition, there was little change in the iNKT subset percentages, nor in comparison of proportions after antigen specific expansion (Pearson's Chi-squared, *p=0.45* [Figure 3.12c]). This suggests vaccination does little to the iNKT repertoire in an already resistant macaque population.

However, correlative analysis of the percentage of $CD8^+$ and $CD4^+$ iNKTs post BCG with disease burden measured post challenge consistently revealed a more favourable disease outcome for animals with an increased percentage of antigen responsive $CD8^+$ iNKTs, and vice versa with regard to $CD4^+$ iNKTs (Figure 3.13). $CD8^+$ iNKT numbers negatively correlated with total pathology score (r=-0.73, *p=0.33*) and total lung score (r=-0.89, *p=0.25*). These results suggest that increased proportions of *in vitro* expanded $CD8^+$ iNKT associate with improved disease pathology in Chinese cynomolgus.

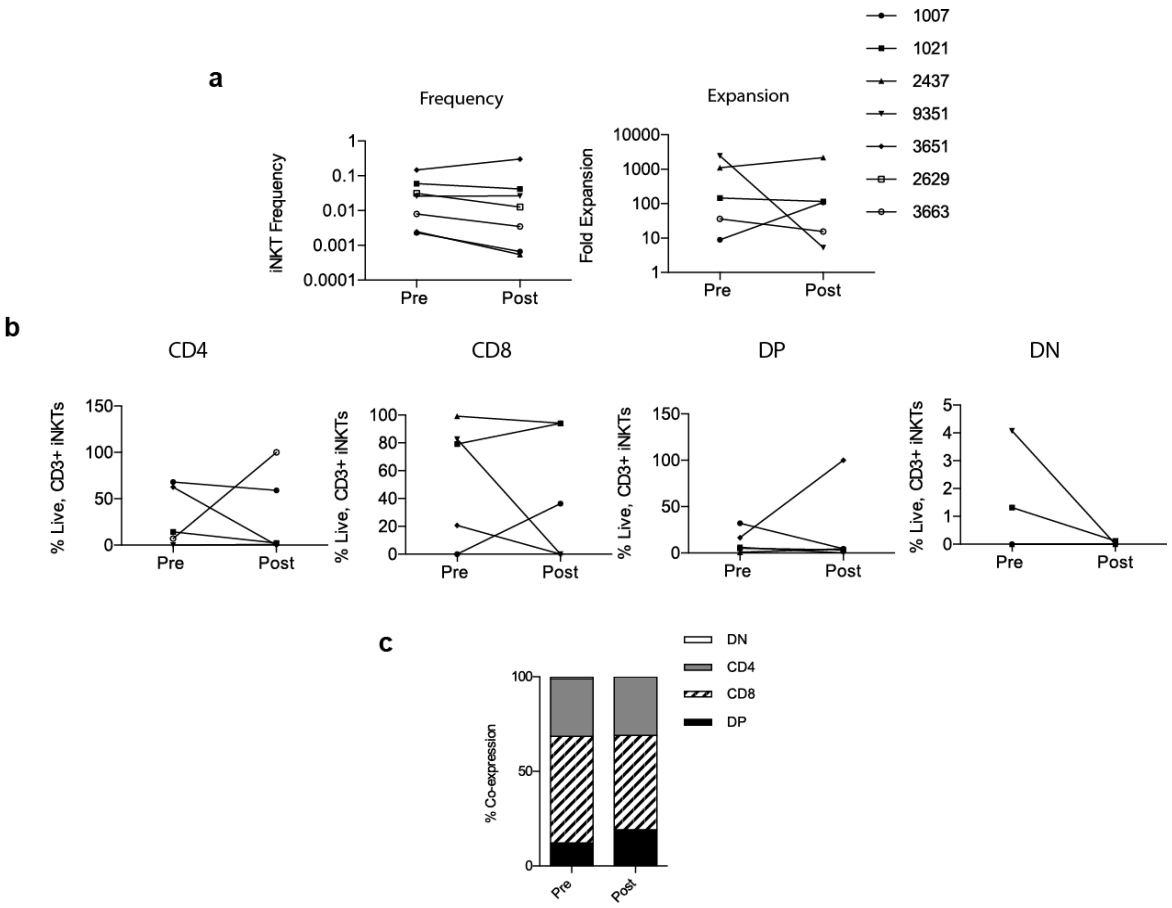

Figure 3.12: Vaccination has little effect on iNKTs in Chinese cynomolgus macaques

iNKT frequency and subset proliferative response were measured two weeks pre vaccination and followed up two weeks post vaccination in 6 Chinese cynomolgus macaques. a) Ex vivo frequency and total iNKT proliferation to antigen pre and post vaccination in 7 animals, data not acquired for some animals. b) Stratification of iNKT subsets post expansion with αGC antigen pre and post vaccination. c) Comparison of expanded iNKT subset proportions using chi squared test with post hoc analysis pre- and post- BCG reveals little change in response pre and post vaccination.

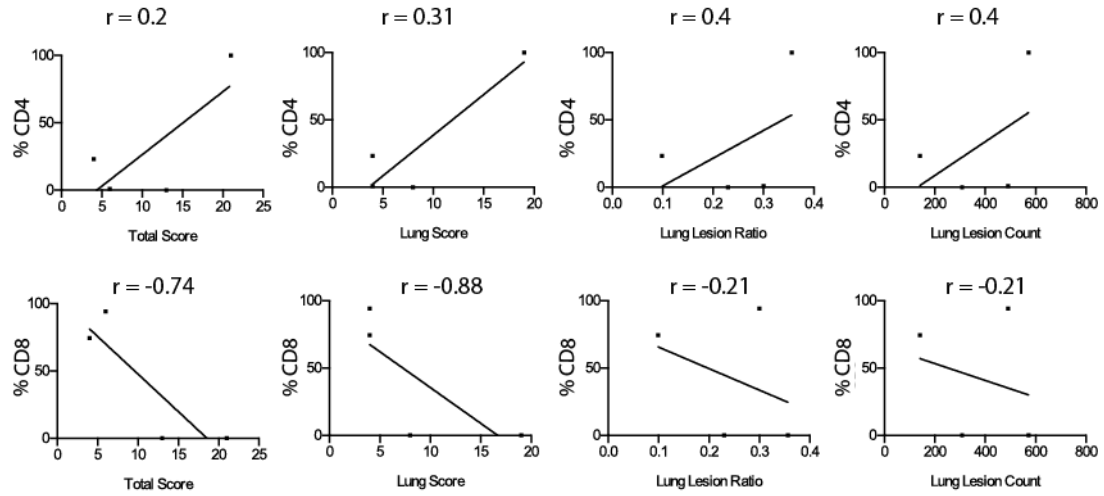

Figure 3.13: $CD8^+$ iNKT profile associates with lower pathology scores after BCG vaccination in Chinese macaques

αGC-mediated iNKT expansion was measured two weeks pre- and two weeks post- BCG vaccination in four Chinese cynomolgus macaques. Correlative analysis of the proportions of antigen responsive $CD4^+/CD8^-$ iNKTs (upper row) or $CD4^-/CD8^+$ iNKTs (lower row) with disease burden measured post challenge with virulent Mtb. A predominant $CD4^-/CD8^+$ iNKT profile correlates with better disease outcome.

3.6 Increased numbers of antigen responsive CD8+ iNKTs in rhesus macaque Mtb controllers

In the Chinese cynomolgus, a greater proportion of expanded $CD8^+$ iNKTs correlated with reduced disease burden, so we rationalised that the next step would be to study iNKTs in macaques with increased susceptibility to Mtb. We chose rhesus macaques as we hypothesised that an iNKT response would be more exaggerated due to their inherent Mtb susceptibility. We could also stratify according to animals that controlled or progressed in this cohort based on their clinical progression during the first 12 weeks after high dose aerosol challenge with Mtb (244, 245). Blood samples were taken two weeks before Mtb challenge of mycobacteria naïve macaques. Comparison of *ex vivo* iNKT frequency (*p=0.23*) and *in vitro* antigen induced expansion (*p=0.36*) revealed little differences between controllers and progressors (Figure 3.14a). However, by subset analysis of antigen responsive iNKTs, we demonstrated a trend toward a greater proportion of $CD8^+$ iNKTs (ratio=0.04) in animals able to control Mtb infection compared to those that developed severe disease (ratio=0.39, *p=0.21* [Figure 3.14b]). Consistent with this, there were higher $CD4^+$ antigen responsive iNKTs in animals that developed severe disease compared to controllers (*p=0.15* [Figure 3.14b]). Analysis of the mean subset proportions revealed statistically significant differences between controllers and progressors (Pearson's Chi-squared *p=0.0002* [Figure 3.14c]). These results corroborate the observations from the BCG study in Chinese cynomolgus and suggest that increased numbers of $CD8^+$ iNKTs associate with protection.

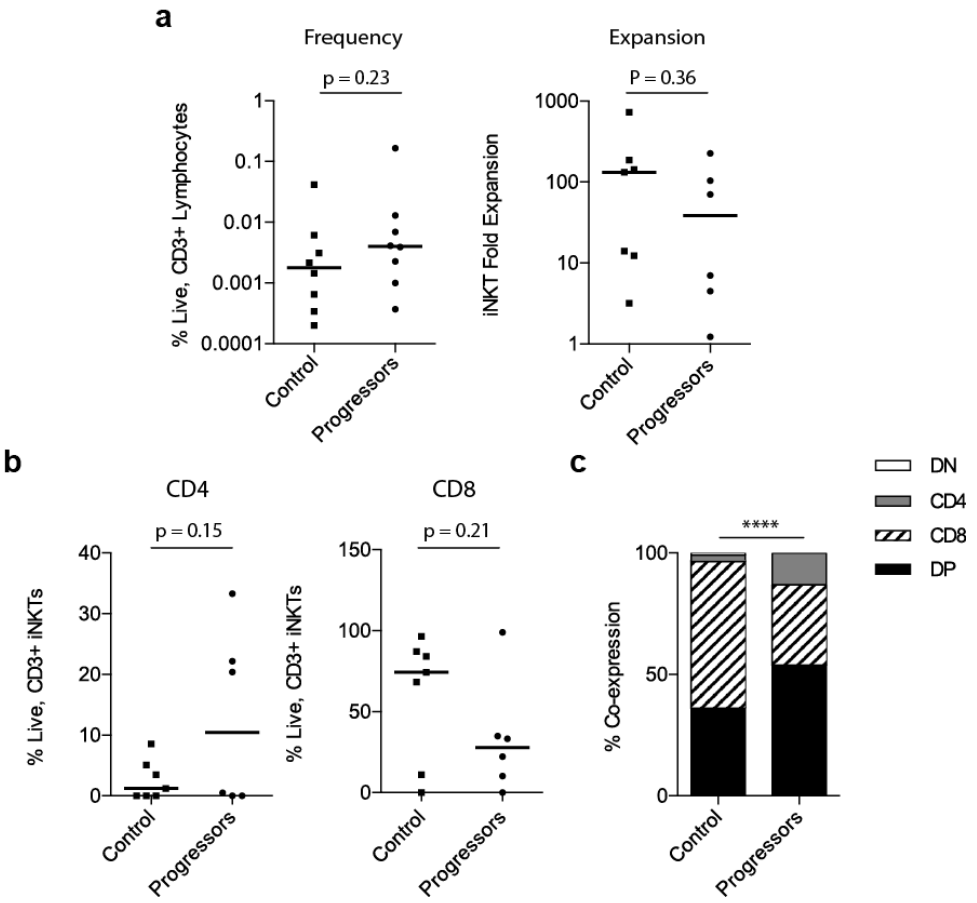

Figure 3.14: CD8$^+$ iNKT numbers are increased after antigen expansion in rhesus macaques that control infection

iNKT profile was analysed in 16 rhesus macaques that had not been vaccinated and were classified into controllers and progressors post challenge. a) Comparison of peripheral blood iNKT numbers (left) and αGC mediated fold expansion of iNKTs (right) in controllers and progressors. No differences were detected. b) CD4$^+$/CD8$^-$ (left) and CD4$^-$/CD8$^+$ (right) iNKT profiles after *in vitro* antigen expansion in controllers and progressors. Controllers tended to have lower CD4$^+$/CD8$^-$ and higher CD4$^-$/CD8$^+$ iNKT. c) Comparison of the proportions of iNKT subsets using chi-squared test with post-hoc analysis after αGC expansion demonstrated a CD8$^+$ predominant iNKT profile in controllers relative to progressors.

3.7 $CD8^+$ iNKTs associate with reduced pathology in BCG-vaccinated rhesus macaques

Next, we hypothesised that BCG vaccination in rhesus macaques may realign the iNKT profile to a ratio that correlates with protection. PBMC samples taken before and after BCG vaccination (245) were analysed and demonstrated an increase in the ratio of $CD8^+$ iNKT from pre vaccination (ratio=0.64) to post vaccination (ratio=0.07). This represented a significant change in the proportion of iNKT subsets after BCG vaccination (CD4 *p=0.028*, CD8 *p=0.067* [Figure 3.15a]). $CD8^+$ iNKTs are the dominant antigen responsive subset after BCG vaccination, when analysed by subset ratio (Pearson's Chi-squared $p=1.44x10^{-6}$ [Figure 3.15b]). Correlations of antigen responsive iNKT subsets with disease burden measures after Mtb challenge revealed similar trends, with a positive correlation between increased total iNKT proliferative response and $CD8^+$ iNKT subset proportions with better disease outcome. Increased $CD8^+$ iNKT percentages inversely correlated with decreased: total pathology (r=-0.2, *p=0.67*), lung lesion number (r=-0.82, *p=0.13*) and weight loss (r=-0.55, *p=0.4*). In contrast, increased $CD4^+$ iNKT percentages consistently correlated with increased: total pathology (r=0.34, *p=0.53*), lung lesion number (r = 0.3, *p=0.68*) and weight loss (r=0.05, *p>0.99*) (Figure 3.15c). Therefore, our results reveal a dominant $CD8^+$ iNKT phenotype after BCG vaccination, which associates with better disease outcome.

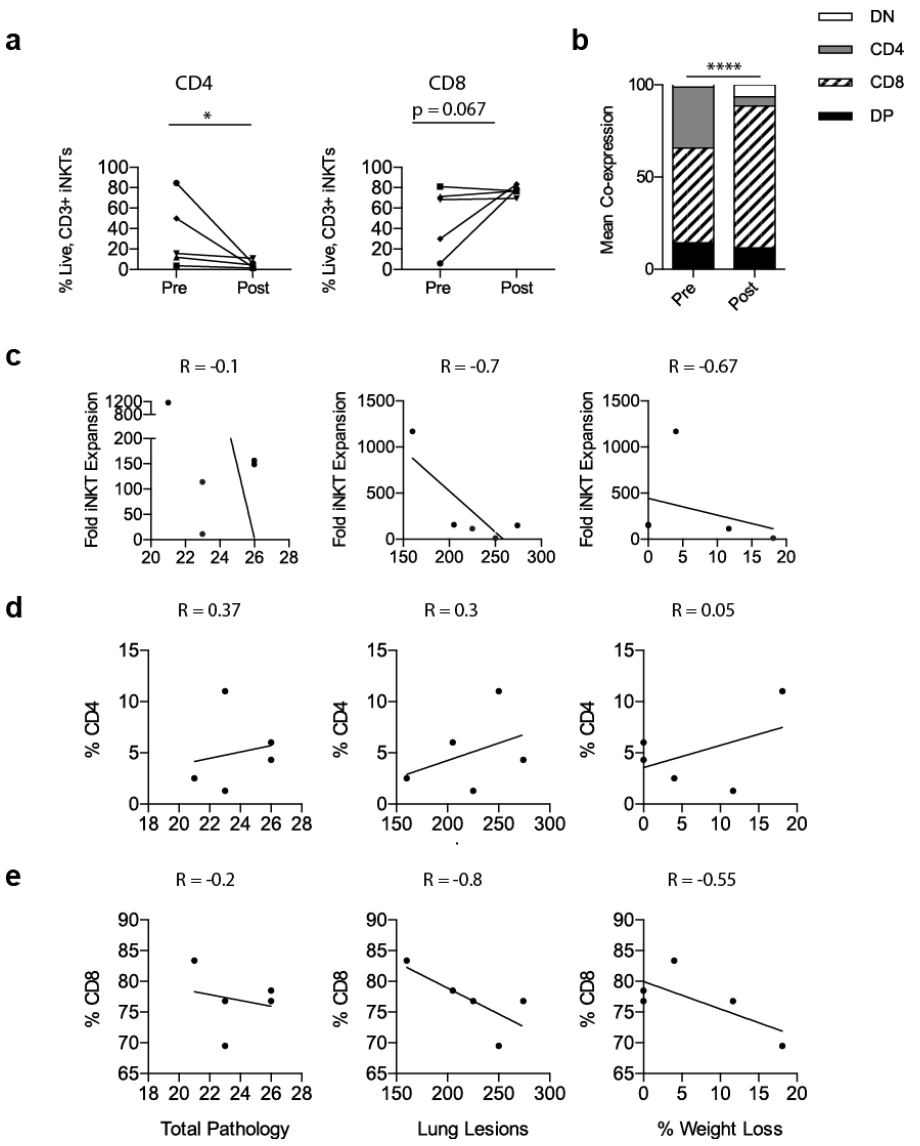

Figure 3.15: Increased $CD8^+$ iNKT proportions after BCG vaccination associates with decreased lung pathology in the TB susceptible rhesus macaques

Five healthy rhesus macaques were vaccinated with BCG and blood samples were taken two weeks pre- and post- vaccination. 21 weeks after BCG vaccination the animals were challenged with virulent Mtb and were stratified into progressors and controllers. a) αGC expanded $CD4^+/CD8^-$ and $CD4^-/CD8^+$ iNKTs are analysed in animals pre-and post- vaccination. $CD4^-/CD8^+$ iNKT subsets are increased after BCG vaccination. b) Summary of the proportions of $CD4+/CD8^-$ and $CD4^-/CD8^+$ iNKT subsets within αGC expanded iNKT pre- and post- BCG vaccination, showing an increase in $CD4^-/CD8^+$ cells post vaccination analysed using chi squared test with post hoc analysis. c) Correlative analysis of proliferative response (upper row) $CD4^+/CD8^-$ (middle row) and $CD4^-/CD8^+$ (lower row) iNKTs against disease burden. $CD8^+$ iNKT associate with reduced disease burden.

Chapter 4: Discussion

To study iNKTs in macaque, we first compared the ability of both the human and macaque CD1d-K7 tetramers to bind and identify iNKTs from macaque. Our data demonstrate that the most efficient tool to identify iNKTs in macaques is the human CD1d-αGC tetramer. We therefore applied these tetramers to investigate iNKT frequency in four genetically distinct groups of macaque that have different susceptibilities to Mtb infection. This study is the first systematic investigation of innate iNKT cells as a predictive marker of disease outcome in BCG vaccination and TB challenge studies in a well-characterised cohort of rhesus and Cynomolgus macaque species. Our results demonstrate that an increased peripheral blood iNKT frequency, and the ratio of $CD4^+/CD8^+$ iNKT subset proportion after *in vitro* antigen expansion, associates with TB resistance in mycobacteria naive animals. Furthermore, we observed increased proportions of antigen expanded $CD8^+$ iNKTs post BCG vaccination in rhesus macaques that controlled infection. Taken together, our study suggests that a dominant $CD8^+$ iNKT response associates with better disease outcome in macaque TB infection.

4.1 Low affinity iNKT/CD1d Interaction in macaques

Our first goal after generating a new macaque CD1d-αGC tetramer, was to compare its binding to human and macaque iNKTs, including clonal populations and PBMCs. We demonstrate that macaque CD1d-αGC tetramers stained iNKT cells with much lower MFI, suggesting reduced binding affinity relative to human CD1d-αGC tetramers. This trend opposes expectations in macaque iNKTs as logic would dictate macaque CD1d-αGC tetramers bind macaque iNKTs with similar or even higher binding affinity than human CD1d-αGC tetramers. Our data may suggest that lower affinity binding of macaque CD1d-αGC tetramers to iNKT cells may be an inherent feature of the macaque iNKT/CD1d interaction. Macaque and human iNKT-TCRs share 89% sequence identity, therefore some amino acid changes may affect the CDR3 loops responsible for mediating the fine interaction with CD1d, causing the observed affinity differences in

tetramer binding (221). Moreover, the CDR3β loop of the human iNKT-TCR contributes only 6% of the TCR/CD1d interaction but is responsible for defining iNKT clonal affinity to CD1d (220). Alternatively, the observed lower affinity binding of macaque CD1d to macaque and human iNKT cells may be due to the CD1d hotspot within the α1 helix to which the CDR3β loop interacts. We have previously established this hotspot as the region on human CD1d that mediates the interaction with the human CDR3β loop. In macaque CD1d, the short seven amino acid hotspot to which the CDR3β loop binds contains two substitutions highlighted in red in (Figure 3.12). Our analysis indicates that this small amino acid sequence is less hydrophobic on macaque CD1d relative to human CD1d. Further analysis of clonal iNKT TCRs and their interaction with macaque CD1d are required to dissect this phenomenon. Generating surface plasmon resonance (SPR) data with human and macaque iNKT TCRs would uncover any affinity differences.

```
Macaque     MGCLLFLLLWALLQAWGSAEVPQRLFPLRCLQISSFANSSWTRTDGLAWLGELQTHSWSN
            MGCLLFLLLWALLQAWGSAEVPQRLFPLRCLQISSFANS*WTRTDGLAWLGELQTHSWSN
Human       MGCLLFLLLWALLQAWGSAEVPQRLFPLRCLQISSFANSNWTRTDGLAWLGELQTHSWSN

Macaque     DSDTVRSLKPWSQGTFSDQQWETLQHIFRVYRSSFTRDVKEFAKMLRLSYPLELQVSAGC
            DSDT*RSLKPWSQGTFSDQQWE*LQ**FRVYRSSFTRDVKEFAKMLRL*Y**ELQVSAGC
Human       DSDTIRSLKPWSQGTFSDQQWEALQRVFRVYRSSFTRDVKEFAKMLRLAYSMELQVSAGC

Macaque     EVHPGNASNNFFHVAFQGKDILSFQGTSWEPTQEAPLWVNLAIQVLNQDKWTRETVQWLL
            EVHPGNAS*NFFHVAFQG*DILSFQGTSWEP*QEAPLWVNLAIQVLNQD*WT*ETVQWLL
Human       EVHPGNASHNFFHVAFQGSDILSFQGTSWEPAQEAPLWVNLAIQVLNQDNWTKETVQWLL

Macaque     NGTCPQFVSGLLESGKSELKKQVKPKAWLSRGPSPGPGRLLLVCHVSGFYPKPVWVKWMR
            N*TCPQFVSGLLESGKSEL*KQVKPKAWLSRGPSPGPGRL*LVCHVSGFYPKPVWVKWMR
Human       NDTCPQFVSGLLESGKSELEKQVKPKAWLSRGPSPGPGRLQLVCHVSGFYPKPVWVKWMR

Macaque     GEQEQQGTQPGDILPNADETWYLRATLDVVAGEAAGLSCRVKHSSLEGQDIVLYWGGSYT
            GEQEQQGTQ*GDILPNADETWYLRATL*V*AGEAAGLSCRVKHSSLEGQDIVLYWGGS*T
Human       GEQEQQGTQRGDILPNADETWYLRATLEVAAGEAAGLSCRVKHSSLEGQDIVLYWGGSHT

Macaque     SMGLIALAVLACLLFL--LIVGFTSRFKRQTSYQGVL
            S*GLIALAVLACLLFL**LIVGFT*RFKRQTSYQG*L
Human       SVGLIALAVLACLLFLLALIVGFTFRFKRQTSYQGIL
```

Figure 4.1: Comparison of macaque and human CD1d sequences

Alignment of human and macaque sequence reveals 24 amino acid changes indicated by asterisk. Red section highlights CD1d membrane distal section of α2 helix responsible for iNKT TCR CDR3 loop binding that contains two amino acid substitutions in macaque. Complete human and macaque sequences have 89% sequence similarity.

4.2 iNKT proliferation in healthy macaque

Lymphoproliferative capacity is commonly used as a functional readout of iNKTs (171, 182, 246). We therefore optimised macaque iNKT expansion using different APCs that are known to express CD1d, the most common of which are monocytes and moDC. Due to their distinct phenotypic differences, we were able to verify moDC differentiation using our *in vitro* culture conditions. We confirmed that CD14, a marker of monocytes, is decreased during differentiation into moDC in human. In macaques however, we showed that CD14 is retained, if not increased. Indeed, this phenotypic difference is also true of different species of macaque (241, 247). We were unable to identify a commercially available cross-reactive anti-CD1d antibody to analyse its expression, however CD1d expression on macaque monocytes has been reported (248). Key markers highly expressed on the surface of moDC in both human and macaque includes CD86, HLA-DR and CD1b. For the latter, we tested three antibody clones to determine which were cross-reactive between species. In addition, the literature states that CD1c and CD11c used in combination could identify all NHP moDCs, markers that had upregulated expression in our moDCs (240, 241). Therefore, our results indicate, along with visual assessment of differentiated monocytes, that we were successfully able to differentiate monocytes into moDCs in macaque.

However, despite moDC generation, we determined that optimal conditions for iNKT expansion were in fact through direct addition of αGC to PBMCs. Moreover, despite optimising the culture conditions for macaque iNKT stimulation and expansion, we found a reduced proliferation in response to αGC compared to human iNKTs, when expansion was performed in the same manner (data not shown) (246). We cannot rule out however that this is donor specific. Previous studies have reported the observation that spleen derived macaque iNKTs are semi-anergic under regular culture conditions (179). CD69, an early T cell activation marker constitutively expressed on the surface of iNKTs in humans and mice (249, 250), was not expressed by spleen derived macaque iNKTs constitutively. They were also unable to proliferate, increase CD25 expression or secrete IL-2 in response to frequent antigen stimulation post PMA/Ionomycin administration (179). Reduced proliferative capacity of macaque iNKTs may be because

these cells exhibit the same semi-anergic state as the spleen derived macaque iNKTs, and so the level of expansion that we achieved was high compared to many reports.

4.3 iNKT based correlates of Mtb Protection in macaque

It has been hypothesised that robust Th1 responses from $CD4^+$ T cells, including polyfunctional $CD4^+$ T cell responses secreting IFN-γ, TNF-α, and IL-2, are associated with protection in Mtb infection. However, a vaccine that produces these immunological traits has not yet been proven efficacious (23, 251, 252). In addition, there is uncertainty about the precise relationship between IFN-γ and TNF-α expression and protection. Indeed, a lack of immune correlates that reliably measure vaccine efficacy have been a major impediment in the development of an effective TB vaccine in humans (253). It is only now becoming clear that, whilst required for better disease outcome, excessive activation of conventional $CD4^+$ T cells seems detrimental in vaccinated infants (254), and may even be a correlate of disease risk (255). Therefore, as an alternative line of investigation, we investigated unconventional iNKT cell subsets in a well characterised animal model that accurately recapitulate human disease (256). This was the first study to associate altered iNKT subset proportion with Mtb immunity, and also provides proof of concept using NHPs to identify new correlates.

iNKTs in the mouse model of TB have been shown capable of providing a protective immune response (170, 171) and are thought to have a role in human Mtb infection (169, 257). Protection stems from the release of soluble effector molecules such as IFN-γ (258), GM-CSF (174) and granulysin (176), as well as through their cytotoxic capacity (172). In addition, iNKTs exist in a poised effector state, able to quickly home to infection sites to orchestrate an immune response (74). Our data associates the most resistant macaque group with significantly higher *ex vivo* peripheral blood iNKTs. Whilst it is a possibility this association may be linked to increased gene flow within the more resistant animal groups (259), reduced peripheral blood iNKT cell numbers correlate with a plethora of human pathologies (229, 232, 260, 261); including active TB where reduced peripheral blood iNKT numbers were suggested as a marker of disease in

patients (262). These diverse observations support a protective role for iNKT in human TB.

Studies from mice and humans have described $CD4^+$ and $CD8^+$ iNKT phenotype as precursor readouts for identifying functionally distinct subsets of iNKTs (250, 263). However, functional characterisation of macaque iNKTs is less well defined, likely due to the semi-anergic nature of cultured macaque iNKTs (179). Indeed, one study in Mauritian cynomolgus found that $CD4^+$ and $CD8^+$ iNKTs produced comparable levels of the Th1 cytokines IFN-γ and TNF-α, but only $CD4^+$ iNKTs produced IL-13 (181). Therefore, $CD4^+$ iNKT cells exhibit a Th0 profile while $CD8^+$ iNKTs exhibit Th1 profiles in similar fashion to human iNKT subsets. The skewing of iNKT $CD4^+/CD8^+$ subsets is a predictive measure of iNKT repertoire defects and a marker of disease in rheumatoid arthritis and HIV infection (232, 264). In addition, iNKT subset skewing associates with differential regulation of dendritic cell and T helper cell responses (169, 232, 264, 265). We observe that greater ratios of $CD8^+$ iNKTs after αGC specific expansion associates with better disease outcome, verified in two animal groups. However, defining the precise mechanisms for these observations needs further study, as we cannot rule out the possibility of $CD4^+$ iNKT homing post vaccination, making them undetectable in the periphery, or alternatively correlating with a different T cell subset which is providing the protective benefit.

The small group sizes used in our studies are an inherent limitation when working with NHPs and may have limited the ability to demonstrate statistical differences for some of our data. Nevertheless, the trends we observed with regard to $CD8^+$ iNKT subsets as associates of protection are worthy of further investigation, as they were consistently observed in both rhesus and cynomolgus species. Further investigation is required for innate cells other than conventional $CD4^+$ T cells that may provide more reliable correlates of protection, and the NHP model is ideal for this as mice do not express group 1 CD1 molecules. Our findings should guide future studies designed to investigate the role of the iNKT repertoire as a potential correlate of protection in macaque TB infection.

In summary, our study suggests that antigen specific expansion of $CD8^+$ iNKT subsets in the peripheral blood of NHP associates with protection of TB infection in NHPs. Detailed functional examination of iNKT subsets in NHP and patients is required, to investigate the underlying mechanism leading to this correlation. iNKTs are putative correlates of protection and deserve validation in future vaccination and challenge studies to determine the relationship with TB vaccine efficacy in NHP and in human preclinical studies.

Chapter 5: Investigating Mtb mycolic acid presentation by CD1b

Mycolic acids are highly abundant in the cell wall of Mtb, which expresses more than 80 species that differ with regard to their lipid backbone structures (189). Structurally, mycolic acids are β-hydroxy fatty acids containing two chains; the first is a long meromycolate chain (up to 60 carbons) that can accommodate up to two functional groups, the second is a shorter, non-functionalised acyl chain (up to 26 carbons) (198). These backbones are either free MAs with a carboxylic acid head group, or can be esterified to glycerol, glucose or trehalose molecules. The hydrocarbon chains sit within the CD1b molecule and the head group is solvent exposed at the CD1b/TCR interface and is therefore recognised directly by the TCR (61). Previous work, based on two different GMMs, are limited to investigating T cell responses toward long and short meromycolate chains (72). These studies have focused on lipid head group alterations, largely ignoring the role of the lipid backbone which is buried within the CD1b binding groove. Furthermore, those MAs were not representative of the naturally occurring MA lipid population expressed by Mtb (198). Hence, structure-function studies on a comprehensive panel of natural Mtb MAs that differ with regard to their meromycolate functional group type and stereochemistry are required for a holistic understanding of mycolate presentation via CD1b.

We hypothesised that differences in MA backbone structure might have a direct impact on the ensuing MA specific functional T cell response. To investigate this, we obtained a panel of synthetic MAs representing the predominant MA lipid species expressed in the lipid rich cell wall of Mycobacterial species, predominantly *Mycobacterium tuberculosis* (198) These were provided by our collaborator, Mark Baird. However, before investigating the TCRs we first asked whether CD1b was expressed at the site of infection to potentially drive a CD1b restricted T cell response. We therefore stained granulomas from human lung sections of Mtb infected donors.

5.1 CD1b expression in human granulomas

Dendritic cells are the professional APC most widely understood to express high levels of CD1b (266). However, there is little evidence of CD1b expression on other cells types such as macrophages, which are the major cell type involved in the first encounter with Mtb (267). Studies have shown expression of CD1a, c and d under most circumstances on macrophages, but not CD1b (45). Furthermore, T cells responsive to CD1b are assumed important in the immune response to Mtb at local infection sites, despite the fact CD1b expression has never been unequivocally described within granulomas. We therefore used human lung sections taken from patients with tuberculosis to investigate CD1b expression within the granuloma. We also compared the staining of anti-CD11c - a marker of dendritic cells and anti-CD68 – a macrophage marker with CD1b, in an attempt to identify which cell type express this molecule.

Of the five lung sections containing more than one granuloma, we found clear evidence of CD1b expression in three. However, there was differing regional expression and levels of CD1b in each individual granuloma. There were two predominant CD1b expression patterns shown in figure 5.1 illustrated by two different granulomas. The first was expression of CD1b on cells positioned on the edge of the caseous necrosis and not within the caeseum itself (Figure 5.1a). Magnification at 4x clearly shows the granuloma most evident with CD68 staining. Increased magnification at 10x and 20x shows caseous necrosis in the top left hand corner and surrounding normal lung tissue. CD11c and CD68 staining of the same area revealed large portions of the caeseum positive for both markers indicating staining of the remnants of cells that have undergone necrosis. CD68, the most highly expressed marker, also shows evidence of whole cells present in the caesium.

The second observation we made was the presences of speckles of CD1b within the caesium itself (Figure 5.1b), suggesting accumulation of cell fragments after death. These two events occurred independently of one another and we did not observe CD1b expression in both the caesium and the periphery in any individual granuloma possibly indicating development stage of the granuloma. Figure 5.1b shows a large granuloma containing a necrotic centre at 4x magnification, with areas strongly positive for CD68

and evidence of CD11c expression. CD1b is seen at 20x and 40x magnification where the necrotic core is evident in the lower right hand corner surrounded by lung tissue in the upper left. These data confirm that major accumulation of macrophages occurs within the granuloma with some dendritic cells present. We cannot confirm the expression of CD1b on either cell type but can for the first time show CD1b expression within both the centre and edge of the granuloma. Cells expressing CD1b therefore have the capacity to present MAs to T cells within the granuloma, consistent with the hypothesis that T cells responding to CD1b-presented mycolic acids will form a component of the host immune response to Mtb.

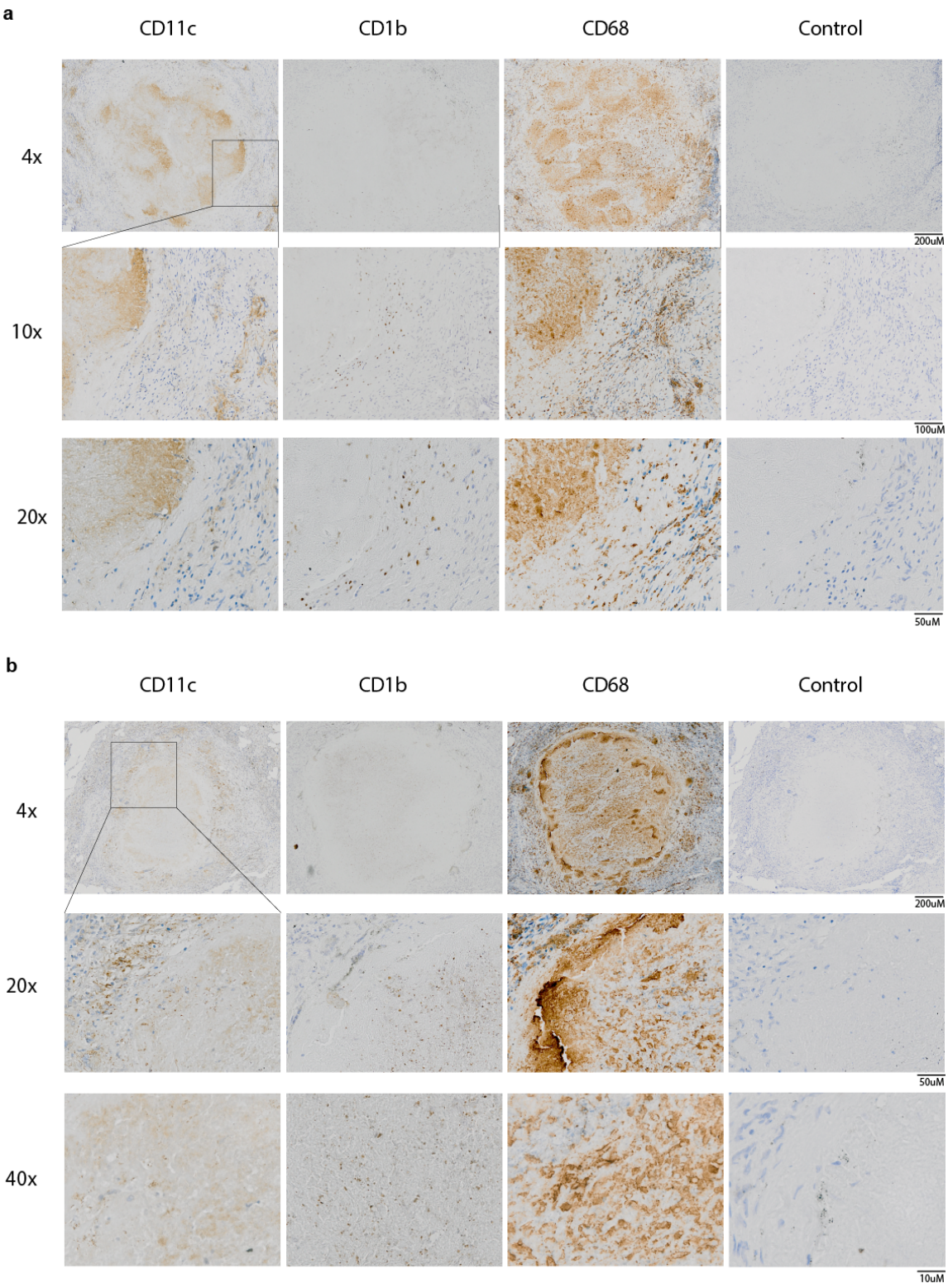

Figure 5.1: Immunohistochemistry staining of lung sections taken from Mtb infected patient.

a) Staining of granuloma with anti-CD11c, CD1b and CD68 antibodies with images at 4x magnification (top row), 10x magnification (middle row) and 20x magnification (bottom row). Images show CD11c and CD68 within the caseous necrosis and visible cells positive for CD1b

around the edge. b) Similar staining of granuloma strongly positive for CD68 with evidence of CD1b within the caseous necrosis. Images taken at 4x magnification (top row), 20x magnification (middle row) and 40x magnification (bottom row) respectively.

5.2 Generation of an *In vitro* T cell reporter line for the study of Mycolic acid structure-function

After visualising CD1b within the granuloma, suggesting a local CD1b restricted T cell response was likely, we next wanted to investigate the T cell responses of donor unrestricted T cells toward a panel of mycolic acids. We therefore developed an *in vitro* cellular reporter system to allow the quantification of TCR mediated T cell activation via CD1b/MA stimulation. This system consisted of T2 lymphoblast cell lines containing stable expression of macaque and human CD1b, and Jurkat T cell lines stably expressing GEM TCRs; including the MA specific TCR clone 18 (C18) and the GMM specific TCR clone 1 (C1) (134).

To achieve this, we attempted to clone macaque and human CD1b as well as MA specific TCRs, into a mammalian lentiviral expression system (268). First, using cDNA from newly generated macaque and human moDC, we used specific primers to amplify CD1b DNA sequences by PCR (Figure 5.2a). The CD1b DNA coding sequences were then cloned into our lentivirus vector (Figure 5.2b-c). Alignment of both human and macaque CD1b revealed 94.6% sequence similarity, the highest of all the CD1 isotypes. This results in 18 amino acid changes of which six are in the α1 domain, four in the α2 domain, six in the α3 domain and two in the transmembrane domain (207). To confirm DNA cloning efficiency, ligation products were digested to produce two DNA bands corresponding to CD1b and the digested lentiviral vector (Figure 5.2d); a first indication for effective cloning.

After additional confirmation of the correct CD1b sequences for both macaque and human by DNA sequencing, we used our cloned CD1b plasmids to produce lentivirus particles that were subsequently used to transduce T2 lymphoblasts with CD1b. After two weeks of cell expansion we analysed cell surface CD1b expression on transduced

T2s via FACS (Figure 5.3). Our results revealed 22% and 31% transduction of macaque and human CD1b respectively, compared to 0% CD1b expression in mock-transduced negative control T2s. To enrich newly generated CD1b expressing cells, we sorted those positive for CD1b by FACS into a $CD1b^{high}$ population. After sorting and further expansion, T2s were 99% positive for human- and 97% positive for macaque- CD1b. These cells were expanded further and used in all subsequent assays.

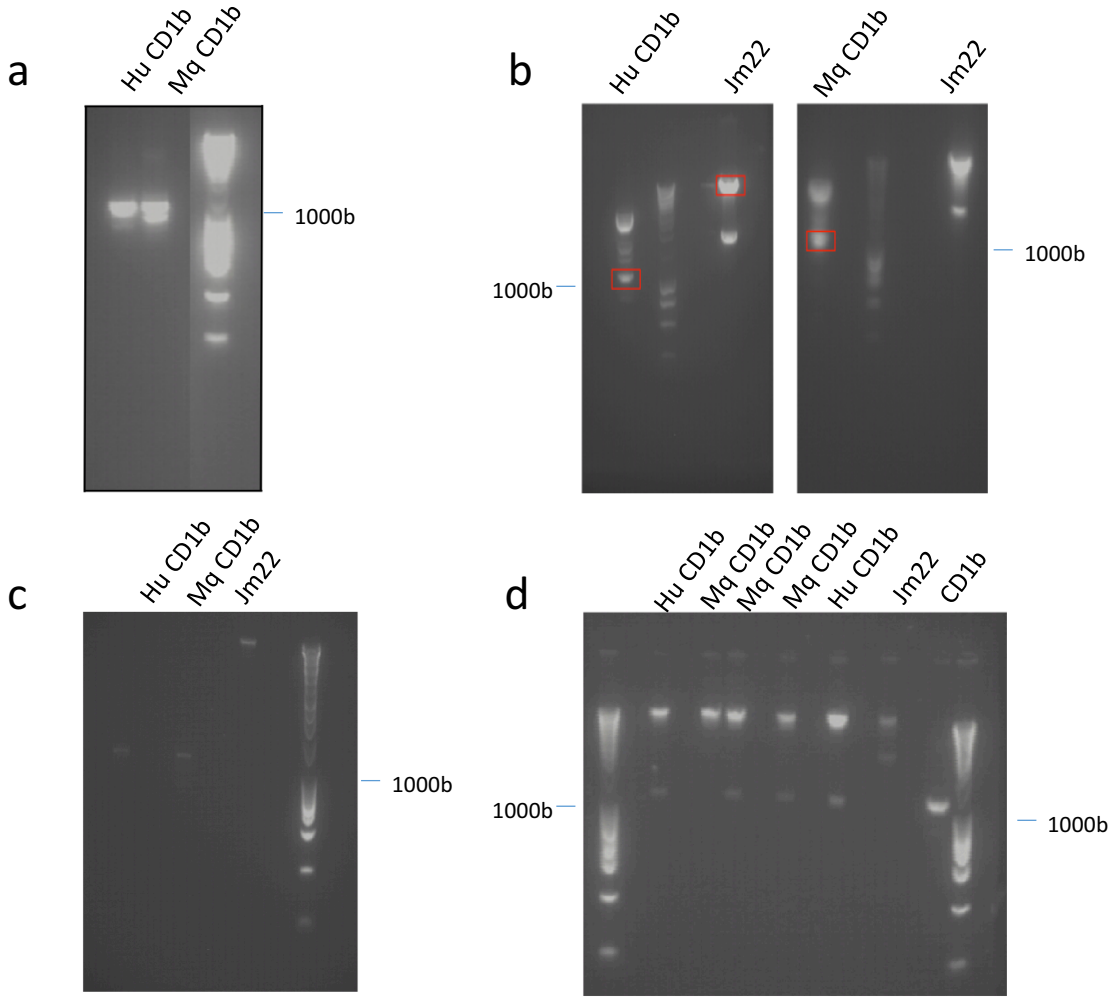

Figure 5.2: Cloning sequence of human and macaque CD1b into lentiviral vectors

DNA gel images showing the sequence of cloning events for CD1b. RNA was isolated from moDCs derived from both macaque and human monocytes using trizol extraction. (a) CD1b DNA PCR products for both macaque and human, each 1,008 bp in length. (b) CD1b DNA products were ligated into an easy cloning vector (pJet) and propagated using *E. coli.* CD1b insert was digested and the product harvested from the gel. In parallel the propagated lentiviral plasmid, which contained the alpha and beta sequences for the MHC restricted TCR JM22, was digested to remove its insert. (c) Purified CD1b and empty lentiviral vector before ligation showing pure products. (d) Digestion of plasmid after ligation of CD1b with the LV vector, confirming the presence of CD1b which was later confirmed by DNA sequencing

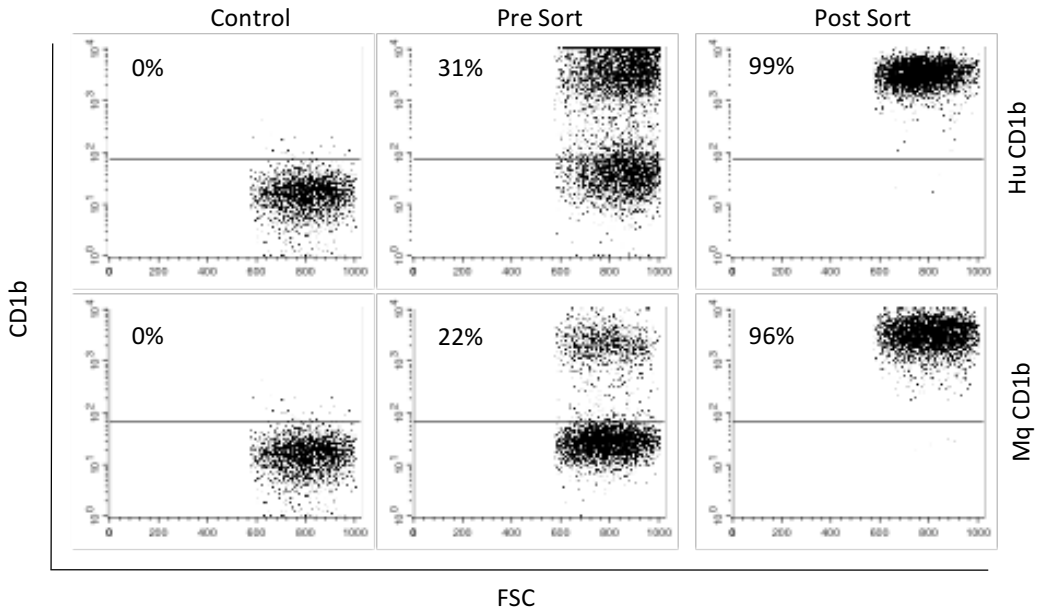

Figure 5.3: CD1b transduction of T2 cells

T2s gated on live cells, stained with anti-CD1b, showing percentage of T2s positive for CD1b expression. T2s negative for CD1b expression (far left), T2s after lentiviral transduction (middle), CD1b positive T2s sorted into 30 cells/well of 96-well plate and cultured for 2 weeks (far right). T2s were transduced with human (Upper panels) and macaque (lower Panels) CD1b.

The GEM T cell subset is defined by C18 which is MA specific, and clones C1, C21 and C42 which are GMM specific (134). For TCR cloning, we used published GEM C18 clone DNA sequences (Genbank accession numbers JQ778257.1 & JQ778258.1) (134) to design a 2A peptide linked alpha (Vα7.2) and beta (Vβ13.2) chains, which ensures equimolar expression of both chains. The DNA sequences were subsequently optimised by GeneArt for efficient mammalian cell expression. The optimised sequences were then synthesised and cloned into our lentiviral expression vector by GeneArt. GEM C1 T cells (Genbank accession numbers JQ778263.1 & JQ778264.1) (134) express a Vα7.2 chain with two amino acid substitutions (leu93α → arg and Asp94a→Val) compared to GEM C18. In contrast, GEM C1 expresses a different beta chain to GEM C18 namely; Vβ20 chain (Genbank accession JQ778264.1). Therefore, GEM C1 Vβ20 DNA sequences were synthesised and cloned into the GEM C18 cassette by GeneArt; replacing the C18 Vβ13.2

sequence. Site-directed mutagenesis was subsequently performed on the alpha chain to yield a complete GEM C1 sequence. Vectors containing GEM TCR sequences were confirmed by DNA sequencing and then employed to generate lentiviral particles to transduce Jurkat T cells (Figure 5.4).

In order to study T cell activation using two different complementary readouts, we not only transduced GEM TCRs into Jurkat sub-clone J.RT3-T3.5 (269), we also transduced the T cell line Jurkat-NFAT-GLuc, containing a plasmid that upon TCR mediated activation secretes the enzyme gaussia luciferase (Figure 5.7). Subsequent addition of luciferase to the supernatant yields luminescence that can be measured directly as a specific marker of T cell activation.

After using our newly constructed plasmid to generate lentivirus for Jurkat transduction, we verified C18 TCR expression via staining with anti-Vα7.2 (Figure 5.4). In comparison to mock transduced Jurkats, C18 transduced Jurkats were 45.85% (J.RT3-T3.5) and 92.37% (NFAT-Gluc) positive for TCR expression, which was increased to 79.78% (J.RT3-T3.5) and 100% (NFAT-GLuc) after FACS sorting and enrichment of TCR positive cells (Figure 5.4a). FACS sorting of C1 Jurkats was not necessary post transduction as the initial efficiency was high at 80% (J.RT3-T3.5) and 92% (NFAT-Gluc) shown in figure 5.4 (lower row).

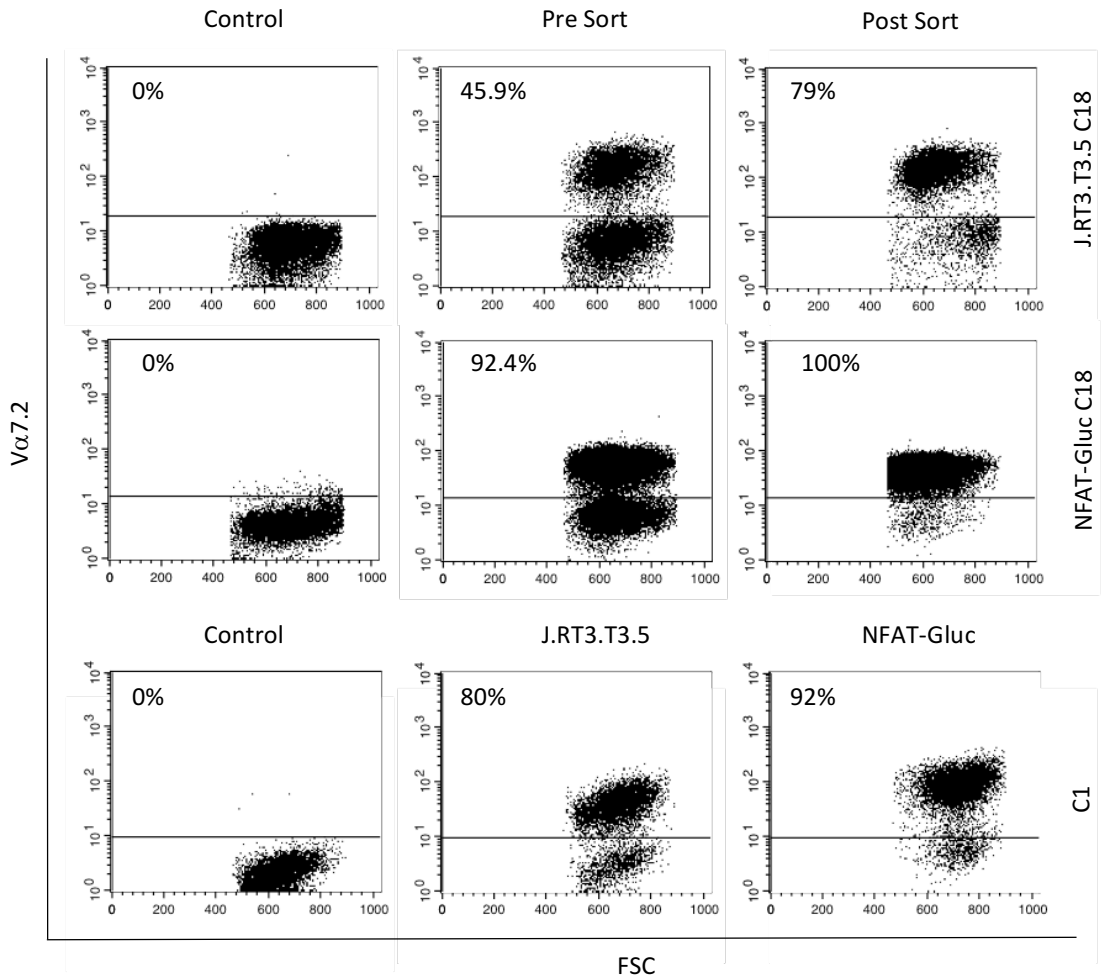

Figure 5.4: GEM TCR transduction of Jurkat T cell lines

Jurkats gated on live CD3 positive cells showing staining of anti-Vα7.2 of the clone 18 and clone 1 GEM TCRs. Upper two panels show expression of C18 transduction of J.RT3.5 Jurkat cells (upper row) and NFAT-GLuc Jurkat cells (middle Panel). Dot plots show Vα7.2 staining of C18 TCR in untransduced cells (left), initial transduction efficiency pre-sort (middle column) and TCR expression post-sort (right column). Bottom row shows expression of C1 TCR on untransduced (left) J.RT3.5 Jurkat cells (middle) and NFAT-GLuc Jurkat cells (right). Initial transduction efficiencies were high for C1 therefore no enrichment via FACS was performed.

To functionally validate our newly generated GEM Jurkats, we stimulated them with a pool of mixed MA pulsed CD1b-T2 APC. Using the cell surface activation marker CD69 as a readout, we demonstrated that our Jurkats were activated by CD1b-T2 only when

loaded with MA compared to mock transduced T2s, T2s lacking CD1b and unpulsed CD1b, (Figure 5.5a-b) (134). Furthermore, we added a soluble C18 GEM TCR tetramer to our co-cultures to block Jurkat activation (Figure 5.5c). By increasing the concentration of tetramer to 30 μg/ml and 50 μg/ml, we were able to significantly inhibit Jurkat activation (p=0.042 and p=0.015 respectively) compared to 1 μg/ml addition of tetramer. We did not see any inhibition when using monomers to block the interaction. Taken together, our results functionally validate this system and suggest Jurkat activation was TCR mediated.

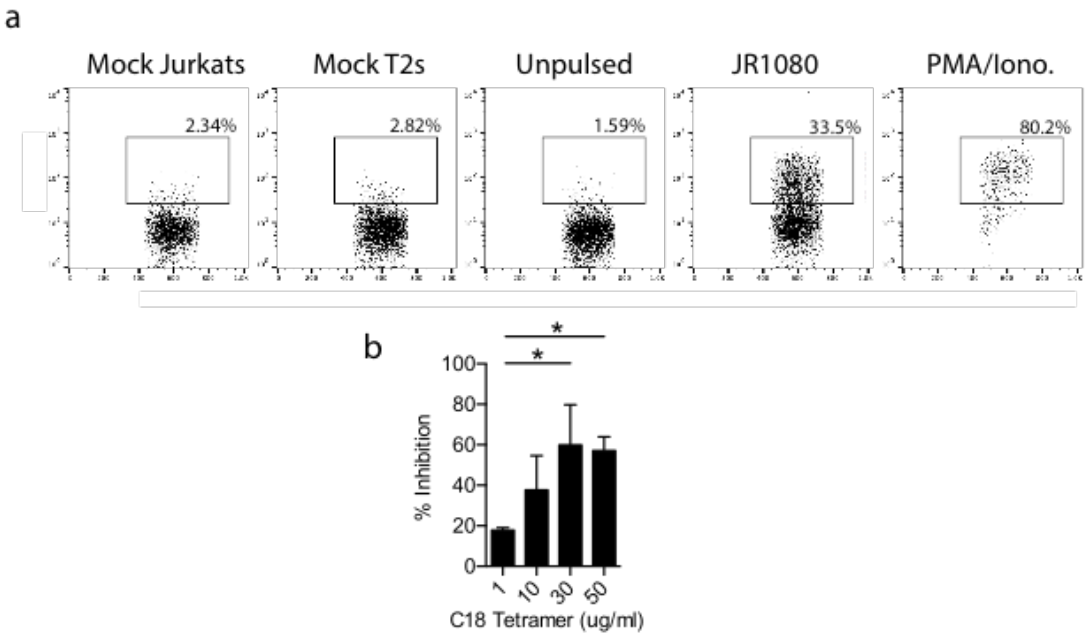

Figure 5.5: Functional validation of *in vitro* cellular system for MA studies

(a) CD69 expression on C18 GEM TCR transduced Jurkats. FACS dot plots gated on live, $CD3^+$ Jurkats. Staining for the early activation marker CD69 on: mock transduced Jurkats stimulated with CD1b transduced T2s pulsed with mixed MA (Sigma), C18 GEM transduced Jurkats stimulated with mock transduced T2s pulsed with MA, C18 transduced Jurkats stimulated with unpulsed CD1b transduced T2s, PMA/Ionomycin treated Jurkats (positive control) and C18 transduced Jurkats activated by mixed MA pulsed CD1b-T2s (Left to Right). Results demonstrate MA specific TCR mediated activation of Jurkat T cell lines. (b) Percentage inhibition of Jurkat response when T2s pulsed with 10 μg/ml and subsequently blocked with: 1, 10, 30 and 50 μg/ml of tetramerised C18 GEM TCR. Response significantly blocked when >30 μg/ml tetramer added for 20 minutes prior to Jurkat addition.

5.3 TCR Specificity

Using our newly validated cellular system, we first compared C18-, C1- and LDN5- TCR ligand specificity as well as their cross-reactivity with macaque CD1b. LDN5 is a well-documented GMM specific TCR, highly sensitive to the glucose head group (65). We employed four ligands with different head groups containing the same meromycolate backbone lipid tail structure to confirm the fine specificity of the TCRs. Ligands included: JR1080 (free MA), OTA-23 (Gro-MM), SMP74 (GMM) and MH176 (TMM) (Table 5.1).

Our data confirmed the specific activation of LDN5 Jurkats by human (Figure 5.6a) and macaque (Figure 5.6d) CD1b-T2 in the presence of GMM. LDN5 activation was absent with MA, Gro-MM and TMM loaded CD1b. GEM C18 was recently demonstrated to confer specificity to free MA (134). In contrast to published studies (134), our results indicate that clone 18 GEM TCR is not only reactive toward MA but also Gro-MM and even GMM presented by human CD1b (Figure 5.6b), albeit to a lesser extent which may suggest a partial blocking of TCR recognition by the glucose head group. These results confirm the key determinant for clone 18 T cell activation is not only the solvent exposed MA head group. In addition, we demonstrated that clone 18 could not be stimulated by macaque CD1b in the presence of ligand (Figure 5.6e). The GEM clone C1, like LDN5, is also specific for GMM (134).We confirm that with our system (Figure 5.6c) while also demonstrating it does not respond to GMM when presented by macaque CD1b (Figure 5.6f). None of the TCRs were activated by TMM, presumably because the double sugar head group ablates TCR recognition (127).

MA	Chemical Structure	Code	Class	Organism	Proximal	Distal
A	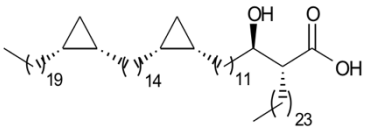	JR1080	alpha	Mtb	Cis, *RS*	*Cis,RS*
B	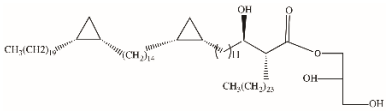	OTA 23	alpha	Mtb	Cis, *RS*	*Cis,RS*
C	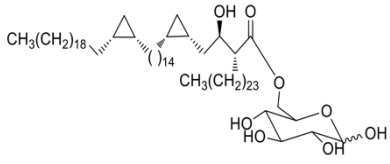	SMP74	alpha	Mtb	Cis, *RS*	Cis, *RS*
D	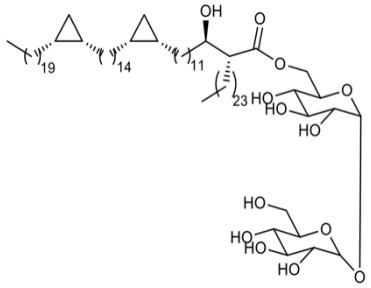	MH176	alpha	Mtb	Cis, *RS*	Cis, *RS*

Table 5.1: GMM and TMM of strong and weak stimulatory MAs

Schematic of free mycolate JR1080 (A) with corresponding Gro-MM (OTA-23) (B), GMM (SMP74) (C) and TMM (MH176) (D). The chemical name indicates MA class based on functional group within the meromycolate chain. The organism column specifies from which species the MA was derived. Proximal and distal columns indicate chirality of respective functional groups. Cis and trans indicate stereochemistry around the functional group, and R, S designates absolute stereochemistry.

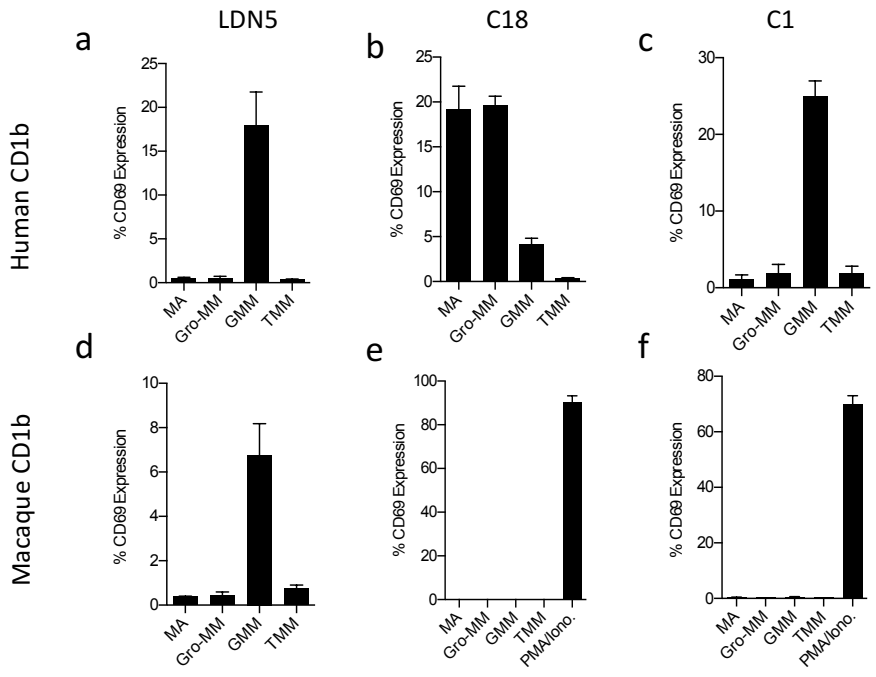

Figure 5.6: CD1b lipid specificity of C18 GEM TCR and LDN5

Specificity of each TCR was examined via CD69 upregulation of Jurkat T cells when added to CD1b expressing T2s pulsed with 10 μg/ml of 4 lipids with the same meromycolate backbone containing different head groups as outlined in table 3; a) LDN5 TCR specifically responds to GMM presented by human CD1b; b) C18 specifically responds to MA, Gro-MM and GMM presented by human CD1b; c) C1 specifically responds to GMM only presented by human CD1b d) LDN5 specifically responds to GMM presented by macaque CD1b; e) C18 has no cross-reactivity with macaque CD1b; f) C1 has no cross-reactivity with macaque CD1b.

5.4 Meromycolate functional groups dictate GEM T cell activation

We hypothesised that MA lipid backbone structure differences could have a direct impact on T cell activation. We therefore used our functionally validated and characterised Jurkat system to systematically investigate the impact of meromycolate lipid tail structure on T cell activation (Table 5.2). Our MA panel consisted of: (A) JR1080, an alpha-MA (45C), (B) MMS131, an alpha-MA (49C), (C) MMS130, an alpha-MA (50C) (D) HA56, a methoxy-MA (54C), (E) JR-RR121, a methoxy-MA (53C), (F) JR-RR124, a methoxy-MA (51C), (G) JR1046, a methoxy-MA (51C), (H) AD129, a keto-MA (48C) (I) MH140, a keto-MA (55C), (J) DZ146, an epoxy-MA (49C), (K) MH95, an alpha-alkene-MA (37C), and (L) MH157, an alpha-diene-MA (51C). MAs A and D-I are derived from cell wall of Mtb and have an acyl chain of 23 carbons while B and C are derived from *Mycobacterium kansasii* and J-L are from *Mycobacterium smegmatis* containing an acyl chain of 21 carbons in length.

MA	Chemical Structure	Code	Class	Organism	Proximal	Distal
A	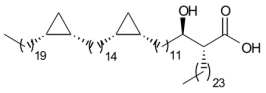	JR1080	Alpha	Mtb	Cis, *RS*	*Cis,RS*
B	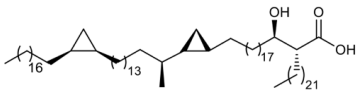	MMS131	Alpha	M. Kansasii	Trans cyclopropane *S-(methyl)*, *RS*	Cis, *SR*
c	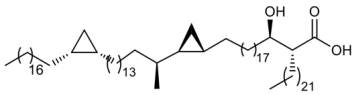	MMS130	Alpha	M. Kansasii	Trans-cyclopropane, *S-(methyl)*, *RS*	Cis, *RS*
D	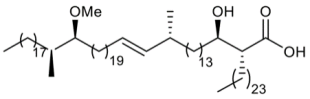	HA56	Methoxy	Mtb	Trans-alkene *R*-(methyl)	SS
E	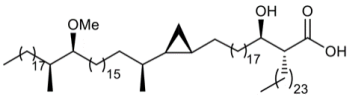	JR-RR121	Methoxy	Mtb	Trans cyclopropane, *S-(methyl)*, *RS*	SS
f	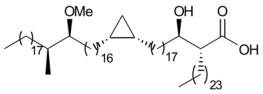	JR-RR124	Methoxy	Mtb	Cis, *RS*	SS
G	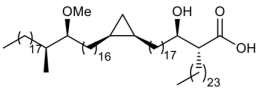	JR1046	Methoxy	Mtb	Cis, *SR*	*SS*
h	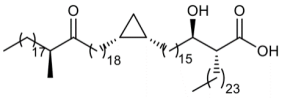	AD129	Keto	Mtb	Cis, *RS*	S
I	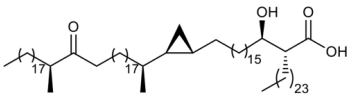	MH140	Keto	Mtb	Trans cyclopropane, *S-(methyl)*, *RS*	S
j	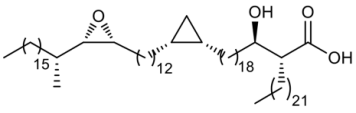	DZ146	Epoxy	M. smeg	Cis, *RS*	Epoxy, *R-(methyl)*, *SS*
K	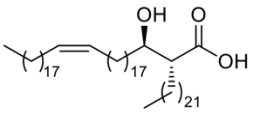	MH95	Alpha' alkene	M. smeg	Cis-alkene	n/a
L	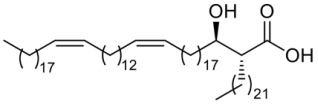	MH157	Alpha' diene	M. smeg	Cis-alkene	Cis-alkene

Table 5.2: Panel of MAs from Mtb, M. smegmatis and M. Kansasii

Schematic of MA meromycolate chains and their orgamism of origin and stereochemistry. (A) JR1080, (B) MMS131, (C) MMS130, (D) HA56, (E) JR-RR121, (F) JR-RR124, (G) JR1046, (H) AD129, (I) MH140, (J) DZ146, (K) MH95, (L) MH157.

We first stimulated our clone 18 Jurkat T cells with free MA loaded CD1b-T2s before measuring T cell activation utilising both CD69 upregulation and luminescence as readout (Figures 5.7a-b). Our initial results indicated that a selection of these MAs could specifically activate the GEM Jurkats (Figure 5.7). Furthermore, our data suggest a hierarchy of MA stimulatory potential ranging from strong to weak in the following order 1) MH157; alpha-diene-MA, 2) JR1080; alpha-MA, 3) HA56; methoxy-MA, 4) DZ146; epoxy-MA, 5) AD129; keto-MA 6) MMS131; alpha-MA, 7) JR-RR124; methoxy-MA, 8) MH95; alpha-alkene-MA, 9) MH140; keto-MA, 10) JR1046; keto-MA, 11) JR-RR121; methoxy-MA and 12) MMS130; alpha-MA. Given that the solvent exposed head group is the same in all these mycolates, our data suggested that lipid backbone modifications, which are buried within the antigen-binding groove of CD1b, can indirectly affect T cell activation.

Having observed C18 reactivity to Gro-MM (Figure 5.6b), we were interested to identify a similar hierarchy with a panel of lipids containing this head group, described in table 5.3. Repeating the stimulation of C18, we found an identical hierarchy, that could be replicated in both CD69 and luminescent Jurkat systems (Figures 5.7c-d). This further supports our hypothesis by demonstrating a hierarchy of T cell activation mediated by meromycolate chain differences. Finally, when we compare T cell activation of our Gro-MM panel (Table 5.3) with their corresponding MAs containing the same meromycolate chain, we see very similar responses (Figure 5.7e). These data suggest that clone 18 TCR does not discriminate between solvent exposed head groups of free MA and Gro-MM, but instead is sensitive to changes in lipid structure buried deep within the CD1b protein.

MA	Chemical Structure	Code	Class	Organism	Proximal	Distal
A	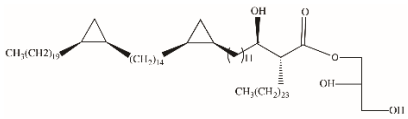	OTA 15	alpha	Mtb	Cis, *SR*	Cis, *SR*
B	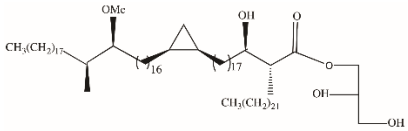	OTA 17	Methoxy	Mtb	Cis, *SR*	*SS*
C	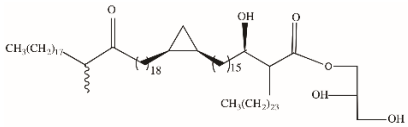	OTA 19	Keto	Mtb	Cis, *SR*	
D	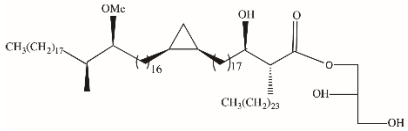	OTA 21	Methoxy	Mtb	Cis, *SR*	*SS*
E	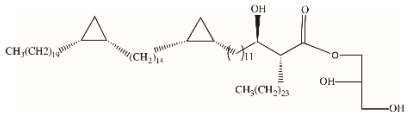	OTA 23	alpha	Mtb	Cis, *RS*	*Cis,RS*
F	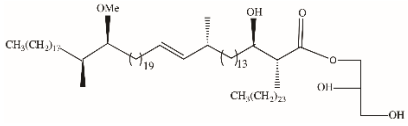	HA 72	Methoxy	Mtb	Trans-alkene *R*-(methyl)	SS

Table 5.3: Panel of synthesised Gro-MMs from Mtb

Schematic of Gro-MM meromycolate chains. A) OTA-15, B) OTA-17, C) OTA-19, D) OTA-21, E) OTA-23 and F) HA72.

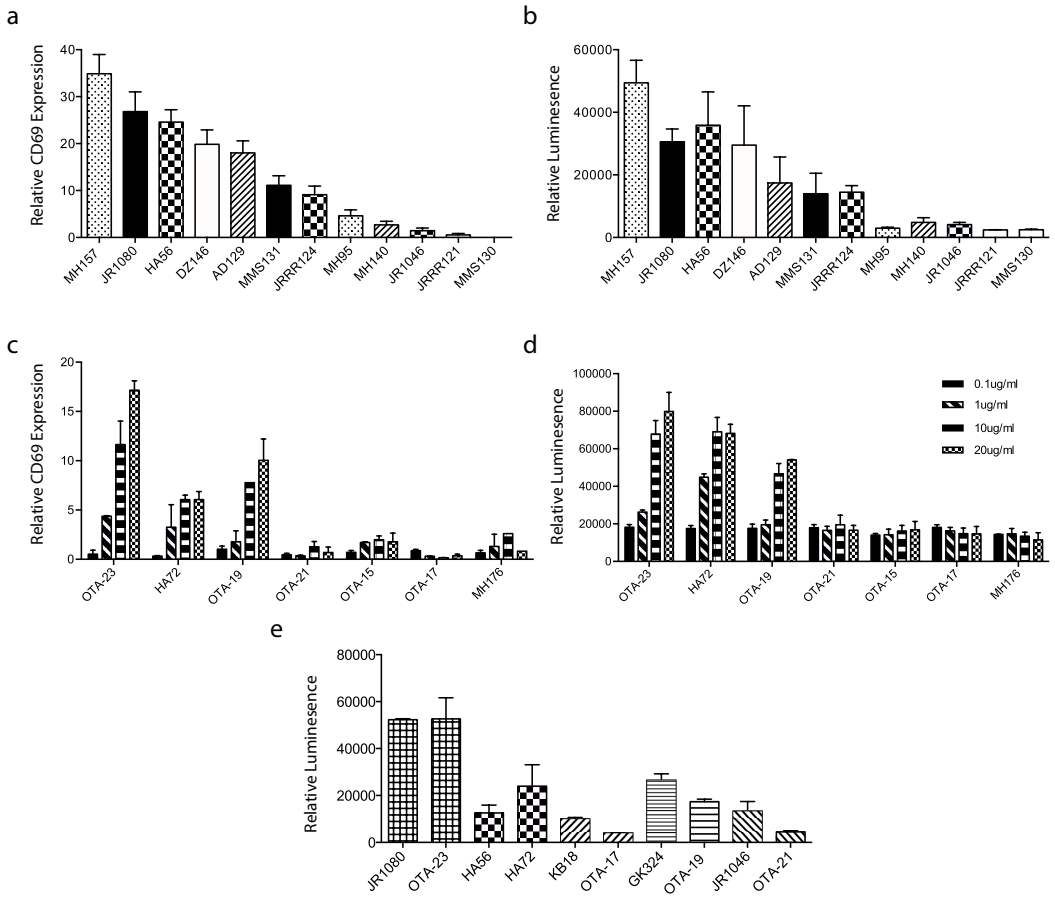

Figure 5.7: Comparison of C18 activation via MAs and Gro-MMs

Activation of C18 TCR transduced Jurkats post stimulation with CD1b T2s presenting Mtb MAs; a) MA panel pulsed at 10 μg/ml measured via CD69; b) MA panel pulsed at 10 μg/ml measured via Gluc secretion (Dots; alkene-MAs), (black; alpha-MAs), (checked;Methoxy-MAs), (empty; expoxy-MA), (diagonal; Keto-MAs) MAs ranged in their ability to stimulate a GEM TCR mediated response, from most potent with MH157 to no stimulation with MMS130. c) Gro-MM panel pulsed in a dose response measured via CD69; d) Gro-MM panel pulsed in a dose response measured via Gluc secretion. Only three of six Gro-MMs are recognised via C18 TCR. MH176 is a TMM. e) Comparison of C18 activation via MA and equivalent Gro-MM, mycolates with the same backbone have similar activation, despite differences in head group.

After demonstrating a T cell activation hierarchy mediated by meromycolate functional groups, we considered whether their relative stereochemistry would result in similar distinctions. We have three α-mycolates containing the same length of meromycolate and acyl chains and same proximal and distal cyclopropane groups at carbon positions 11 and 25 as JR1080, but different functional group stereochemistry (Table 5.4). In a dose response experiment, T cell activation mediated by these MAs again demonstrated a clear hierarchy based on stereo-arrangement of the cyclopropane groups. We found CDL12DU and JR1080 were both very similar in their stimulatory ability and were the most potently activating (Figure 5.8), even at very low concentrations. The hierarchy of stereoisomers were reproducible when measuring both CD69 and luminescence as markers of Jurkat activation.

MA	Chemical Structure	Code	Class	Organism	Proximal	Distal
A	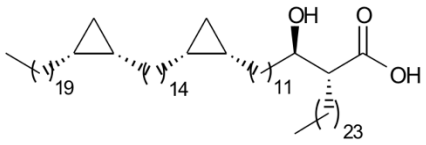	JR1080	alpha	Mtb	Cis, *RS*	*Cis,RS*
B	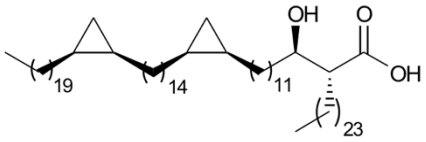	JR-MM267C	alpha	Mtb	Cis, *SR*	Cis, *SR*
C		CDL 12UD	alpha	Mtb	Cis, *SR*	Cis, *RS*
D	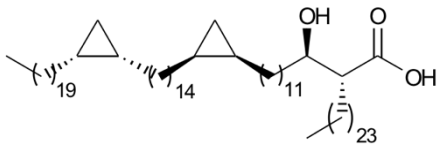	CDL 12DU	alpha	Mtb	Cis, *RS*	Cis, *SR*

Table 5.4: Stereoisomers of stimulatory alpha mycolate JR1080

Schematic of alpha mycolate stereochemistry. (A) JR1080, (B) JR-MM267C, (C) CDL12UD and (D) CDL12DU

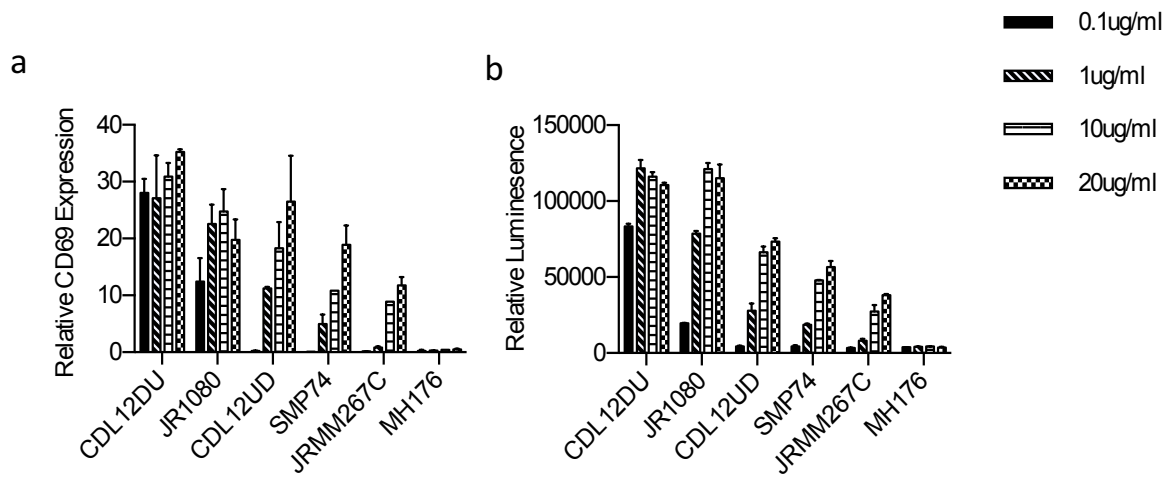

Figure 5.8: Dose response of stereoisomers of JR1080

CD1b-T2s were pulsed with increasing concentrations (0.1 μg/ml-20 μg/ml) of 4 stereoisomers of the stimulatory alpha mycolate JR1080 and presented to GEM transduced J.RT3.T3.5 Jurkats or NFAT GLuc Jurkats in a 1:1 ratio and subsequent CD69 expression and GLuc secretion was measured. (A) Relative CD69 expression measured by FACS analysis. (B) Relative GLuc secretion measured by luminescence. Stereochemistry of meromycolate functional group impacts C18 Jurkat T cell activation.

Finally, to investigate whether other mycolate specific TCRs are also sensitive to MA lipid backbone differences; we employed C1 and LDN5 TCRs, both specific for GMM (72, 134). We demonstrate an observable hierarchy for C1 against our panel of GMMs (Table 5.5). Our strongest GMM (SMP74) and weakest (SMP75) are significantly different (p=0.05 and p=0.029, Mann whitney-U) at 20 μg/ml when stimulating C1 using CD69 and luminescence as readouts respectively (Figure 5.9a). However, the strongest (SMP74) and weakest (SMP71) GMM are not significantly different at 20 μg/ml when activating LDN5 (Figure 5.9b). In addition, stimulation of LDN5 via the same GMM panel presented by macaque CD1b reveals no visible hierarchy (Figure 5.9c). Taken together this data suggests that the GEM TCRs are sensitive to changes in the meromycolate backbone, whereas LDN5 responds similarly to all GMMs.

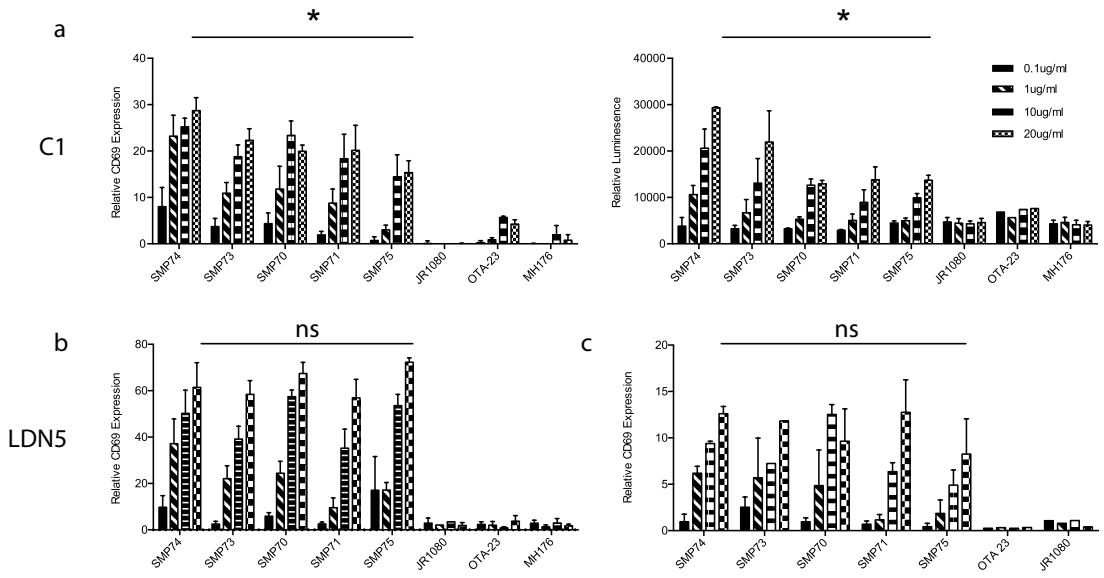

Figure 5.9: Meromycolate mediated activation hierarchy is a feature of GEMs

Stimulation of GMM specific TCRs C1 and LDN5 by GMM panel. a) C1 activation by GMM in a dose response measured via CD69; b) C1 activation by GMM panel in a dose response measured by Gluc secretion; c) LDN5 activation by GMM in a dose response presented by human CD1b; d) LDN5 activation by GMM panel in a dose response presented by macaque CD1b. Significant difference in C1 hierarchy which is absent in LDN5. Mann whitney-U test performed on SMP74 and SMP75 pulsed at 20 μg/ml.

5.5 Processing-independent mechanism for activation hierarchy

Using mycolates containing two different head groups comprising of an array of mycolate species and stereo-arrangements, we demonstrate that proximal and distal functional groups within the meromycolate chain causes differing levels of GEM C18 T cell activation. This hierarchy also occurs with C1 activation mediated by GMMs differing in meromycolate backbone structures. We therefore considered the mechanism for this hierarchy, either arising because of differing MA processing efficiencies within the cell, yielding differentially loaded CD1b molecules on the APC cell surface, or due to similar loading efficiencies but an altered stability of MA within CD1b. To investigate this, we took advantage of C18's ability to respond to GMMs (Figure 5.6b) listed in table 5.

MA	Chemical Structure	Code	Class	Organism	Proximal	Distal
A	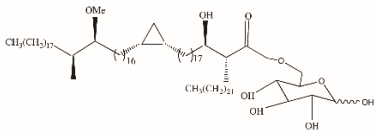	SMP70	Methoxy	Mtb	Cis, *RS*	*SS*
B	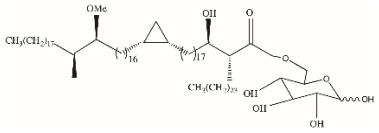	SMP71	Methoxy	Mtb	Cis, *RS*	SS
C	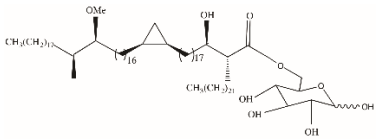	SMP73	Methoxy	Mtb	Cis, *SR*	*SS*
D	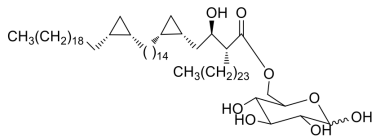	SMP74	Alpha	Mtb	Cis, *RS*	Cis, *RS*
E	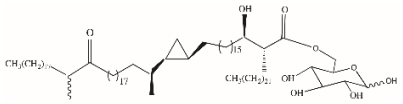	SMP75	Keto	Mtb	Tras-cyclopropane	

Table 5.5: Panel of synthesised GMMs from Mtb

Schematic of GMM meromycolate chains, their organism of origin and stereochemical arrangement. A) SMP70, B) SMP71, (C) SMP73, (D) SMP74 and (E) SMP75.

While LDN5 responds in an equal manner to all GMMs when presented by both human CD1b (Figure 5.9b) and macaque CD1b (Figure 5.9c), C18 recognises only SMP73, SMP74 and SMP75, consistently shown by both CD69 and luminescent expression by Jurkats (Figures 5.10a-b). We infer from these findings that while the GMMs are loaded and presented equally on the surface of APCs, as indicated by LDN5 responses, C18 recognition of these lipids differ. This strongly indicates that lipid tail backbone structure, independent of lipid processing, strongly impacts on GEM T cell activation.

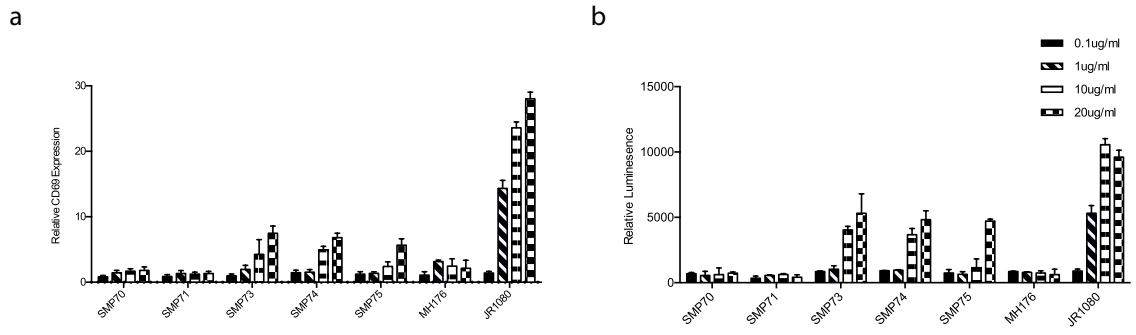

Figure 5.10: Antigen processing independent mechanism for activation hierarchy

Activation of C18 TCR transduced Jurkats post stimulation with a panel of GMMs pulsed at increasing concentrations (0.1 μg/ml-20 μg/ml); a) activation of C18 Jurkats by human CD1b presenting GMM; b) activation of C18 transduced NFAT Jurkats by human CD1b presenting GMM. LDN5 responds without a hierarchy to all GMMs in the panel (figure 5.9b & c) while C18 responds to only SMP73, SMP74 and SMP75.

5.6 Synthetic mycolates activate T cells derived from Mtb infected clinical samples and conform to hierarchy

For the purpose of investigating *ex vivo* T cell responses to our synthetic mycolate panel, we wanted to demonstrate CD1b expression on the surface of moDC for use as an autologous APC. Also CD14, a marker of human monocytes, is only expressed minimally on moDC, we therefore used it in addition to CD1b to track monocyte differentiation (Figure 5.11). We exposed freshly purified monocytes to 20 ng/ml of IL-4 and 25 ng/ml of GM-CSF for 6 days. Each day $2x10^5$ cells were stained to elucidate CD1 and CD14 expression on the cell surface. Our results show that every 24 hours, CD1b expression was increased while CD14 expression was decreased, as demonstrated by the MFI (Figure 5.11). CD14 expression on monocytes is initially very high and although it decreased during differentiation, it was retained to some degree on moDCs. Conversely, CD1b expression is very low on monocytes and its expression increased on moDC.

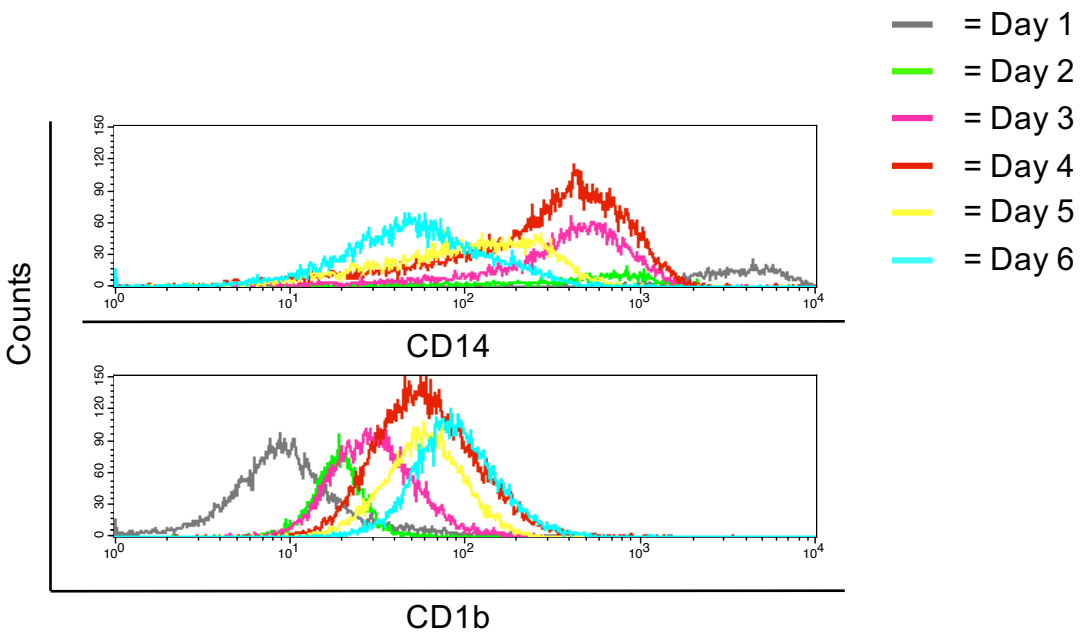

Figure 5.11: CD14 and CD1b expression on differentiating human monocytes

Differentiation of human monocytes *in vitro* with IL-4 and GM-CSF. Each day during differentiation, cells were stained with anti-CD1b and anti-CD14 and fluorescence was measured. There is a decrease in CD14 expression over 6 days (top), and increase in expression of CD1b of the same 6-day period (bottom), suggesting correct differentiation from monocytes into moDCs.

To further improve CD1b expression on moDC from both macaque and human, we investigated the potential of rifampicin to up-regulate CD1b expression. A previous report has shown that rifampicin can up-regulate cytokine induced expression of CD1b (270), which is interesting as rifampicin is a critical antibiotic in the treatment of TB. We therefore added 10 μg/ml of rifampicin to cultured cells on day 3, 4 and 5 to assess its effects on CD1b expression. Our data suggested that addition of rifampicin on day 3 was optimal with greater CD1b expression compared to cultures that received it on day 4 and 5 (Figure 5.12). Overall our data suggest that differentiated moDC can be used as APC to stimulate autologous T cells, and that rifampicin can further increase this expression.

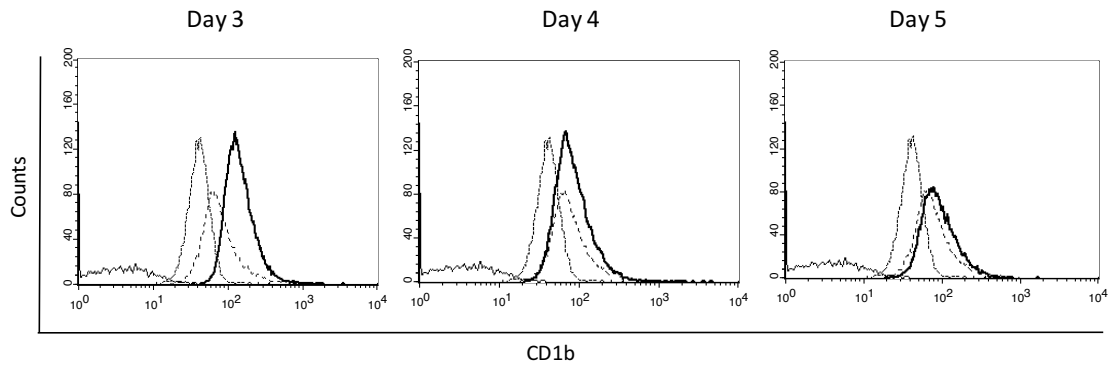

= Unstained
= Isotype
= No Rifampicin
= Rifampicin

Figure 5.12: Effect of rifampicin on CD1b expression in moDC

CD1b expression on monocytes differentiated into moDC over a 6-day period. Dark line shows expression after addition of rifampicin on the indicated days. Effect of rifampicin on CD1b expression was most pronounced when added to cultures on day 3 when compared to GM-CSF and IL-4 cytokine differentiation alone.

Using autologous moDC with confirmed CD1b expression, we investigated the *ex vivo* T cell response to our synthetic mycolates. PBMCs from ten latently infected TB patients were collected and cytokine responses were measured against our MAs (Figure 5.13). We chose a strongly activating MA (JR1080), two weakly activating MAs (MMS130 and JRR121), a GMM and a Gro-MM (SMP74 and OTA-23) where the latter two contained the same backbone as JR1080. Using intracellular cytokine staining to measure numbers of cells responsive toward each ligand, we show a hierarchy with regard to the number of cells responsive to each lipid, complementing our *in vitro* data. Significantly more cells released detectable levels of IL-2 toward JR1080 (Median = 2.5%) than with MMS130 (Median = 0.99%, P = 0.045) and JRR121 (Median = 1.02%, P = 0.02). There were also significantly more cells releasing IFN-γ toward JR1080 (Median = 2.08%) than JRR121 (Median = 0.81%, P = 0.039) and MMS130 although this did not reach significance (Median = 0.63%, p = 0.2). Finally, the same pattern occurred with cells releasing TNF-α, as more cells responded to JR1080 (Median = 1.17%) compared to MMS130 (Median =

1.045%, p = 0.18) and JRR121 (Median = 0.82%, P = 0.0086). In addition, the GMM SMP74 has more responsive cells releasing IL-2, IFN-γ and TNF-α (Median = 1.43%, 1.41%, 1.15% respectively) than its Gro-MM counterpart OTA-23 (0.96%, 1.02%, 0.9% P = 0.099, 0.03, 0.1 respectively), and the two weakly activating MAs, reaching statistical significance in some cases. This agrees with existing literature that the GMM T cell response is dominant in latently infected patients (135). It also confirmed our synthetic mycolates are stimulatory in an *ex vivo* T cell population from human TB patients, but also preserved the activation hierarchy in a polyclonal T cell population gated on $CD161^-$, $CD3^+$ T cells which includes GEMs.

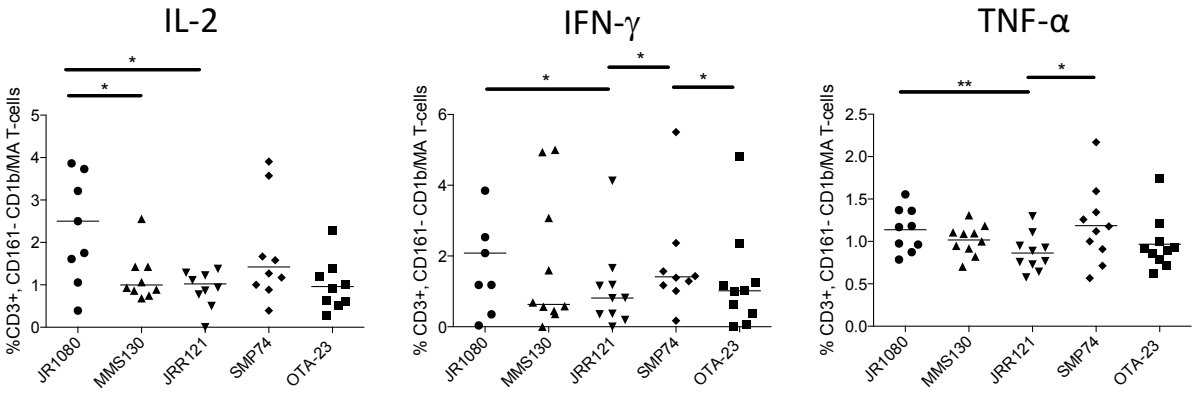

Figure 5.13: *Ex vivo* T cell activation using strong and weakly active mycolates

T cell samples from 10 latently infected patients were presented to autologous moDC pulsed with each MA for 24 hours. Anti-CD28 was also added to each stimulation at 2.5 μg/ml. Cells were then intracellularly stained for acquisition on the FACS Aria, number of cells expressing either IL-2, IFN-γ and TNF-α were measured. Cells were pre-gated on live, $CD3^+$, $CD161^-$ T cells. A negative control for each donor included T cells added to un-pulsed moDC and anti-CD28, results were normalised to the negative control. In each case there is an increase in the number of cytokine positive T cells when activated by the strong mycolate JR1080 compared to weak.

5.7 Dissecting CD1b/MA interactions and complex stability

To further support our processing/loading independent mechanism for the observed T cell activation hierarchy, we used *in silico* modelling techniques to understand CD1b/MA interactions and complex stability. Using molecular dynamics, a simulation of how the lipid interacts with the protein can be modelled over a period of time as a trajectory. Lipid movement can then be quantified when compared to the previously resolved structure. However, there was initial difficulty arranging the ligand pose within the groove, as no existing crystal structure of CD1b has been determined with hydrocarbon chains in excess of 80C (61). After multiple simulations, it was clear that while the mycolate acyl chain can protrude from the C' portal opening, beneath the α2 helix at the side of the molecule, this did not yield stable complexes (Figure 5.14a & b). A more plausible arrangement therefore was generated from initial simulation work, which we called the 'tucked' arrangement, this allowed a more stable conformation and more consistent results between simulations (Figure 5.14c & d). Thus, results were generated applying this acyl chain arrangement.

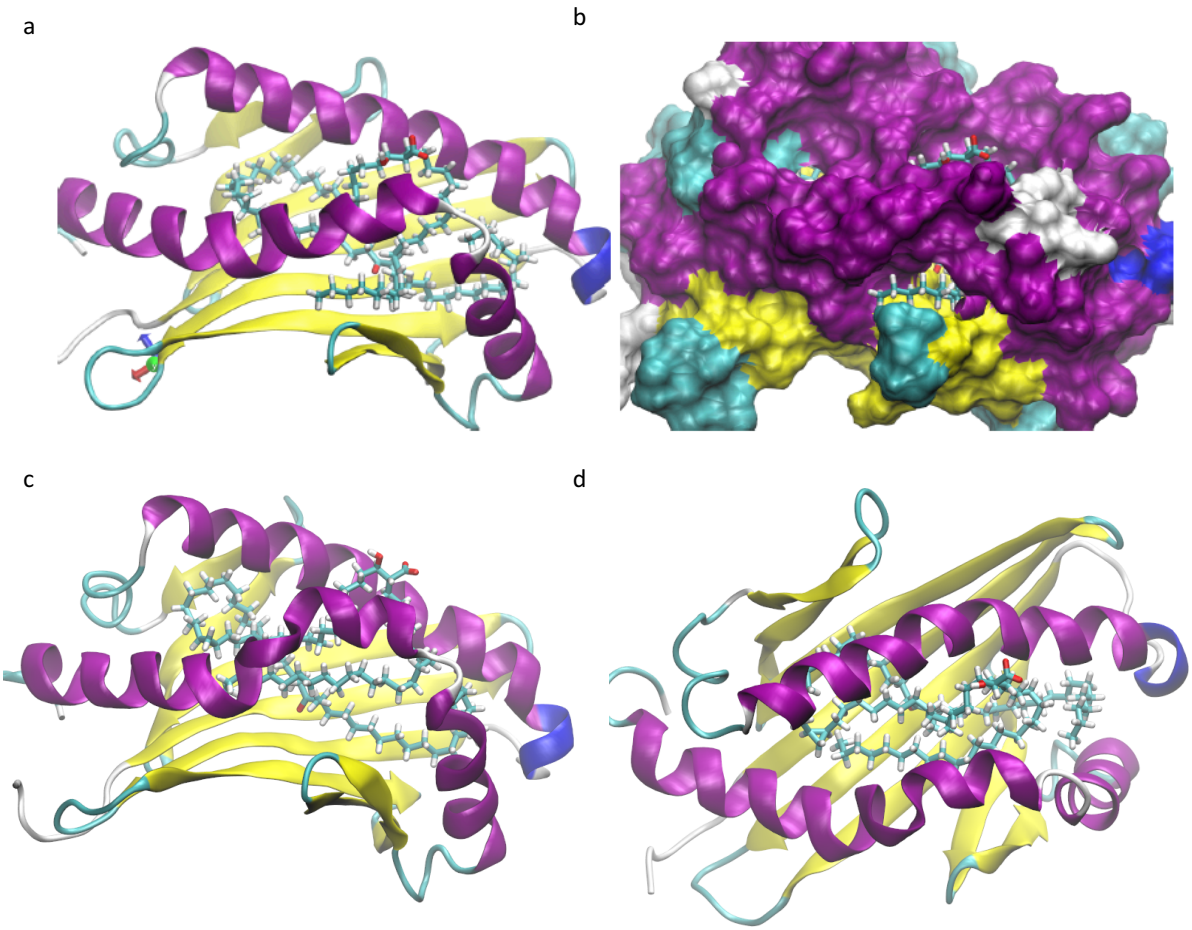

Figure 5.14: MA orientation within the CD1b antigen binding groove

MA ligand pose within the groove of CD1b. a) Side view of CD1b represented as ribbon structure containing JR1080 in initial ligand pose. b) Surface representation of CD1b showing initial ligand poses. c) Side view of CD1b containing JR1080 in tucked arrangement. d) Above view of CD1b containing JR1080 in the tucked position, the acyl chain folds back into the protein. Purple indicates alpha helices and yellow indicates the heavy chain.

Over the trajectory time course, we examined the position and behaviour of the ligand head group and meromycolate chain substitutions. Head group mobility was measured via the distance moved in references to the head group of GMM in the existing crystal structure of CD1b in complex with GMM. Root mean squared deviation (RMSD) values were calculated to provide a measure of structural similarity to the putative productive

conformation of CD1b-GMM (Fig 5.15a). This highlighted the stimulatory JR1080 as adopting similar conformations and the weakly stimulatory JRRR121 as adopting markedly different conformations to the head group of CD1b-GMM. Whilst not recreating the full hierarchy of stimulatory behaviours, this analysis shows the ability of ligand chain substituents to influence head group positioning and behaviour.

Study of the meromycolate chains was carried out through visualisation and comparison of substituent centroid positions. Striking differences in centroid localisation and dynamics were apparent between stimulatory and weak-stimulatory mycolic acids. The weakly stimulatory mycolic acids JRRR121 and JR1046 showed much more pronounced localisation of substituent centroids in the T' tunnel (distal) and A' channel (proximal) (figure 5.15b) than the simulated stimulatory ligands. Investigation of the structural features of CD1b revealed that the localisation resulted from the insertion of the larger distal chain substituent of these ligands into a small crevice of the T' tunnel (Fig 5.15c) in an “anchoring” mechanism. This strongly suggests that constraining the meromycolate chain within the binding pocket influences positioning of the ligand head group that restricts the ability to adopt productive conformations for T-cell binding.

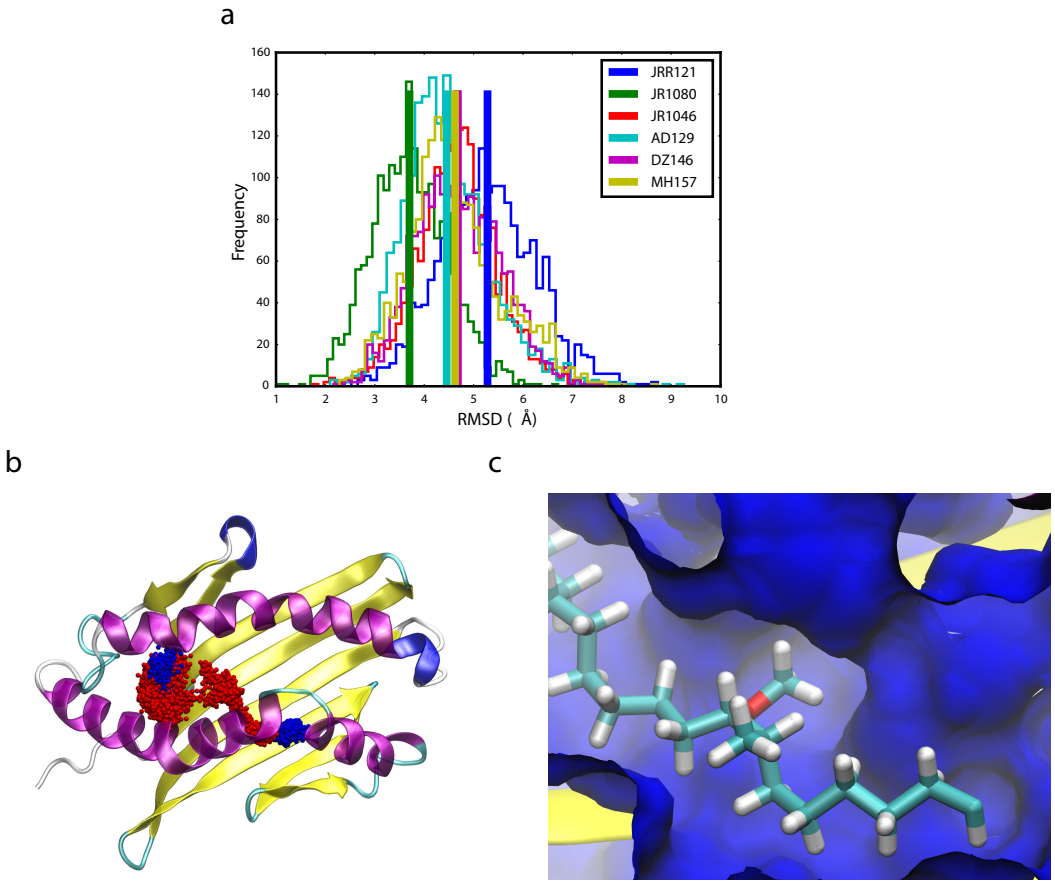

Figure 5.15: Quantification of lipid stability in CD1b groove

a) Histogram of head group RMSD value for mycolic acid head group movement relative to the solvent exposed head group of GMM in published CD1b-GMM complex (1UQS). Higher RMSD values indicate conformations less similar to that observed in 1UQS whilst a greater spread of values indicates increased mobility of ligand head group. Vertical bars mark mean values for histograms of the corresponding colour. b) Meromycolate substituent centroids from molecular dynamics trajectory. A representative weak-stimulatory ligand (JRR121) is shown in red and a stimulatory ligand (MH157) in blue. c) Distal meromycolate chain of JRR121 inserted into a small crevice of the T' tunnel.

5.8 Investigating the therapeutic potential of GEM transduced T cells

To understand the functional relevance of MA lipid backbone differences, we transduced primary human T cells with GEM C18, LDN5, and the CD1c restricted TCR NM4 (62). Figure 5.16 shows representative dot plots of viral transduction efficiencies from addition of concentrated virus to three healthy donor $CD14^-$ PBMCs. TCR expression was measured using and anti-beta chain antibody. Table 5.6 summarises the percentage transduction efficiencies within the $CD3^+$ T cells as well as $CD8^+$ T cells to assess use as a cytotoxic population. T2 CD1b cells were pulsed with three strong (CDL12DU, JR1080, DZ146) and three weak MAs (JRR121, MMS130, JR1046) and functional response of activated T cells was measured using a cell viability assay and measuring cytokine release within the supernatant. Figure 5.17 shows relative cell killing after 24 hours incubation of C18 transduced T cells with lipid pulsed APCs. Results demonstrate the prototypic ligand, JR1080, induced more cell death than any other MA, reaching significance in each case when compared to the weak ligands (JRR121 - p=0.009, MMS130 – p=0.003, JR1046 – p=0.0071). CDL12DU also reached significance when compared to each of the weak ligands (JRR121 – p=0.048, MMS130 – p=0.025, JR1046 – p=0.029). Finally, T cells activated by DZ146 resulted in a lower number of viable cells compared to (MMS130 - p=0.057, JRR121 - p=0.1 and JR1046 - p=0.05). Our results suggest strongly activating MAs cause more cell killing via activation of GEM C18 transduced T cells.

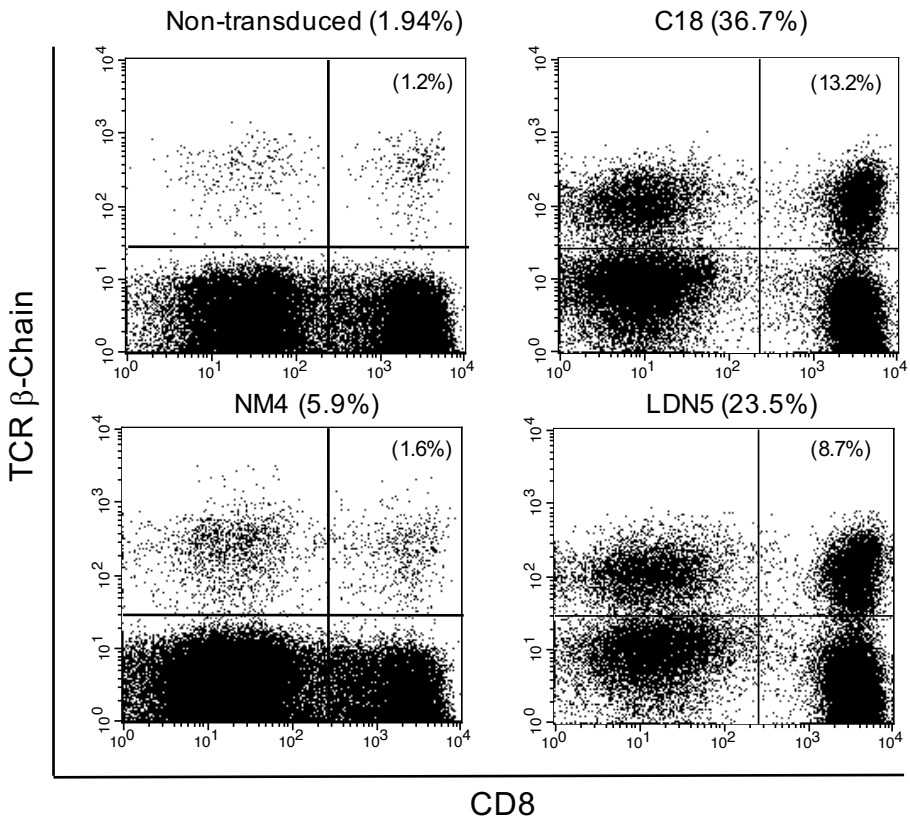

Figure 5.16: Viral TCR transduction of CD14 depleted PBMCs

PBMCs depleted of $CD14^+$ cells by magnetic separation were virally transduced with each TCR indicated and subsequently stained for specific TCR expression using anti-beta chain antibodies. Cells were pre-gated on live, $CD3^+$ lymphocytes and CD8 co-stain is shown. Total percentage TCR transduction of $CD3^+$ T cells is indicated in title of each plot. Upper right hand quadrant percentage indicates transduction efficiency of $CD8^+$ T cells.

Donor		NTD	C1	C18	NTD	NM4	NTD	LDN5
A	**CD3 (%)**	2.45	3.17	13.54	2.01	3.1	3.02	17
	CD8 (%)	1.89	2.39	6.94	1.37	1.23	1.41	5.86
B	**CD3 (%)**	1.94	2.36	36.67	2.59	5.29	1.72	23.5
	CD8 (%)	1.2	1.53	13.19	0.83	1.61	1.24	8.37
C	**CD3 (%)**	4.16	4.81	25.26	1.18	5.44	1.36	18.8
	CD8 (%)	3.09	3.68	15.48	0.6	2.51	0.694	7.4

Table 5.6: Percentage T cell transduction with CD1 specific TCRs

CD1b expressing T2 cells were pulsed with a panel of six MAs including 3 strongly activating and 3 weakly activating for use as APC. After adding C18 transduced T cells in a ratio of 1:2 for 24 hours supernatant was stored and killing measured. Figure 1.13 shows that the lipid activation hierarchy is preserved with stronger lipids inducing greater cell death compared to weak. Statistical significance was reached in every case comparing the three most activating MAs to MMS130 in two repeat experiments performed in triplicate. This result is consistent with our previous data, and also highlights the functional relevance of greater levels of GEM T cell activation in transduced PBMC.

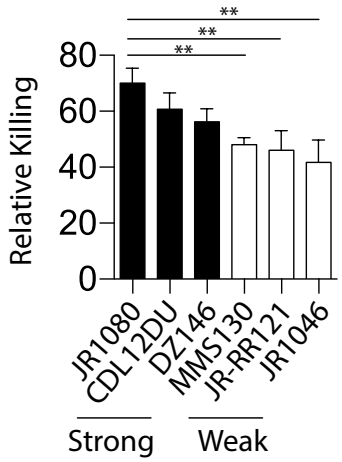

Figure 5.17: Cytotoxicity induced by C18 transduced T cells against strong and weak MAs

Cell cytotoxicity was measured in the cultures of GEM C18 transduced T cells added to T2 APC, pulsed with three strong lipids include, JR1080, CDL12DU and DZ146 and three weak lipids include MMS130, JRR121 and JR1046. Bar graph shows percentage killing of all cells in the well. Graph is representative of two repeat experiments each performed in triplicate.

In the same experiment, culture supernatant was analysed with a 10-plex luminex assay. The panel of cytokines assessed contained both proinflammatory and anti-inflammatory cytokines important in Mtb infection. In all cases, transduced T cells stimulated with the three stronger lipids secreted more cytokine than any of the weaker lipids (Figure 5.18) which was significant in all cases. Strong responses were noted from IFN-γ, GM-CSF and IL-2 which were secreted >10,000pg/ml by all of the strong mycolates, suggestive of a proinflammatory response from these cells. The lowest cytokine secretion was of IL-4, IL-10, IL-17a and IL-6 which were all at levels <100pg/ml for both strong and weak lipids. IL-12p70 was also measured and not detected in any of the wells. Figure 5.19 is a heat map representing normalised secretion quantities displaying relative levels of cytokine released by each MA. Both the strong and the weak lipids stimulate a greater Th1 response compared to a Th2, with greater levels of IFN-γ, IL-2 and GM-CSF. Unsupervised clustering shows differences between strong and weak lipids as well as

differences in relative levels of Th1 and Th2 cytokines. In summary, these data demonstrate the therapeutic potential of our lipids, indicating T cell responses can be tailored using different MAs. Finally, these cells confirm the activation hierarchy of our lipids, which is preserved in both killing and cytokine secretion.

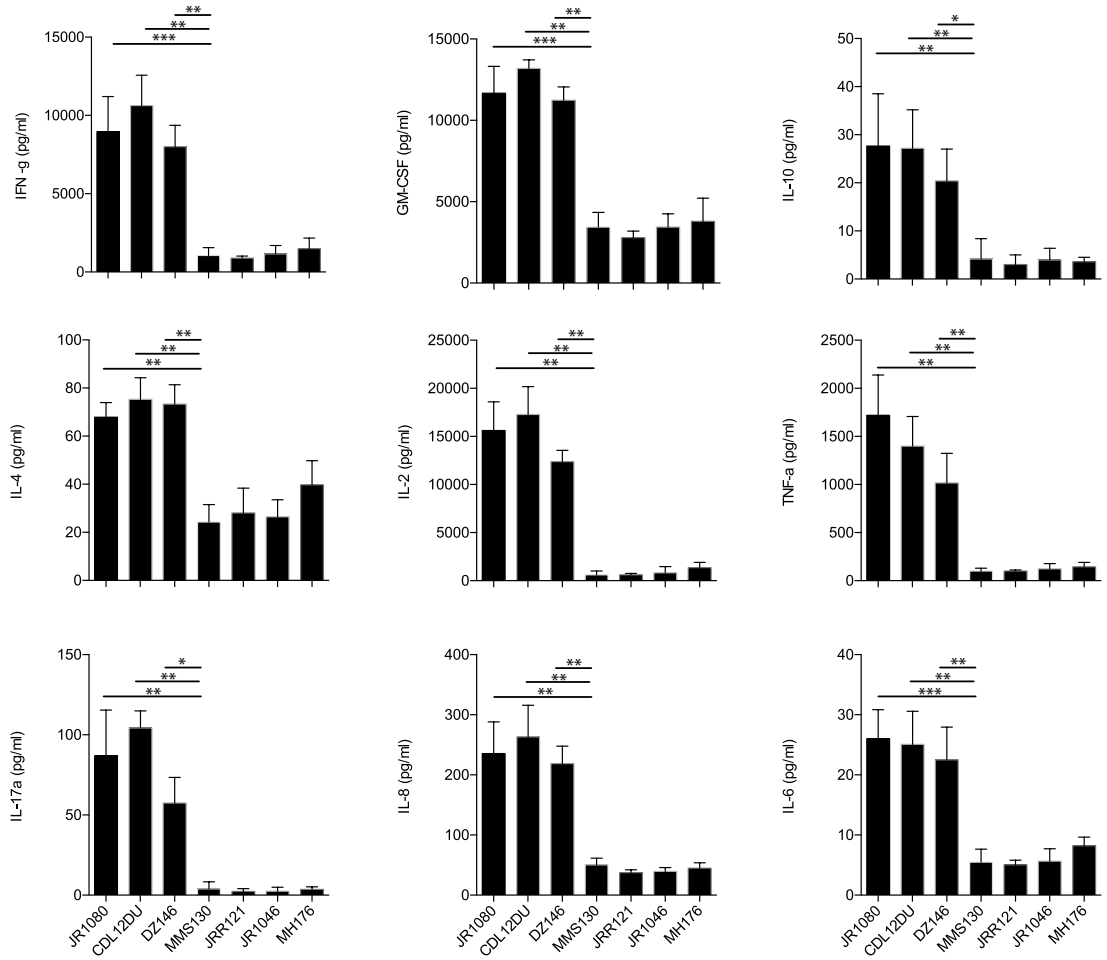

Figure 5.18: Cytokine production from transduced T cells against strong and weak MAs

Supernatant was removed from GEM C18 transduced T cells stimulated with 10 μg/ml of three weak and three strong lipids, and analysed via a 10-plex luminex. Three strong lipids include, JR1080, CDL12DU and DZ146 and three weak lipids include MMS130, JRR121 and JR1046. In addition, a TMM (MH176) which is not recognised by C18 was used to show background levels of cytokine. Data representative of mean cytokine release from one donor across two experiments each performed in triplicate.

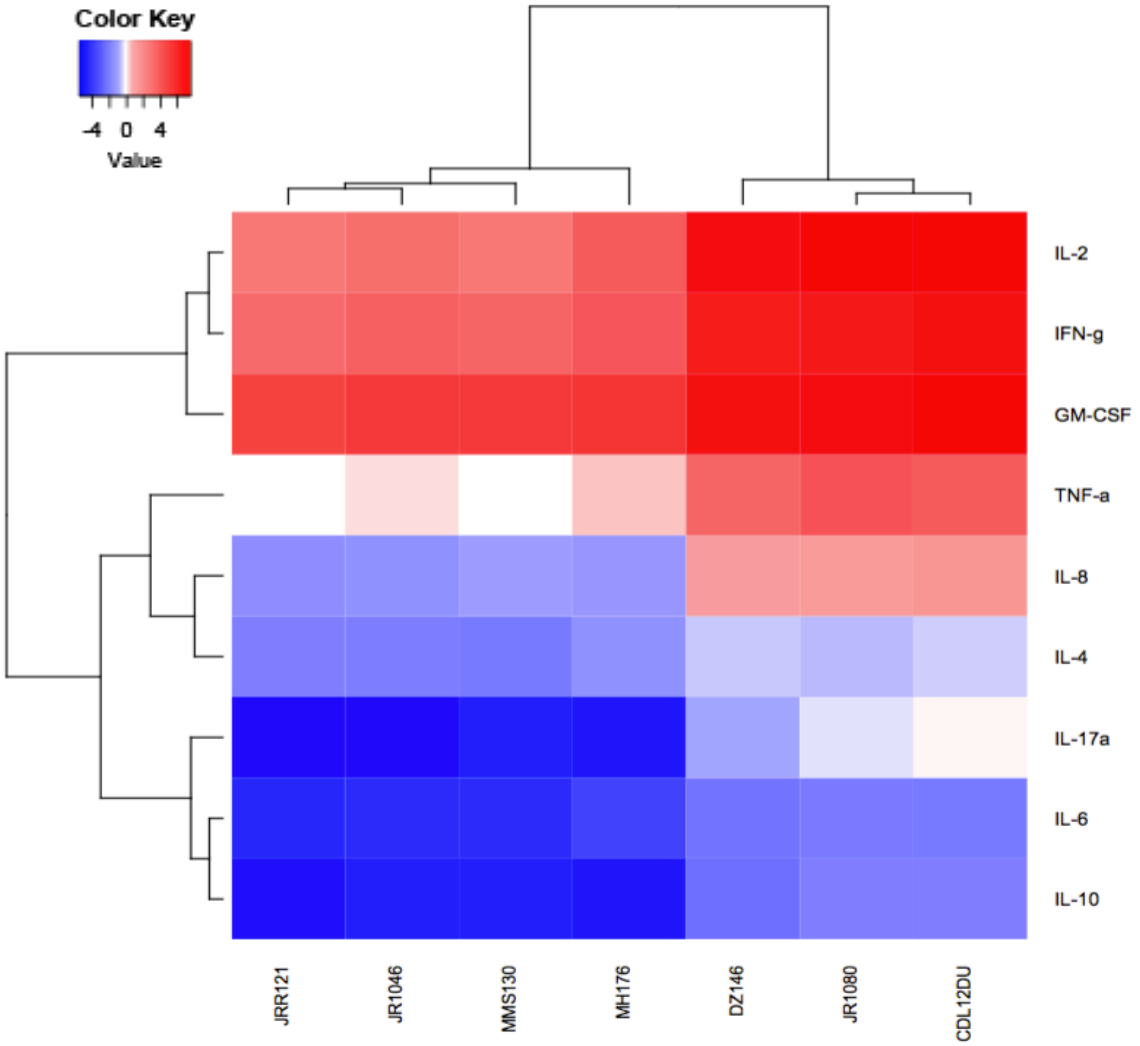

Figure 5.19: Heat map of cytokine release from transduced T cells

Heatmap depicting the relative levels of cytokines secreted from GEM C18 transduced T cells by respective lipids when presented by T2 cells expressing CD1b. Hierarchical clustering was performed using euclidean correlation metric to calculate distances and clustered using complete linkage. Cytokine levels were $\log_2$ transformed and normalized by median cytokine level across all lipids and cytokines. Red and blue indicate greater and lower expression, respectively, compared to the median.

Chapter 6: Discussion

CD1 group 1 molecules are likely to have a central role in the host immune response to tuberculosis infection (107, 132). However, our knowledge of this arm of the human immune system remains relatively poor. Current evidence suggests that CD1b has a key role in Mtb lipid antigen presentation to T cell populations that express an invariant TCR called GEMs (130, 271). We therefore investigated the T cell response towards MAs with a particular focus on GEM T cells. Utilising a panel of, pure, synthetic mycolates which are representative of the most abundant families present in the cell wall of Mtb (272), we demonstrated an inherent ability for GEM T cells to detect structural alterations in the meromycolate chains of MA, GMM and Gro-MM, which dictated the potency of the T cell response. This pattern was verified using diverse experimental and *in silico* methods and it was independent of antigen processing. Furthermore, we demonstrate the divergent cytokine induction of our mycolate lipids, revealing their potential use for future TB therapy that may target GEM T cells.

6.1 CD1b expression in the granuloma

Granuloma formation, in the most part, is initiated by infection of a single macrophage with a single Mtb bacilli (273). This in turn usually leads to production of proinflammatory cytokines and chemokines such as monocyte chemoattractant protein (MCP-1), causing an accumulation of phagocytes, sometimes resulting in a granuloma (274). T cells are thought to later join and form a ring around a developed granuloma, traditionally thought to wall off infection (274). Despite the mechanisms deployed by Mtb to prevent MHC expression, classical T cells are understood to eventually become activated through peptide presented on an abundant supply of epithelial cells, macrophages, foam cells and dendritic cells (112). Activation of lipid antigen specific T cells however, is less well understood, since expression of group 1 CD1 is far more restricted. CD1b has perhaps the most restricted expression, predominantly residing on the surface of dendritic cells, and *a priori* is not expressed on macrophages.

Lipid antigen mediated activation of T cells therefore chiefly occurs via dendritic cells. In addition, investigation in mouse suggests T cell contact with dendritic cells takes place mainly at distal sites, such as the mediastinal lymph nodes (275). As such there is little evidence in human disease that CD1b is expressed at the site of disease, or that dendritic cells are able to prime T cells in the local inflammatory site of the granuloma. However, our immunochemical staining of CD1b in human lung sections containing clear granuloma formation suggests otherwise. Our results show CD1b expression both in the central, necrotic areas as well as in the granuloma periphery. This suggests that CD1b presenting cells are active at the local site of infection, capable of inducing CD1b restricted T cells. Our attempts to identify the cell type responsible are inconclusive. However, the large areas of CD68 positive tissue in proximity to CD1b, suggest the possibility of CD1b antigen presentation via macrophages. Confocal imaging of cell stained with both CD68 and CD1b labelled with different fluorophores is required for verification.

6.2 MA Structure-function – Backbone directly influences T cell activation

MAs are crucial for Mtb survival, contributing toward bacterial structure, pathogenicity, virulence, and drug resistance (11, 188, 189, 194, 276). Investigations in mice have suggested that there are differences in innate immune responses directed towards different MA structures, and structure–function studies have also been undertaken in antibody responses toward MAs in humans (272, 277). Interestingly, meromycolate lipid tails of MA are the most diverse structural feature of tuberculosis mycolates. However, there has been no systematic study to date investigating the effect of this diversity with regard to CD1b antigen presentation and how it may impact the subsequent T cell response. To investigate MA antigen presentation, we developed and functionally validated CD1b-expressing T2 APCs and Jurkat T cell lines expressing mycolate specific TCRs including GEMs.

It is clear from a growing body of evidence that single amino acid changes in the key binding loops of TCRs can change their binding affinity towards lipid antigen in the

context of CD1 (221, 278). Using our cellular *in vitro* system, we were first able to verify TCR specificity which is determined by lipid head group, a concept maintained throughout CD1 restricted T cell populations (81, 126, 127, 134). As a result, we identified novel specificity of the C18 GEM TCR, as it is not only activated by MA but also Gro-MM and GMM, which differs from published data (134). Head group discrimination suggests that the TCR forms stabilising interactions with smaller OH groups, due to lower activation with GMM. On the other hand, clone 1 has the same dependency of the glucose head group as LDN5. Insights from structural data of clone 18 and clone 42 (134) (another GMM specific GEM TCR) suggest that specificity is dictated by the exchange of amino acid in the CDR3β loop (Leu107β–Arg107β), providing mobility to the CDR3α loop. Increased flexibility in clone 42 presumably allows for accommodation of the larger glucose head group (134). Our data therefore suggest MA head is an important determinant of GMM specific TCRs, however GEM C18 has less dependency.

Evidence exists suggesting the buried hydrophobic chains in ligands that bind CD1b, CD1c and CD1d influence T cell activity (141, 211, 279, 280). In CD1d, the clearest example is in the affinity and functional outcome of α-GC and OCH binding with CD1d (280). OCH contains a truncated sphingosine chain, which results in lower binding affinity to the iNKT TCR as well as lower proliferative capability and ability to stimulate cytokine production (280, 281). Furthermore, regarding CD1c, mycoketide synthesis revealed the T cell clone CD8-1 was more potently activated by synthetic ligands that more accurately mimicked the natural branched mycobacterial mannosyl phosphopolyketides (MPMs) (141). It was determined that the length, the methyl branching pattern and the stereochemistry of the protein buried polyketide chain significantly impacted T cell responses (141). Moreover, sulfoglycolipid is another mycobacterial lipid, presented by CD1b (282). Using a panel of synthetic analogues that contained the same trehalose-sulfate polar head, but different acyl chains to stimulate T cells, revealed how the chiral centres and the C-methyl substituents on the fatty acid chain governed T cell activity (279).

In addition, previous analysis of LDN5 activation toward GMM revealed that the long chain length, cyclopropanation, double bonds and R groups were not antigenic determinants (72). In this case, T cell activation was solely determined by the hydrophilic

head. Other MAs studied include Gro-MM, which was found to be the specific antigen for the T cell clone Z5B71 (211). This clone demonstrated activity only toward C80 Gro-MM and not the C32, thereby indicating the importance of the hydrocarbon chain. Therefore, the antigenic determinants of the hydrophobic moiety of mycolic acids have been largely unappreciated. Our study represents the first systematic investigation of the effect of meromycolate functional group and stereo arrangement on T cell activation; in particular, the recently described donor unrestricted GEM TCRs.

Contrary to existing paradigms that meromycolate chains bind CD1b non-specifically with no effect on T cell responses (72), our data suggests that differences in meromycolate functional group structure, position as well as its stereochemistry strongly impacts on GEM T cell activation. The observed hierarchy was verified in MAs, GMMs and Gro-MMs using both clone 18 and clone 1 TCRs. There are two possible mechanisms for the hierarchy, the first due to potential differences in antigen presentation and processing and therefore loading efficiency of lipids onto CD1b. In contrast, the observed hierarchy in T cell activation may reflect stable MA CD1b complexes for stronger stimulatory lipids and vice versa. The former scenario of divergent processing is unlikely, as our data suggest equal GMM loading capability when presented to LDN5 despite functional group differences. This is in agreement with previous reports suggesting that dramatic alterations in hydrocarbon chain length of GMMs are recognised equally by LDN5 (208). This strongly suggests that while GMM loading is equal, subtle changes in the CD1b/MA interactions lead to a ‘stronger’ or ‘weaker’ TCR binding platform, seemingly detected by GEM TCRs, which is mediated by simple alterations in the meromycolate chain. Thus, these data indicate an antigen processing independent mechanism for the observed hierarchy. This agrees with current data suggesting that Mtb-derived MAs are not processed by any cellular mechanism (283).

Stereochemical changes of meromycolate functional groups have an impact on T cell activation. JR1080 has two cyclopropane functional groups in its hydrocarbon chain that can naturally exist as four stereoisomers in cis (Table 4.3) (272). The alpha chain is more stimulatory when in a cis-SR, cis-RS or cis-RS, cis-SR (proximal and distal respectively), than when in a cis-SR, cis-SR or cis-SR, cis-RS orientation. One reason for the highly

stimulatory potential of CDL12DU and CDL12UD may be due to cyclopropane functional groups that are positioned at distances down the meromycolate chain for optimal fit in the CD1b super-channel, similar to the CD1d/αGC system (280). If they are positioned at the junction of both the A'-T' and T'-F' channels, they may possess increased rigidity thereby reducing ligand mobility within the groove (207). This may enhance rigidity of the complex, in turn reducing loss of entropy, allowing for a minimal binding energy for bound TCRs. Evidence to suggest that changes in meromycolate functional groups affect T cell activation has been generated in unpublished computational modelling of ligand/CD1b interactions with the MA specific TCR DN1 (208). Chemical modifications preferentially locate themselves in specific areas of the CD1b A' channel (207). This may also be a mechanism as to how MA meromycolate backbone influences the geometry of the solvent exposed portion of the MA head group.

These results therefore refine our previous understanding of T cell interactions with CD1b/mycolate. Our data suggests there are three types of mycolate recognition from LDN5, C1 and C18. The first is LDN5, which has absolute dependency on lipid head group detecting no changes in the lipid tail. The second is C1, which has dependency on lipid head group for specificity but also detects alterations in lipid tails. Finally, C18 whose interaction is not principally dependant on head group, and activation is dramatically altered by subtle meromycolate changes.

6.3 Inferences from LDN5 activation by macaque CD1b

LDN5 has previously been shown to cross-react with macaque CD1b when presenting GMM (41), an observation we also verified. Therefore, LDN5 is seemingly less sensitive than the GEM clones to amino acid changes in the α1 and α2 helix in macaque CD1b. In addition, while the glucose head group is absolutely required, LDN5 TCR binding is less reliant on strong meromycolate/CD1b binding as there is no observable hierarchy using our GMM panel. Therefore, the GEM TCRs may make critical interactions with human CD1b which is absent in LDN5.

Previous mutational analysis of the α1 and α2 helices of CD1b revealed a greater contribution of the residues forming the α1 helix than the α2 in DN1 (MA specific) TCR binding, suggesting that the β-chain which sits directly above the α1 helix, dominates this interaction (210). MHC class I interactions usually entail a vertical tilt of the TCR α-chain toward the α2 helix in TCR/MHC class I interaction (284). This may be the opposite for CD1b interactions where a vertical tilt towards the α1 helix is the dominant interaction (284). A binding mechanism that may be more critical in the clone 18 GEM interaction because of its greater requirement for protein/protein interactions. In support of this suggested binding mechanism, DN1 was more sensitive than LDN5 to point mutations in the CD1b alpha helices (210). LDN5 was affected by only 3 of 18 amino acid substitutions compared to DN1 that was sensitive to almost half (210). DN1 is therefore likely to act as the MA specific clone 18 GEM TCR and lack binding toward macaque CD1b. Point mutations of the macaque CD1b sequence in the α1 and α2 helices that restore binding of clone 18 GEM TCR will reveal the requirements for TCR interaction with CD1b. Figure 4.15 shows the aligned CD1b sequences from both human and macaque, highlighting the amino acid differences within the α1 and α2 helices. There are six amino acid differences in the α1 helix and six in the α2 helix. Future structural studies to determine TCR binding to MA loaded CD1b are needed to reveal the molecular mechanisms for these interactions.

Figure 6.1: Comparison of human and macaque CD1b sequences

(Red) Leader sequence, (green) α1 domain sequence, (blue) α2 domain sequence, (purple) α3 domain sequence, (orange) transmembrane domain. Amino acid changes indicated by asterisk.

6.4 *Ex vivo* T cell CD1b/MA responses replicate *in vitro* observations

To confirm our hierarchical observations, we investigated mycolate stimulation of *ex vivo* T cell populations from latently infected TB patient donors. We used intracellular cytokine staining as a readout for T cell responses toward MAs. Monocyte derived dendritic cells are well established APCs, derived in culture from monocytes because of the low number of both plasmocytoid and myeloid DCs available for harvest in the blood (239). We used moDC as an autologous APC in our intracellular cytokine staining (145) studies due to their efficiency in presenting long hydrophobic lipids such as MAs (72). To ensure proper monocytic differentiation and high CD1b expression, we tracked CD14 (a

monocytic marker) and CD1b expression on these cells each day during differentiation (239). We demonstrated a decrease in CD14 expression and a simultaneous increase in CD1b, making moDC an ideal APC for presenting MAs. Furthermore, we also confirm rifampicin has the capacity to increase CD1b expression, as shown previously (270). This may have important implications as rifampicin is a first line drug against Mtb, which may also have undescribed immunomodulatory effects.

Our ICS gating strategy focused on live, $CD3^{+}$, $CD161^{-}$ T cells, as these are suggested markers of GEM T cells (134). Using this we were able to confirm the mycolate hierarchy via cytokine release. Our attempts to identify GEMs using the invariant TCR chain as a marker were not successful, presumably due to low expression once activated (data not shown) (285). However, we demonstrate that more T cells release cytokine toward strongly activating MAs than weakly activating. There was little difference in the quantity of cytokine secreted by individual cells as measured by MFI. Thus, stronger MAs may be identifying different populations other than GEMs that are reactive to CD1b/MA but have a lower affinity, so do not produce cytokine in response to weaker MAs. It would be interesting to investigate these T cell populations further. Notwithstanding, these results not only confirmed the functional validity of our synthetic TB lipids in human *ex vivo* samples, but also demonstrated the strong and weak stimulatory potential of these mycolates.

6.5 Molecular Dynamics eludes to a mechanism that's governed by CD1b/MA complex stability

We infer that MA meromycolate alterations directly impact TCR binding and thus affect T cell activation, independent of antigen processing. To support this, we performed molecular dynamics (286) studies in collaboration with Prof. Jon Essex and Prof. Chris Sklyaris (School of Chemistry, Southampton University). This technique provides insights into lipid interactions with CD1b, its binding conformation and overall stability of the complex. Of the existing crystal structures of CD1b, only one contains a mycolate (GMM), whose length is 49 carbons long in the meromycolate chain and 8 in the acyl

chain (61). However, our lipids are substantially longer with the same length meromycolate chain but 21-23 carbons in the acyl chain. As this was the first MD study performed using lipids with a total length of 80C, this posed an issue accommodating the acyl chain within the C'. Multiple simulations with the solvent exposed acyl chain protruding from the distal C' portal, previously proposed as a mechanism to allow C80 lipid binding, were unstable (69). The hydrophobic lipid tail tucked back into the C' channel, which enabled more consistent simulation repeats and reflected a more stable and therefore plausible lipid binding pose.

Once this likely binding conformation was modelled, three 'strong' and three 'weak' MAs were simulated in a blinded study, revealing increased mobility of 'weaker' ligands in the CD1b groove. Previous study of αGC analogues have demonstrated acyl chain differences do not dramatically alter the CD1d binding mode or footprint of the iNKT TCR (280). However, they led to fewer stabilising interactions with CD1d and therefore more ligand mobility leading to lower TCR affinity and reduced iNKT function (280). Furthermore, CD1d studies indicate that the forces stabilising the lipid hydrocarbon side chains with the groove are made up of weak hydrophobic and Van der Waals interactions, and modification of lipid acyl chains such as fluorination and inclusion of a phenyl ring can increase ligand stability in the groove (287). Our data demonstrated a similar mechanism by which structural changes within MA lipid tails directly impact on T cell activation. This also further supports an antigen processing independent activation hierarchy.

6.6 C18 transduced T cell function supports antimycobacterial role

Using our *in vitro* system, we have characterised the activation of CD1b/MA restricted T cells against a panel of mycolates which is supported by polyclonal *ex vivo* T cell populations and molecular dynamic studies. We also investigated the functional consequences of changing the meromycolate structure by virally transducing polyclonal T cell populations with clone 18 and LDN5 TCRs with high expression to use as reporter cells. This technique is used to dissect functional aspects of TCR affinities and translation

potential of antigen specific T cells (288, 289). In MHC peptide presentation, T cell function measured by cytokine release generally correlates with TCR affinity (290). This is also true of CD1d when independent of any cellular processing, likely due to reduced loss of entropy with more stable ligands (280, 290). It therefore follows, MAs that more potently activate T cells have higher TCR binding affinity when bound to CD1b. However, definite proof of this hypothesis would be provided by investigating the affinity of GEM TCRs to MA ligand loaded CD1b complexes by surface plasmon resonance.

The mycolate specific TCRs DN1 and LDN5 are well understood, and studies characterising GEM TCRs are lacking (208). Indeed, this is the first study examining the potential therapeutic role of purified T cells transduced with mycolate specific TCRs. Although it is not clear what immune response is appropriate for protection in Mtb infection, it is generally accepted controlled cell death or apoptosis mediated by Fas ligand for example, is more beneficial than necrosis (291, 292). We measured protease activity as a marker of cell necrosis within cultures containing APC pulsed with strong and weak lipids and C18 transduced T cells. The activity hierarchy of our lipids is maintained, with stronger lipids resulting in less cell viability within the cultures. Necrosis can be triggered through multiple innate pathways such as TLR3/4 pathway activation and ROS production (293). However, T cells are able to trigger necrosis through TNF-α production which activates Fas receptor associated death domain (FADD), ultimately leading to loss of membrane integrity (294, 295). Therefore, cell cytotoxicity assays suggest increased release of TNF-α from T cells against stronger lipids, which ultimately may not be beneficial in Mtb growth.

In addition to T cell cytotoxicity, we also measured cytokine release in the same cultures. *Ex vivo* T cell TCR transduction with peptide specific TCRs has revealed that increased antigen affinity increases T cell polyfunctionality (289). Stimulation with strong MAs revealed secretion of large amounts of each cytokine compared to weakly stimulating MAs. Similar experiments taking affinity measurements of the iNKT TCR against different αGC analogues revealed a correlation with iNKT proliferation and levels of IFN-γ produced (280). This may suggest the increased cytokine production from our strongly activating lipids is a reflection of increased C18 TCR binding with CD1b bound to

a strong MA, which supports our *in vitro* and MD data. Using these synthetic MAs, it is therefore possible to tailor the GEM T cell response.

6.7 3D Immunoaugmentation – Dissecting MA responsive T cells in TB

In Mtb infection, the desired immune response for robust protection has not yet been elucidated, and it is likely a complex, multifaceted response. An emerging concept is that either a deficit or excess of specific mediators may be deleterious. Traditional *in vitro* Mtb modelling aimed at solving this consists of 2D cell culture where events dramatically differ from *in vivo* (296, 297). Furthermore, the extracellular matrix is partly responsible for regulation of cell biology and the host immune response and has been broadly omitted from 2D cell culture (298, 299). Therefore, we employ a novel 3D cell culture model that includes human PBMC, extracellular matrix and virulent Mtb to assess the role C18 transduced T cells could have as a potential therapy. Not only can we measure Mtb growth via luminescence, but also host cell viability and cytokine release. Validation experiments have been performed including manipulation via addition of chemotherapy agents and individual cytokines that control or exacerbate Mtb growth as predicted (unpublished data).

Emerging data suggests T cell responses can be detrimental in Mtb pathology, and even a correlate of disease risk (255). However, evidence from the HIV pandemic and detailed work in the mouse model has demonstrated T cells are necessary for long term control of Mtb (111, 113). During the development of TB pathology *in vivo*, some lung lesions are sterilised by the host, while others progress to form necrotic cores (300). Different local T cell responses driving Mtb killing are likely responsible for the apparent disparity in granuloma development, as well as tissue injury, and it is clear that the 'correct' response is desirable. Addition of C18 transduced T cells in our model consistently show increased Mtb growth compared to infected PBMCs alone. This agrees with previous model data demonstrating an increase in iNKTs, ESAT-6 or CFP-10 peptide specific T cells also increase Mtb growth compared to control. These data suggest a mere increase in T cell activation generates a favourable environment for Mtb. It is not certain whether the

ex vivo proliferation of these cells has made them permissive to Mtb growth, or more simply that they are becoming activated and releasing an array of cytokines that reduce macrophage control of Mtb growth. However, further dissection of T cell responses in this model may elucidate a T cell profile that provides protection against Mtb.

6.8 Relevance of mycolate structure in host immunity

The repertoire of MA groups in each mycobacterium species differ with regard to average meromycolate chain length and functional group (198). These differences not only have profound effects on cell wall function, and also on pathogen virulence and manipulation of host immune responses (301-303). *Mycobacterium tuberculosis* mutants have been developed, some containing deletions in MA functional groups while others lack trans-cyclopropane rings to investigate the consequences on immune responses (201, 202, 301, 302). Innate immunity toward these strains has been described and demonstrated that although isolates lacking oxygenated groups are attenuated, the resultant host immunity is dampened (301). Other studies suggest mutants lacking cyclopropane groups were hypo-inflammatory for macrophages, developing less severe granulomatous lesions (201). Also, that cyclopropanation causes, lethal, chronic and persistent Mtb infection in mice (201). However, no mechanism is offered describing how innate immunity differentiates between mycolate structures. The current study reflects adaptive immunity; although similar consequences are observed in as much as cyclopropanation in our alpha mycolates causes increased GEM T cell activation. Likewise, B cell responses to MA are elicited toward various classes, where antibody binding differed hugely depending on functional group and stereochemistry (272). Thus, our study supports the notion that MAs elicit immune responses in a meromycolate structure-dependent way. Mtb is therefore seemingly able to modulate immune responses by changing MA class content in its cell wall, dictating virulence and pathogenicity. This is represented in the fact that virulent and non-virulent Mtb strains have different MA compositions in their cell walls, with Mtb containing largely alpha mycolates with cyclopropane groups in *cis*- stereo-arrangement, most similar in structure to our prototypic ligand JR1080 (304). This lends itself as another

possible mechanism where virulent Mtb drives an immune response to its advantage. Understanding these immune responses will be vital in development of new vaccines and therapeutics.

6.9 Unresolved immunity to Mtb

Immunity toward infection is complex crosstalk between pathogen, innate and adaptive cells, generating an environmental milieu of pro- and anti-inflammatory mediators that require fine balancing. In Mtb-directed immunity, response time is also very likely just as important as the response itself (95). Early recognition of Mtb pathogen associated molecular patterns (PAMPs) such as LAM, PIM, ESAT-6 and CFP-10 through PRRs contribute to macrophage activation and release of anti- mycobacterial effectors (24), events that prove important in downstream containment of Mtb. However, many of these critical innate responses can be blocked or modulated by Mtb itself limiting their effectiveness. Nevertheless, the outcome invariably leads to a chemokine and cytokine milieu designed to attract lymphocytes and polarise a response into either Th1 or Th2. The infinite possibilities of which then dictate the nature of infection outcome along a spectrum ranging from sterilisation to aggressive active disease. Simultaneously, aggregation of immune cells in the infection locality leads to granuloma formation, a hallmark physiological feature that although once assumed to contain infection may now incubate and protect Mtb bacilli (274). Despite the first description of granulomas in the early 1900s, it was only revealed in 2015 the polyfunctional nature of granulomas. Where although most are derived from a single bacterium, heterogeneous lesions occurred through differential Mtb killing leading to highly individual outcomes (300), highlighting a lack of understanding surrounding early immune responses in Mtb infection.

However, a lack of clarity is not limited to early immune events, as contraindication can be found on the issue of host cell death within the granuloma. The central tenet of which focuses on apoptosis as beneficial to the host generating controlled cell death allowing, efficient Mtb killing. In contrast, necrosis is seen as detrimental leading to

caseation and an environment where bacterial numbers far exceed that in lesions with no necrosis (274). However, the conditions leading to necrosis are not well characterised and therefore cannot be targeted for modulation. Moreover, apoptosis can often promote bacterial dissemination, through preservation of viable bacteria within apoptotic vesicles, becoming phagocytosed by passing macrophages subsequently allowing bacterial growth and possible secondary infection (305).

Finally, once recruited, classical T cells contribute to long-term bacterial control, and are essential for mouse survival and infection control and specifically kill infected macrophages and Mtb directly through well characterised mechanisms (111, 113, 114, 116). However, evidence now suggests that while protective, over-activation of T cells can lead to increased bacterial dissemination and tissue pathology, which is ultimately detrimental to the host. An observation we also found in our immunoaugmentation studies. This brings into question the logic behind of a number of vaccines currently in development and clinical trials, that are designed to consolidate robust T cell responses. Some of these have failed and in parallel revealed activated T cells in infants are a correlate of increased disease risk (255). Indeed, in this study we have detailed unconventional CD1b restricted T cell responses toward a panel of mycolates ultimately demonstrating the possibility of customising the response generated by a conserved T cells population. This work contains many of the elements required to enable widely applicable vaccine and therapeutic development. However, the underlying question remains of what is the desirable immunological consequence of such customisation. Deconvolution of the optimal host immune response to TB is ongoing, and will require careful consideration of immunity as a whole.

Chapter 7: Future work and concluding remarks

7.1 Future Work – Investigating the role of iNKTs in Macaque model of *Mtb* infection

An interesting observation made in this project was lower affinity iNKT interaction to macaque CD1d compared to human CD1d, when loaded with αGC. This is a possible first route of investigation, analysing iNKT clones from these different species to gain an understanding of the basic biological differences surrounding the CD1d system. Cloning macaque iNKTs for further characterisation, which is not as trivial as with human iNKTs, would need to be optimised allowing investigation of the repertoire of iNKT TCRs in macaques. Clones can then be sequenced to investigate CDR loop amino acid changes at points critical for the interaction with CD1d. Previous work in rat and mouse CD1 from our group could be included to gain a full appreciation of species differences. Phenotypical and functional work may be performed on these clones, however it would be interesting to investigate whether high and low affinity clonal populations that exist in humans are maintained across all species. These investigations would allow further characterisation of iNKTs in relevant animal models of Mtb.

In addition, our study associates skewed iNKT subset ratios, and increased antigen responsive $CD4^+$ iNKTs post BCG with greater disease susceptibility and worse infection outcome. Therefore, this observation firstly needs validation in a larger cohort of macaques. In addition, detailed functional experiments of $CD4^+$, $CD8^+$ and double positive iNKT subsets across the four macaque groups are necessary. This would highlight any differences in iNKT subsets between species that could more readily explain the inherent resistance hierarchy. To investigate the functional relevance with regard to Mtb infection, the 3D bioelectrospray system developed in Southampton could be employed. This model incorporates virulent Mtb, PBMCs and collagen in a 3D cell culture model that has been validated, demonstrating modelling advantages compared to traditional 2D cell culture. Ultimately, this would allow a mechanistic understanding of the potential protective qualities of iNKTs. Indeed, validation and

identification of a protective mechanism of iNKT related correlates in Mtb would aid development of better therapeutics and vaccines, and potentially also diagnostic markers.

7.2 Future Work – Role of CD1b/MA restricted T cell in Mtb infection

To harness the potential of mycolates to elicit T cell responses for use as vaccines and therapeutics, further understanding of the basic biology is required. Our CD1b study takes one step toward understanding T cell response to diverse MAs. However, to fully characterise these responses, it would be useful to generate correctly refolded CD1b containing weak and strong MAs. This would not only enable SPR, to directly assess MA impact of affinity but also tetramer and dextramer development. These tools would allow tracking of restricted T cell population in disease, detailed phenotypic and functional cell investigation and efficient cloning to fully appreciate the T cell repertoire. Finally, soluble CD1b/MA would enable crystallisation and co-crystallisation with relevant TCRs. These structures would unequivocally reveal how such long meromycolate chain interact with CD1b, as well as elucidate the critical interactions involved in TCR binding.

The appropriate protective immune response in Mtb infection is currently not well understood and is likely complex. Therefore, to tease apart the impact of different MA structures and restricted T cell populations; the 3D bioengineered Mtb model could be employed. Not only can other TCR transduced T cell populations be incorporated into the model as we have demonstrated with the GEM C18 TCR, but also *in vitro* enriched CD1b/MA and GMM specific lines. Polyclonal lines enriched for CD1b/mycolate specific cells can be generated though persistent cell culture with lipid loaded autologous dendritic cells. Using the tractability of the 3D system, multiple readouts could be achieved dissecting the role of these T cells in controlling infection. Furthermore, there is scope for addition of strong and weak lipids which we have demonstrated can tailor the response from GEM T cells. Ultimately, this would allow a detailed investigation of

mycolates and the T cell response to delineate a protective or indeed destructive mechanism that could be harnessed for future vaccines and therapies.

Finally, the ultimate translational goal of this work is to assess the potential of mycolates as vaccines and therapeutics. This would require the use of suitable animal models, NHPs in particular due to the lack of group 1 CD1 in mice. Therefore, understanding the CD1b/mycolate system would allow investigation of the effects of strong and weak lipids administered *in vivo*.

7.3 Conclusions

NHPs are the penultimate animal model before humans, it is vital therefore to fully appreciate immune correlates for therapeutic and vaccine development. Unconventional T cells are an understudied and thus far unappreciated T cell category that likely have a central role in Mtb infection. We associate iNKT subset proportions with varying disease susceptibilities and outcome in the first investigation of iNKTs across well-characterised macaque groups. We then demonstrate an association of higher peripheral $CD8^+$ iNKTs post antigen exposure with better disease outcome in two species of macaques, and also show this subset ratio is conferred by BCG vaccination. Our study for the first time implicates iNKT subset ratios with Mtb susceptibility and disease outcome.

We also systematically investigate the effect of structurally different mycolates on a conserved T cell population called GEMs using a large panel of mycolates containing different head groups and functional lipid tail groups accurately representing those found in nature. We reveal differences in their potential to activate GEMs based on meromycolate chain functional group type and stereo-arrangements. Not only do we demonstrate this in a controlled cell system, but also in *ex vivo* polyclonal T cells and transduced T cell using multiple readouts. Finally, we show this activation hierarchy is processing independent, supported by molecular dynamics, which identify weak MAs have increased mobility within the CD1b binding groove. Given the public nature of the

GEM T cell population and the ability of our MAs to tailor the response, the implications of these findings extend to MA derived vaccine and therapeutic development.

As is the case for many infectious diseases, tissue destruction mediated by immunity is often more detrimental to the host than the pathogen itself. Initial recognition of Mtb activates innate cells, which interact with both Mtb and adaptive immunity to define whether pathology develops or infection is resolved. Immune regulation therefore is clearly vital in generating an effective response to remove the pathogen while preventing permanent tissue damage. Although this project focuses on CD1b and CD1d restricted T cells, resolution of TB infection needs to be considered on a more holistic level involving more than one cell type or cytokine. To properly deal with infection, there needs to be a well-organised and rapid response, with a good balance of inflammatory and anti-inflammatory cytokines. Orchestrating an appropriate immune response is perhaps co-ordinated by CD1d restricted iNKTs and in part executed by CD1b restricted T cells, given the fundamental importance of lipids to Mtb, particularly mycolates. Understanding these responses is the first step to their manipulation for more consistent protection against TB.

Chapter 8: Bibliography

1. Barral DC, Brenner MB. CD1 antigen presentation: how it works. Nature reviews Immunology. 2007;7(12):929-41.

2. Nunes-Alves C, Booty MG, Carpenter SM, Jayaraman P, Rothchild AC, Behar SM. In search of a new paradigm for protective immunity to TB. Nat Rev Microbiol. 2014;12(4):289-99.

3. Dorman SE. New diagnostic tests for tuberculosis: bench, bedside, and beyond. Clinical infectious diseases : an official publication of the Infectious Diseases Society of America. 2010;50 Suppl 3:S173-7.

4. Hunter RL, Olsen MR, Jagannath C, Actor JK. Multiple roles of cord factor in the pathogenesis of primary, secondary, and cavitary tuberculosis, including a revised description of the pathology of secondary disease. Annals of clinical and laboratory science. 2006;36(4):371-86.

5. Wolf AJ, Linas B, Trevejo-Nunez GJ, Kincaid E, Tamura T, Takatsu K, et al. Mycobacterium tuberculosis infects dendritic cells with high frequency and impairs their function in vivo. Journal of immunology. 2007;179(4):2509-19.

6. Bermudez LE, Goodman J. Mycobacterium tuberculosis invades and replicates within type II alveolar cells. Infection and immunity. 1996;64(4):1400-6.

7. Quast TM, Browning RF. Pathogenesis and clinical manifestations of pulmonary tuberculosis. Disease-a-month : DM. 2006;52(11-12):413-9.

8. Dheda K, Booth H, Huggett JF, Johnson MA, Zumla A, Rook GA. Lung remodeling in pulmonary tuberculosis. The Journal of infectious diseases. 2005;192(7):1201-9.

9. Russell DG. Mycobacterium tuberculosis: Here today, and here tomorrow. Nat Rev Mol Cell Bio. 2001;2(8):569-77.

10. Vergne I, Chua J, Singh SB, Deretic V. Cell biology of mycobacterium tuberculosis phagosome. Annual review of cell and developmental biology. 2004;20:367-94.

11. Smith I. Mycobacterium tuberculosis pathogenesis and molecular determinants of virulence. Clinical microbiology reviews. 2003;16(3):463-96.

12. Peyron P, Vaubourgeix J, Poquet Y, Levillain F, Botanch C, Bardou F, et al. Foamy macrophages from tuberculous patients' granulomas constitute a nutrient-rich reservoir for M. tuberculosis persistence. PLoS pathogens. 2008;4(11):e1000204.

13. Knechel NA. Tuberculosis: pathophysiology, clinical features, and diagnosis. Critical care nurse. 2009;29(2):34-43; quiz 4.

14. Silva Miranda M, Breiman A, Allain S, Deknuydt F, Altare F. The tuberculous granuloma: an unsuccessful host defence mechanism providing a safety shelter for the bacteria? Clinical & developmental immunology. 2012;2012:139127.

15. Yamada H, Mizumo S, Horai R, Iwakura Y, Sugawara I. Protective role of interleukin-1 in mycobacterial infection in IL-1 alpha/beta double-knockout mice. Lab Invest. 2000;80(5):759-67.

16. Sugawara I, Yamada H, Hua S, Mizuno S. Role of interleukin (IL)-1 type 1 receptor in mycobacterial infection. Microbiol Immunol. 2001;45(11):743-50.

17. Gopal R, Monin L, Slight S, Uche U, Blanchard E, Fallert Junecko BA, et al. Unexpected role for IL-17 in protective immunity against hypervirulent Mycobacterium tuberculosis HN878 infection. PLoS pathogens. 2014;10(5):e1004099.

18. Khader SA, Guglani L, Rangel-Moreno J, Gopal R, Junecko BA, Fountain JJ, et al. IL-23 is required for long-term control of Mycobacterium tuberculosis and B cell follicle formation in the infected lung. Journal of immunology. 2011;187(10):5402-7.

19. Khader SA, Partida-Sanchez S, Bell G, Jelley-Gibbs DM, Swain S, Pearl JE, et al. Interleukin 12p40 is required for dendritic cell migration and T cell priming after Mycobacterium tuberculosis infection. The Journal of experimental medicine. 2006;203(7):1805-15.

20. Altare F, Durandy A, Lammas D, Emile JF, Lamhamedi S, Le Deist F, et al. Impairment of mycobacterial immunity in human interleukin-12 receptor deficiency. Science. 1998;280(5368):1432-5.

21. Appelberg R, Castro AG, Pedrosa J, Minoprio P. Role of interleukin-6 in the induction of protective T cells during mycobacterial infections in mice. Immunology. 1994;82(3):361-4.

22. Saunders BM, Frank AA, Orme IM, Cooper AM. Interleukin-6 induces early gamma interferon production in the infected lung but is not required for generation of specific immunity to Mycobacterium tuberculosis infection. Infection and immunity. 2000;68(6):3322-6.

23. Flynn JL, Chan J, Triebold KJ, Dalton DK, Stewart TA, Bloom BR. An essential role for interferon gamma in resistance to Mycobacterium tuberculosis infection. The Journal of experimental medicine. 1993;178(6):2249-54.

24. Herbst S, Schaible UE, Schneider BE. Interferon gamma activated macrophages kill mycobacteria by nitric oxide induced apoptosis. PloS one. 2011;6(5):e19105.

25. Redford PS, Mayer-Barber KD, McNab FW, Stavropoulos E, Wack A, Sher A, et al. Influenza A virus impairs control of Mycobacterium tuberculosis coinfection through a type I interferon receptor-dependent pathway. The Journal of infectious diseases. 2014;209(2):270-4.

26. Berry MP, Graham CM, McNab FW, Xu Z, Bloch SA, Oni T, et al. An interferon-inducible neutrophil-driven blood transcriptional signature in human tuberculosis. Nature. 2010;466(7309):973-7.

27. Slight SR, Khader SA. Chemokines shape the immune responses to tuberculosis. Cytokine Growth Factor Rev. 2013;24(2):105-13.

28. Algood HM, Lin PL, Flynn JL. Tumor necrosis factor and chemokine interactions in the formation and maintenance of granulomas in tuberculosis. Clinical infectious diseases : an official publication of the Infectious Diseases Society of America. 2005;41 Suppl 3:S189-93.

29. Hickman SP, Chan J, Salgame P. Mycobacterium tuberculosis induces differential cytokine production from dendritic cells and macrophages with divergent effects on naive T cell polarization. Journal of immunology. 2002;168(9):4636-42.

30. Calderon VE, Valbuena G, Goez Y, Judy BM, Huante MB, Sutjita P, et al. A humanized mouse model of tuberculosis. PloS one. 2013;8(5):e63331.

31. De Groote MA, Gilliland JC, Wells CL, Brooks EJ, Woolhiser LK, Gruppo V, et al. Comparative studies evaluating mouse models used for efficacy testing of experimental drugs against Mycobacterium tuberculosis. Antimicrobial agents and chemotherapy. 2011;55(3):1237-47.

32. Flynn JL. Lessons from experimental Mycobacterium tuberculosis infections. Microbes and infection / Institut Pasteur. 2006;8(4):1179-88.

33. Helke KL, Mankowski JL, Manabe YC. Animal models of cavitation in pulmonary tuberculosis. Tuberculosis. 2006;86(5):337-48.

34. Felio K, Nguyen H, Dascher CC, Choi HJ, Li S, Zimmer MI, et al. CD1-restricted adaptive immune responses to Mycobacteria in human group 1 CD1 transgenic mice. The Journal of experimental medicine. 2009;206(11):2497-509.

35. Kaushal D, Mehra S, Didier PJ, Lackner AA. The non-human primate model of tuberculosis. Journal of medical primatology. 2012;41(3):191-201.

36. Berg RD, Ramakrishnan L. Insights into tuberculosis from the zebrafish model. Trends in molecular medicine. 2012;18(12):689-90.

37. Gupta UD, Katoch VM. Animal models of tuberculosis. Tuberculosis. 2005;85(5-6):277-93.

38. Barclay WR, Busey WM, Dalgard DW, Good RC, Janicki BW, Kasik JE, et al. Protection of monkeys against airborne tuberculosis by aerosol vaccination with bacillus Calmette-Guerin. The American review of respiratory disease. 1973;107(3):351-8.

39. Good RC. Biology of the mycobacterioses. Simian tuberculosis: immunologic aspects. Annals of the New York Academy of Sciences. 1968;154(1):200-13.

40. Hu SL. Non-human primate models for AIDS vaccine research. Current drug targets Infectious disorders. 2005;5(2):193-201.

41. Morita D, Katoh K, Harada T, Nakagawa Y, Matsunaga I, Miura T, et al. Trans-species activation of human T cells by rhesus macaque CD1b molecules. Biochemical and biophysical research communications. 2008;377(3):889-93.

42. McMichael AJ, Pilch JR, Galfre G, Mason DY, Fabre JW, Milstein C. A human thymocyte antigen defined by a hybrid myeloma monoclonal antibody. European journal of immunology. 1979;9(3):205-10.

43. Martin LH, Calabi F, Milstein C. Isolation of CD1 genes: a family of major histocompatibility complex-related differentiation antigens. Proceedings of the National Academy of Sciences of the United States of America. 1986;83(23):9154-8.

44. Facciotti F, Cavallari M, Angenieux C, Garcia-Alles LF, Signorino-Gelo F, Angman L, et al. Fine tuning by human CD1e of lipid-specific immune responses. Proceedings of the National Academy of Sciences of the United States of America. 2011;108(34):14228-33.

45. Guerin L, Wu V, Houser B, Tilburgs T, de Jong A, Moody DB, et al. CD1 Antigen Presentation and Autoreactivity in the Pregnant Human Uterus. Am J Reprod Immunol. 2015;74(2):126-35.

46. Melian A, Geng YJ, Sukhova GK, Libby P, Porcelli SA. CD1 expression in human atherosclerosis. A potential mechanism for T cell activation by foam cells. The American journal of pathology. 1999;155(3):775-86.

47. Canchis PW, Bhan AK, Landau SB, Yang L, Balk SP, Blumberg RS. Tissue distribution of the non-polymorphic major histocompatibility complex class I-like molecule, CD1d. Immunology. 1993;80(4):561-5.

48. Porcelli SA. The CD1 family: a third lineage of antigen-presenting molecules. Advances in immunology. 1995;59:1-98.

49. Zajonc DM, Crispin MD, Bowden TA, Young DC, Cheng TY, Hu J, et al. Molecular mechanism of lipopeptide presentation by CD1a. Immunity. 2005;22(2):209-19.

50. Dascher CC, Brenner MB. Evolutionary constraints on CD1 structure: insights from comparative genomic analysis. Trends in immunology. 2003;24(8):412-8.

51. Porcelli SA. Bird genes give new insights into the origins of lipid antigen presentation. Proceedings of the National Academy of Sciences of the United States of America. 2005;102(24):8399-400.

52. Han M, Hannick LI, DiBrino M, Robinson MA. Polymorphism of human CD1 genes. Tissue antigens. 1999;54(2):122-7.

53. Mirones I, Oteo M, Parra-Cuadrado JF, Martinez-Naves E. Identification of two novel human CD1E alleles. Tissue antigens. 2000;56(2):159-61.

54. Porcelli SA. Bird genes give new insights into the origins of lipid antigen presentation. Proceedings of the National Academy of Sciences of the United States of America. 2005;102(24):8399-400.

55. Sugita M, Jackman RM, van Donselaar E, Behar SM, Rogers RA, Peters PJ, et al. Cytoplasmic tail-dependent localization of CD1b antigen-presenting molecules to MIICs. Science. 1996;273(5273):349-52.

56. Moody DB, Porcelli SA. CD1 trafficking: invariant chain gives a new twist to the tale. Immunity. 2001;15(6):861-5.

57. Sugita M, Grant EP, van Donselaar E, Hsu VW, Rogers RA, Peters PJ, et al. Separate pathways for antigen presentation by CD1 molecules. Immunity. 1999;11(6):743-52.

58. Cernadas M, Cavallari M, Watts G, Mori L, De Libero G, Brenner MB. Early recycling compartment trafficking of CD1a is essential for its intersection and presentation of lipid antigens. Journal of immunology. 2010;184(3):1235-41.

59. Sugita M, van Der Wel N, Rogers RA, Peters PJ, Brenner MB. CD1c molecules broadly survey the endocytic system. Proceedings of the National Academy of Sciences of the United States of America. 2000;97(15):8445-50.

60. Cala-De Paepe D, Layre E, Giacometti G, Garcia-Alles LF, Mori L, Hanau D, et al. Deciphering the role of CD1e protein in mycobacterial phosphatidyl-myo-inositol mannosides (PIM) processing for presentation by CD1b to T lymphocytes. The Journal of biological chemistry. 2012;287(37):31494-502.

61. Batuwangala T, Shepherd D, Gadola SD, Gibson KJ, Zaccai NR, Fersht AR, et al. The crystal structure of human CD1b with a bound bacterial glycolipid. Journal of immunology. 2004;172(4):2382-8.

62. Mansour S, Tocheva AS, Cave-Ayland C, Machelett MM, Sander B, Lissin NM, et al. Cholesteryl esters stabilize human CD1c conformations for recognition by self-reactive T cells. Proceedings of the National Academy of Sciences of the United States of America. 2016;113(9):E1266-75.

63. Koch M, Stronge VS, Shepherd D, Gadola SD, Mathew B, Ritter G, et al. The crystal structure of human CD1d with and without alpha-galactosylceramide. Nature immunology. 2005;6(8):819-26.

64. Ernst WA, Maher J, Cho S, Niazi KR, Chatterjee D, Moody DB, et al. Molecular interaction of CD1b with lipoglycan antigens. Immunity. 1998;8(3):331-40.

65. Moody DB, Guy MR, Grant E, Cheng TY, Brenner MB, Besra GS, et al. CD1b-mediated T cell recognition of a glycolipid antigen generated from mycobacterial lipid and host carbohydrate during infection. The Journal of experimental medicine. 2000;192(7):965-76.

66. Shamshiev A, Donda A, Prigozy TI, Mori L, Chigorno V, Benedict CA, et al. The alphabeta T cell response to self-glycolipids shows a novel mechanism of CD1b loading and a requirement for complex oligosaccharides. Immunity. 2000;13(2):255-64.

67. Van Rhijn I, van Berlo T, Hilmenyuk T, Cheng TY, Wolf BJ, Tatituri RV, et al. Human autoreactive T cells recognize CD1b and phospholipids. Proceedings of the National Academy of Sciences of the United States of America. 2016;113(2):380-5.

68. Garcia-Alles LF, Versluis K, Maveyraud L, Vallina AT, Sansano S, Bello NF, et al. Endogenous phosphatidylcholine and a long spacer ligand stabilize the lipid-binding groove of CD1b. EMBO J. 2006;25(15):3684-92.

69. Gadola SD, Zaccai NR, Harlos K, Shepherd D, Castro-Palomino JC, Ritter G, et al. Structure of human CD1b with bound ligands at 2.3 A, a maze for alkyl chains. Nature immunology. 2002;3(8):721-6.

70. Moody DB, Briken V, Cheng TY, Roura-Mir C, Guy MR, Geho DH, et al. Lipid length controls antigen entry into endosomal and nonendosomal pathways for CD1b presentation. Nature immunology. 2002;3(5):435-42.

71. Brennan PJ, Lehane DP. Composition of the phospholipid fraction of Corynebacterium diphtheriae. The Biochemical journal. 1969;115(3):8P.

72. Moody DB, Reinhold BB, Guy MR, Beckman EM, Frederique DE, Furlong ST, et al. Structural requirements for glycolipid antigen recognition by CD1b-restricted T cells. Science. 1997;278(5336):283-6.

73. Lawton AP, Kronenberg M. The Third Way: Progress on pathways of antigen processing and presentation by CD1. Immunology and cell biology. 2004;82(3):295-306.

74. Brennan PJ, Brigl M, Brenner MB. Invariant natural killer T cells: an innate activation scheme linked to diverse effector functions. Nature reviews Immunology. 2013;13(2):101-17.

75. Kim J, Kim JH, Winau F. Thinking inside the box: endogenous alpha-anomeric lipid antigens. Immunity. 2014;41(4):505-6.

76. O'Konek JJ, Illarionov P, Khursigara DS, Ambrosino E, Izhak L, Castillo BF, 2nd, et al. Mouse and human iNKT cell agonist beta-mannosylceramide reveals a distinct mechanism of tumor immunity. The Journal of clinical investigation. 2011;121(2):683-94.

77. Godfrey DI, Kronenberg M. Going both ways: immune regulation via CD1d-dependent NKT cells. The Journal of clinical investigation. 2004;114(10):1379-88.

78. Matsuda JL, Naidenko OV, Gapin L, Nakayama T, Taniguchi M, Wang CR, et al. Tracking the response of natural killer T cells to a glycolipid antigen using CD1d tetramers. The Journal of experimental medicine. 2000;192(5):741-54.

79. Behar SM, Podrebarac TA, Roy CJ, Wang CR, Brenner MB. Diverse TCRs recognize murine CD1. Journal of immunology. 1999;162(1):161-7.

80. Brigl M, Bry L, Kent SC, Gumperz JE, Brenner MB. Mechanism of CD1d-restricted natural killer T cell activation during microbial infection. Nature immunology. 2003;4(12):1230-7.

81. Kinjo Y, Illarionov P, Vela JL, Pei B, Girardi E, Li X, et al. Invariant natural killer T cells recognize glycolipids from pathogenic Gram-positive bacteria. Nature immunology. 2011;12(10):966-74.

82. Brennan PJ, Tatituri RV, Brigl M, Kim EY, Tuli A, Sanderson JP, et al. Invariant natural killer T cells recognize lipid self antigen induced by microbial danger signals. Nature immunology. 2011;12(12):1202-11.

83. Brigl M, Tatituri RV, Watts GF, Bhowruth V, Leadbetter EA, Barton N, et al. Innate and cytokine-driven signals, rather than microbial antigens, dominate in natural killer T cell activation during microbial infection. The Journal of experimental medicine. 2011;208(6):1163-77.

84. Sriram V, Du W, Gervay-Hague J, Brutkiewicz RR. Cell wall glycosphingolipids of Sphingomonas paucimobilis are CD1d-specific ligands for NKT cells. European journal of immunology. 2005;35(6):1692-701.

85. Mattner J, Debord KL, Ismail N, Goff RD, Cantu C, 3rd, Zhou D, et al. Exogenous and endogenous glycolipid antigens activate NKT cells during microbial infections. Nature. 2005;434(7032):525-9.

86. Kinjo Y, Wu D, Kim G, Xing GW, Poles MA, Ho DD, et al. Recognition of bacterial glycosphingolipids by natural killer T cells. Nature. 2005;434(7032):520-5.

87. Amprey JL, Im JS, Turco SJ, Murray HW, Illarionov PA, Besra GS, et al. A subset of liver NK T cells is activated during Leishmania donovani infection by CD1d-bound lipophosphoglycan. The Journal of experimental medicine. 2004;200(7):895-904.

88. Lotter H, Gonzalez-Roldan N, Lindner B, Winau F, Isibasi A, Moreno-Lafont M, et al. Natural killer T cells activated by a lipopeptidophosphoglycan from Entamoeba histolytica are critically important to control amebic liver abscess. PLoS pathogens. 2009;5(5):e1000434.

89. Gapin L. iNKT cell autoreactivity: what is 'self' and how is it recognized? Nature reviews Immunology. 2010;10(4):272-7.

90. Zhou D, Mattner J, Cantu C, 3rd, Schrantz N, Yin N, Gao Y, et al. Lysosomal glycosphingolipid recognition by NKT cells. Science. 2004;306(5702):1786-9.

91. Speak AO, Salio M, Neville DC, Fontaine J, Priestman DA, Platt N, et al. Implications for invariant natural killer T cell ligands due to the restricted presence of isoglobotrihexosylceramide in mammals. Proceedings of the National Academy of Sciences of the United States of America. 2007;104(14):5971-6.

92. Sanderson JP, Brennan PJ, Mansour S, Matulis G, Patel O, Lissin N, et al. CD1d protein structure determines species-selective antigenicity of isoglobotrihexosylceramide (iGb3) to invariant NKT cells. European journal of immunology. 2013;43(3):815-25.

93. Coquet JM, Chakravarti S, Kyparissoudis K, McNab FW, Pitt LA, McKenzie BS, et al. Diverse cytokine production by NKT cell subsets and identification of an IL-17-producing CD4-NK1.1- NKT cell population. Proceedings of the National Academy of Sciences of the United States of America. 2008;105(32):11287-92.

94. Crowe NY, Coquet JM, Berzins SP, Kyparissoudis K, Keating R, Pellicci DG, et al. Differential antitumor immunity mediated by NKT cell subsets in vivo. The Journal of experimental medicine. 2005;202(9):1279-88.

95. Winslow GM, Cooper A, Reiley W, Chatterjee M, Woodland DL. Early T-cell responses in tuberculosis immunity. Immunological reviews. 2008;225:284-99.

96. Ehrt S, Schnappinger D. Mycobacterial survival strategies in the phagosome: defence against host stresses. Cell Microbiol. 2009;11(8):1170-8.

97. Seitzer U, Kayser K, Hohn H, Entzian P, Wacker HH, Ploetz S, et al. Reduced T-cell receptor CD3zeta-chain protein and sustained CD3epsilon expression at the site of mycobacterial infection. Immunology. 2001;104(3):269-77.

98. Mahon RN, Rojas RE, Fulton SA, Franko JL, Harding CV, Boom WH. Mycobacterium tuberculosis cell wall glycolipids directly inhibit CD4+ T-cell activation by interfering with proximal T-cell-receptor signaling. Infection and immunity. 2009;77(10):4574-83.

99. Baena A, Porcelli SA. Evasion and subversion of antigen presentation by Mycobacterium tuberculosis. Tissue antigens. 2009;74(3):189-204.

100. Schaible UE, Winau F, Sieling PA, Fischer K, Collins HL, Hagens K, et al. Apoptosis facilitates antigen presentation to T lymphocytes through MHC-I and CD1 in tuberculosis. Nature medicine. 2003;9(8):1039-46.

101. Newton K, Dixit VM. Signaling in innate immunity and inflammation. Cold Spring Harb Perspect Biol. 2012;4(3).

102. Akira S, Hemmi H. Recognition of pathogen-associated molecular patterns by TLR family. Immunology letters. 2003;85(2):85-95.

103. Hugues S, Fetler L, Bonifaz L, Helft J, Amblard F, Amigorena S. Distinct T cell dynamics in lymph nodes during the induction of tolerance and immunity. Nature immunology. 2004;5(12):1235-42.

104. Chen YH, Chiu NM, Mandal M, Wang N, Wang CR. Impaired NK1+ T cell development and early IL-4 production in CD1-deficient mice. Immunity. 1997;6(4):459-67.

105. Stetson DB, Mohrs M, Reinhardt RL, Baron JL, Wang ZE, Gapin L, et al. Constitutive cytokine mRNAs mark natural killer (NK) and NK T cells poised for rapid effector function. The Journal of experimental medicine. 2003;198(7):1069-76.

106. Huang S, Moody DB. Donor-unrestricted T cells in the human CD1 system. Immunogenetics. 2016;68(8):577-96.

107. Montamat-Sicotte DJ, Millington KA, Willcox CR, Hingley-Wilson S, Hackforth S, Innes J, et al. A mycolic acid-specific CD1-restricted T cell population contributes to acute and memory immune responses in human tuberculosis infection. The Journal of clinical investigation. 2011;121(6):2493-503.

108. Pawlowski A, Jansson M, Skold M, Rottenberg ME, Kallenius G. Tuberculosis and HIV co-infection. PLoS pathogens. 2012;8(2):e1002464.

109. Hogan LH, Macvilay K, Barger B, Co D, Malkovska I, Fennelly G, et al. Mycobacterium bovis strain bacillus Calmette-Guerin-induced liver granulomas contain a diverse TCR repertoire, but a monoclonal T cell population is sufficient for protective granuloma formation. Journal of immunology. 2001;166(10):6367-75.

110. Nunes-Alves C, Booty MG, Carpenter SM, Rothchild AC, Martin CJ, Desjardins D, et al. Human and Murine Clonal CD8+ T Cell Expansions Arise during Tuberculosis Because of TCR Selection. PLoS pathogens. 2015;11(5):e1004849.

111. Caruso AM, Serbina N, Klein E, Triebold K, Bloom BR, Flynn JL. Mice deficient in CD4 T cells have only transiently diminished levels of IFN-gamma, yet succumb to tuberculosis. Journal of immunology. 1999;162(9):5407-16.

112. Egen JG, Rothfuchs AG, Feng CG, Horwitz MA, Sher A, Germain RN. Intravital imaging reveals limited antigen presentation and T cell effector function in mycobacterial granulomas. Immunity. 2011;34(5):807-19.

113. Serbina NV, Lazarevic V, Flynn JL. CD4(+) T cells are required for the development of cytotoxic CD8(+) T cells during Mycobacterium tuberculosis infection. Journal of immunology. 2001;167(12):6991-7000.

114. Sud D, Bigbee C, Flynn JL, Kirschner DE. Contribution of CD8+ T cells to control of Mycobacterium tuberculosis infection. Journal of immunology. 2006;176(7):4296-314.

115. Brookes RH, Pathan AA, McShane H, Hensmann M, Price DA, Hill AV. CD8+ T cell-mediated suppression of intracellular Mycobacterium tuberculosis growth in activated human macrophages. European journal of immunology. 2003;33(12):3293-302.

116. Canaday DH, Wilkinson RJ, Li Q, Harding CV, Silver RF, Boom WH. CD4(+) and CD8(+) T cells kill intracellular Mycobacterium tuberculosis by a perforin and Fas/Fas ligand-independent mechanism. Journal of immunology. 2001;167(5):2734-42.

117. Flynn JL, Goldstein MM, Triebold KJ, Koller B, Bloom BR. Major histocompatibility complex class I-restricted T cells are required for resistance to Mycobacterium tuberculosis infection. Proceedings of the National Academy of Sciences of the United States of America. 1992;89(24):12013-7.

118. Darrah PA, Patel DT, De Luca PM, Lindsay RW, Davey DF, Flynn BJ, et al. Multifunctional TH1 cells define a correlate of vaccine-mediated protection against Leishmania major. Nature medicine. 2007;13(7):843-50.

119. Caccamo N, Guggino G, Joosten SA, Gelsomino G, Di Carlo P, Titone L, et al. Multifunctional CD4(+) T cells correlate with active Mycobacterium tuberculosis infection. European journal of immunology. 2010;40(8):2211-20.

120. Forbes EK, Sander C, Ronan EO, McShane H, Hill AV, Beverley PC, et al. Multifunctional, high-level cytokine-producing Th1 cells in the lung, but not spleen, correlate with protection against Mycobacterium tuberculosis aerosol challenge in mice. Journal of immunology. 2008;181(7):4955-64.

121. Kalsdorf B, Scriba TJ, Wood K, Day CL, Dheda K, Dawson R, et al. HIV-1 infection impairs the bronchoalveolar T-cell response to mycobacteria. American journal of respiratory and critical care medicine. 2009;180(12):1262-70.

122. Qiu Z, Zhang M, Zhu Y, Zheng F, Lu P, Liu H, et al. Multifunctional CD4 T cell responses in patients with active tuberculosis. Sci Rep. 2012;2:216.

123. Godfrey DI, Uldrich AP, McCluskey J, Rossjohn J, Moody DB. The burgeoning family of unconventional T cells. Nature immunology. 2015;16(11):1114-23.

124. Kasmar AG, Van Rhijn I, Magalhaes KG, Young DC, Cheng TY, Turner MT, et al. Cutting Edge: CD1a tetramers and dextramers identify human lipopeptide-specific T cells ex vivo. Journal of immunology. 2013;191(9):4499-503.

125. Kasmar AG, van Rhijn I, Cheng TY, Turner M, Seshadri C, Schiefner A, et al. CD1b tetramers bind alpha beta T cell receptors to identify a mycobacterial glycolipid-reactive T cell repertoire in humans. Journal of Experimental Medicine. 2011;208(9):1741-7.

126. Ly D, Kasmar AG, Cheng TY, de Jong A, Huang S, Roy S, et al. CD1c tetramers detect ex vivo T cell responses to processed phosphomycoketide antigens. The Journal of experimental medicine. 2013;210(4):729-41.

127. de Jong A, Cheng TY, Huang S, Gras S, Birkinshaw RW, Kasmar AG, et al. CD1a-autoreactive T cells recognize natural skin oils that function as headless antigens. Nature immunology. 2014;15(2):177-85.

128. Bourgeois EA, Subramaniam S, Cheng TY, De Jong A, Layre E, Ly D, et al. Bee venom processes human skin lipids for presentation by CD1a. The Journal of experimental medicine. 2015;212(2):149-63.

129. de Jong A, Pena-Cruz V, Cheng TY, Clark RA, Van Rhijn I, Moody DB. CD1a-autoreactive T cells are a normal component of the human alphabeta T cell repertoire. Nature immunology. 2010;11(12):1102-9.

130. Rosat JP, Grant EP, Beckman EM, Dascher CC, Sieling PA, Frederique D, et al. CD1-restricted microbial lipid antigen-specific recognition found in the CD8+ alpha beta T cell pool. Journal of immunology. 1999;162(1):366-71.

131. Moody DB, Young DC, Cheng TY, Rosat JP, Roura-Mir C, O'Connor PB, et al. T cell activation by lipopeptide antigens. Science. 2004;303(5657):527-31.

132. Zhao J, Siddiqui S, Shang S, Bian Y, Bagchi S, He Y, et al. Mycolic acid-specific T cells protect against Mycobacterium tuberculosis infection in a humanized transgenic mouse model. Elife. 2015;4.

133. Ulrichs T, Moody DB, Grant E, Kaufmann SH, Porcelli SA. T-cell responses to CD1-presented lipid antigens in humans with Mycobacterium tuberculosis infection. Infection and immunity. 2003;71(6):3076-87.

134. Van Rhijn I, Kasmar A, de Jong A, Gras S, Bhati M, Doorenspleet ME, et al. A conserved human T cell population targets mycobacterial antigens presented by CD1b. Nature immunology. 2013;14(7):706-13.

135. Seshadri C, Lin L, Scriba TJ, Peterson G, Freidrich D, Frahm N, et al. T Cell Responses against Mycobacterial Lipids and Proteins Are Poorly Correlated in South African Adolescents. Journal of immunology. 2015;195(10):4595-603.

136. Sieling PA, Chatterjee D, Porcelli SA, Prigozy TI, Mazzaccaro RJ, Soriano T, et al. CD1-restricted T cell recognition of microbial lipoglycan antigens. Science. 1995;269(5221):227-30.

137. Gilleron M, Stenger S, Mazorra Z, Wittke F, Mariotti S, Bohmer G, et al. Diacylated sulfoglycolipids are novel mycobacterial antigens stimulating CD1-restricted T cells during infection with Mycobacterium tuberculosis. The Journal of experimental medicine. 2004;199(5):649-59.

138. Busch M, Herzmann C, Kallert S, Zimmermann A, Hofer C, Mayer D, et al. Lipoarabinomannan-responsive Polycytotoxic T Cells are Associated With Protection in Human Tuberculosis. American journal of respiratory and critical care medicine. 2016.

139. Beckman EM, Melian A, Behar SM, Sieling PA, Chatterjee D, Furlong ST, et al. CD1c restricts responses of mycobacteria-specific T cells. Evidence for antigen presentation by a second member of the human CD1 family. Journal of immunology. 1996;157(7):2795-803.

140. Moody DB, Ulrichs T, Muhlecker W, Young DC, Gurcha SS, Grant E, et al. CD1c-mediated T-cell recognition of isoprenoid glycolipids in Mycobacterium tuberculosis infection. Nature. 2000;404(6780):884-8.

141. de Jong A, Arce EC, Cheng TY, van Summeren RP, Feringa BL, Dudkin V, et al. CD1c presentation of synthetic glycolipid antigens with foreign alkyl branching motifs. Chemistry & biology. 2007;14(11):1232-42.

142. Scharf L, Li NS, Hawk AJ, Garzon D, Zhang T, Fox LM, et al. The 2.5 A structure of CD1c in complex with a mycobacterial lipid reveals an open groove ideally suited for diverse antigen presentation. Immunity. 2010;33(6):853-62.

143. Shinkai K, Locksley RM. CD1, tuberculosis, and the evolution of major histocompatibility complex molecules. The Journal of experimental medicine. 2000;191(6):907-14.

144. Kjer-Nielsen L, Patel O, Corbett AJ, Le Nours J, Meehan B, Liu L, et al. MR1 presents microbial vitamin B metabolites to MAIT cells. Nature. 2012;491(7426):717-23.

145. Meierovics A, Yankelevich WJ, Cowley SC. MAIT cells are critical for optimal mucosal immune responses during in vivo pulmonary bacterial infection. Proceedings of the National Academy of Sciences of the United States of America. 2013;110(33):E3119-28.

146. Le Bourhis L, Martin E, Peguillet I, Guihot A, Froux N, Core M, et al. Antimicrobial activity of mucosal-associated invariant T cells. Nature immunology. 2010;11(8):701-8.

147. Gold MC, Napier RJ, Lewinsohn DM. MR1-restricted mucosal associated invariant T (MAIT) cells in the immune response to Mycobacterium tuberculosis. Immunological reviews. 2015;264(1):154-66.

148. Morita CT, Beckman EM, Bukowski JF, Tanaka Y, Band H, Bloom BR, et al. Direct presentation of nonpeptide prenyl pyrophosphate antigens to human gamma delta T cells. Immunity. 1995;3(4):495-507.

149. Kabelitz D, Bender A, Prospero T, Wesselborg S, Janssen O, Pechhold K. The primary response of human gamma/delta + T cells to Mycobacterium tuberculosis is restricted to V gamma 9-bearing cells. The Journal of experimental medicine. 1991;173(6):1331-8.

150. Garcia VE, Sieling PA, Gong J, Barnes PF, Uyemura K, Tanaka Y, et al. Single-cell cytokine analysis of gamma delta T cell responses to nonpeptide mycobacterial antigens. Journal of immunology. 1997;159(3):1328-35.

151. Munk ME, Gatrill AJ, Kaufmann SH. Target cell lysis and IL-2 secretion by gamma/delta T lymphocytes after activation with bacteria. Journal of immunology. 1990;145(8):2434-9.

152. Tsukaguchi K, Balaji KN, Boom WH. CD4+ alpha beta T cell and gamma delta T cell responses to Mycobacterium tuberculosis. Similarities and differences in Ag recognition, cytotoxic effector function, and cytokine production. Journal of immunology. 1995;154(4):1786-96.

153. Barnes PF, Grisso CL, Abrams JS, Band H, Rea TH, Modlin RL. Gamma delta T lymphocytes in human tuberculosis. The Journal of infectious diseases. 1992;165(3):506-12.

154. MacDonald HR, Radtke F, Wilson A. T cell fate specification and alphabeta/gammadelta lineage commitment. Current opinion in immunology. 2001;13(2):219-24.

155. Ioannidis V, Beermann F, Clevers H, Held W. The beta-catenin--TCF-1 pathway ensures CD4(+)CD8(+) thymocyte survival. Nature immunology. 2001;2(8):691-7.

156. Wilkinson RW, Anderson G, Owen JJ, Jenkinson EJ. Positive selection of thymocytes involves sustained interactions with the thymic microenvironment. Journal of immunology. 1995;155(11):5234-40.

157. Noel PJ, Alegre ML, Reiner SL, Thompson CB. Impaired negative selection in CD28-deficient mice. Cell Immunol. 1998;187(2):131-8.

158. Wong P, Barton GM, Forbush KA, Rudensky AY. Dynamic tuning of T cell reactivity by self-peptide-major histocompatibility complex ligands. The Journal of experimental medicine. 2001;193(10):1179-87.

159. Dautigny N, Lucas B. Developmental regulation of TCR efficiency. European journal of immunology. 2000;30(9):2472-8.

160. Lucas B, Stefanova I, Yasutomo K, Dautigny N, Germain RN. Divergent changes in the sensitivity of maturing T cells to structurally related ligands underlies formation of a useful T cell repertoire. Immunity. 1999;10(3):367-76.

161. Bendelac A, Rivera MN, Park SH, Roark JH. Mouse CD1-specific NK1 T cells: development, specificity, and function. Annual review of immunology. 1997;15:535-62.

162. Shimamura M, Ohteki T, Beutner U, MacDonald HR. Lack of directed V alpha 14-J alpha 281 rearrangements in NK1+ T cells. European journal of immunology. 1997;27(6):1576-9.

163. Bendelac A, Savage PB, Teyton L. The biology of NKT cells. Annual review of immunology. 2007;25:297-336.

164. Lantz O, Bendelac A. An invariant T cell receptor alpha chain is used by a unique subset of major histocompatibility complex class I-specific CD4+ and CD4-8- T cells in mice and humans. The Journal of experimental medicine. 1994;180(3):1097-106.

165. Kishimoto H, Sprent J. The thymus and negative selection. Immunologic research. 2000;21(2-3):315-23.

166. Arstila TP, Casrouge A, Baron V, Even J, Kanellopoulos J, Kourilsky P. A direct estimate of the human alphabeta T cell receptor diversity. Science. 1999;286(5441):958-61.

167. Nikolich-Zugich J, Slifka MK, Messaoudi I. The many important facets of T-cell repertoire diversity. Nature reviews Immunology. 2004;4(2):123-32.

168. Gellert M. V(D)J recombination: RAG proteins, repair factors, and regulation. Annu Rev Biochem. 2002;71:101-32.

169. Montoya CJ, Catano JC, Ramirez Z, Rugeles MT, Wilson SB, Landay AL. Invariant NKT cells from HIV-1 or Mycobacterium tuberculosis-infected patients express an activated phenotype. Clinical immunology. 2008;127(1):1-6.

170. Sugawara I, Yamada H, Mizuno S, Li CY, Nakayama T, Taniguchi M. Mycobacterial infection in natural killer T cell knockout mice. Tuberculosis. 2002;82(2-3):97-104.

171. Chackerian A, Alt J, Perera V, Behar SM. Activation of NKT cells protects mice from tuberculosis. Infect Immun. 2002;70(11):6302-9.

172. Sada-Ovalle I, Chiba A, Gonzales A, Brenner MB, Behar SM. Innate invariant NKT cells recognize Mycobacterium tuberculosis-infected macrophages, produce interferon-gamma, and kill intracellular bacteria. PLoS pathogens. 2008;4(12):e1000239.

173. Sada-Ovalle I, Skold M, Tian T, Besra GS, Behar SM. Alpha-galactosylceramide as a therapeutic agent for pulmonary Mycobacterium tuberculosis infection. American journal of respiratory and critical care medicine. 2010;182(6):841-7.

174. Rothchild AC, Jayaraman P, Nunes-Alves C, Behar SM. iNKT Cell Production of GM-CSF Controls Mycobacterium tuberculosis. PLoS pathogens. 2014;10(1):e1003805.

175. Pitabut N, Sakurada S, Tanaka T, Ridruechai C, Tanuma J, Aoki T, et al. Potential function of granulysin, other related effector molecules and lymphocyte subsets in patients with TB and HIV/TB coinfection. International journal of medical sciences. 2013;10(8):1003-14.

176. Gansert JL, Kiessler V, Engele M, Wittke F, Rollinghoff M, Krensky AM, et al. Human NKT cells express granulysin and exhibit antimycobacterial activity. Journal of immunology. 2003;170(6):3154-61.

177. Ochoa MT, Stenger S, Sieling PA, Thoma-Uszynski S, Sabet S, Cho S, et al. T-cell release of granulysin contributes to host defense in leprosy. Nature medicine. 2001;7(2):174-9.

178. Kashiwase K, Kikuchi A, Ando Y, Nicol A, Porcelli SA, Tokunaga K, et al. The CD1d natural killer T-cell antigen presentation pathway is highly conserved between humans and rhesus macaques. Immunogenetics. 2003;54(11):776-81.

179. Gansuvd B, Hubbard WJ, Hutchings A, Thomas FT, Goodwin J, Wilson SB, et al. Phenotypic and functional characterization of long-term cultured rhesus macaque spleen-derived NKT cells. Journal of immunology. 2003;171(6):2904-11.

180. Rout N, Else JG, Yue S, Connole M, Exley MA, Kaur A. Paucity of CD4+ natural killer T (NKT) lymphocytes in sooty mangabeys is associated with lack of NKT cell depletion after SIV infection. PloS one. 2010;5(3):e9787.

181. Rout N, Greene J, Yue S, O'Connor D, Johnson RP, Else JG, et al. Loss of effector and anti-inflammatory natural killer T lymphocyte function in pathogenic simian immunodeficiency virus infection. PLoS pathogens. 2012;8(9):e1002928.

182. Exley MA, Hou R, Shaulov A, Tonti E, Dellabona P, Casorati G, et al. Selective activation, expansion, and monitoring of human iNKT cells with a monoclonal antibody specific for the TCR alpha-chain CDR3 loop. European journal of immunology. 2008;38(6):1756-66.

183. Fernandez CS, Jegaskanda S, Godfrey DI, Kent SJ. In-vivo stimulation of macaque natural killer T cells with alpha-galactosylceramide. Clinical and experimental immunology. 2013;173(3):480-92.

184. Gansuvd B, Goodwin J, Asiedu CK, Jiang XL, Jargal U, Andrades P, et al. Invariant natural killer T cells from rhesus macaque spleen and peripheral blood are phenotypically and functionally distinct populations. Journal of medical primatology. 2008;37(1):1-11.

185. Chung Y, Chang WS, Kim S, Kang CY. NKT cell ligand alpha-galactosylceramide blocks the induction of oral tolerance by triggering dendritic cell maturation. European journal of immunology. 2004;34(9):2471-9.

186. Osman Y, Kawamura T, Naito T, Takeda K, Van Kaer L, Okumura K, et al. Activation of hepatic NKT cells and subsequent liver injury following administration of alpha-galactosylceramide. European journal of immunology. 2000;30(7):1919-28.

187. Fernandez CS, Cameron G, Godfrey DI, Kent SJ. Ex-vivo alpha-galactosylceramide activation of NKT cells in humans and macaques. Journal of immunological methods. 2012;382(1-2):150-9.

188. Brennan PJ. Structure, function, and biogenesis of the cell wall of Mycobacterium tuberculosis. Tuberculosis. 2003;83(1-3):91-7.

189. Sekanka G, Baird M, Minnikin D, Grooten J. Mycolic acids for the control of tuberculosis. Expert Opin Ther Pat. 2007;17(3):315-31.

190. Jarlier V, Nikaido H. Permeability barrier to hydrophilic solutes in Mycobacterium chelonei. Journal of bacteriology. 1990;172(3):1418-23.

191. Trias J, Benz R. Permeability of the cell wall of Mycobacterium smegmatis. Molecular microbiology. 1994;14(2):283-90.

192. Engelhardt H, Heinz C, Niederweis M. A tetrameric porin limits the cell wall permeability of Mycobacterium smegmatis. The Journal of biological chemistry. 2002;277(40):37567-72.

193. Xu WX, Zhang L, Mai JT, Peng RC, Yang EZ, Peng C, et al. The Wag31 protein interacts with AccA3 and coordinates cell wall lipid permeability and lipophilic drug resistance in Mycobacterium smegmatis. Biochemical and biophysical research communications. 2014;448(3):255-60.

194. Trias J, Jarlier V, Benz R. Porins in the cell wall of mycobacteria. Science. 1992;258(5087):1479-81.

195. Liu J, Barry CE, 3rd, Besra GS, Nikaido H. Mycolic acid structure determines the fluidity of the mycobacterial cell wall. The Journal of biological chemistry. 1996;271(47):29545-51.

196. Liu J, Nikaido H. A mutant of Mycobacterium smegmatis defective in the biosynthesis of mycolic acids accumulates meromycolates. Proceedings of the National Academy of Sciences of the United States of America. 1999;96(7):4011-6.

197. Jackson M, Raynaud C, Laneelle MA, Guilhot C, Laurent-Winter C, Ensergueix D, et al. Inactivation of the antigen 85C gene profoundly affects the mycolate content and alters the permeability of the Mycobacterium tuberculosis cell envelope. Molecular microbiology. 1999;31(5):1573-87.

198. Verschoor JA, Baird MS, Grooten J. Towards understanding the functional diversity of cell wall mycolic acids of Mycobacterium tuberculosis. Progress in lipid research. 2012;51(4):325-39.

199. Rossjohn J, Pellicci DG, Patel O, Gapin L, Godfrey DI. Recognition of CD1d-restricted antigens by natural killer T cells. Nature reviews Immunology. 2012;12(12):845-57.

200. Rao V, Gao F, Chen B, Jacobs WR, Jr., Glickman MS. Trans-cyclopropanation of mycolic acids on trehalose dimycolate suppresses Mycobacterium tuberculosis -induced inflammation and virulence. The Journal of clinical investigation. 2006;116(6):1660-7.

201. Rao V, Fujiwara N, Porcelli SA, Glickman MS. Mycobacterium tuberculosis controls host innate immune activation through cyclopropane modification of a glycolipid effector molecule. The Journal of experimental medicine. 2005;201(4):535-43.

202. Glickman MS, Cahill SM, Jacobs WR, Jr. The Mycobacterium tuberculosis cmaA2 gene encodes a mycolic acid trans-cyclopropane synthetase. The Journal of biological chemistry. 2001;276(3):2228-33.

203. Villeneuve M, Kawai M, Kanashima H, Watanabe M, Minnikin DE, Nakahara H. Temperature dependence of the Langmuir monolayer packing of mycolic acids from Mycobacterium tuberculosis. Biochimica et biophysica acta. 2005;1715(2):71-80.

204. Villeneuve M, Kawai M, Watanabe M, Aoyagi Y, Hitotsuyanagi Y, Takeya K, et al. Conformational behavior of oxygenated mycobacterial mycolic acids from Mycobacterium bovis BCG. Biochimica et biophysica acta. 2007;1768(7):1717-26.

205. Groenewald W, Baird MS, Verschoor JA, Minnikin DE, Croft AK. Differential spontaneous folding of mycolic acids from Mycobacterium tuberculosis. Chemistry and physics of lipids. 2014;180:15-22.

206. Villeneuve M, Kawai M, Horiuchi K, Watanabe M, Aoyagi Y, Hitotsuyanagi Y, et al. Conformational folding of mycobacterial methoxy- and ketomycolic acids facilitated by alpha-methyl trans-cyclopropane groups rather than cis-cyclopropane units. Microbiology. 2013;159(Pt 11):2405-15.

207. Niazi K, Chiu M, Mendoza R, Degano M, Khurana S, Moody D, et al. The A' and F' pockets of human CD1b are both required for optimal presentation of lipid antigens to T cells. Journal of immunology. 2001;166(4):2562-70.

208. Grant EP, Beckman EM, Behar SM, Degano M, Frederique D, Besra GS, et al. Fine specificity of TCR complementarity-determining region residues and lipid antigen hydrophilic moieties in the recognition of a CD1-lipid complex. Journal of immunology. 2002;168(8):3933-40.

209. Grant EP, Degano M, Rosat JP, Stenger S, Modlin RL, Wilson IA, et al. Molecular recognition of lipid antigens by T cell receptors. The Journal of experimental medicine. 1999;189(1):195-205.

210. Melian A, Watts GF, Shamshiev A, De Libero G, Clatworthy A, Vincent M, et al. Molecular recognition of human CD1b antigen complexes: evidence for a common pattern of interaction with alpha beta TCRs. Journal of immunology. 2000;165(8):4494-504.

211. Layre E, Collmann A, Bastian M, Mariotti S, Czaplicki J, Prandi J, et al. Mycolic acids constitute a scaffold for mycobacterial lipid antigens stimulating CD1-restricted T cells. Chemistry & biology. 2009;16(1):82-92.

212. Porcelli S, Brenner MB, Greenstein JL, Terhorst C, Balk SP, Bleicher PA. Recognition of Cluster of Differentiation 1 Antigens by Human CD4-CD8- CytolyticT Lymphocyte. Nature. 1989. 341: 447-450. 1989. Journal of immunology. 2010;184(7):3306-9.

213. Van Rhijn I, Gherardin NA, Kasmar A, de Jager W, Pellicci DG, Kostenko L, et al. TCR Bias and Affinity Define Two Compartments of the CD1b-Glycolipid-Specific T Cell Repertoire. Journal of immunology. 2014.

214. Sugita M, Cao X, Watts GF, Rogers RA, Bonifacino JS, Brenner MB. Failure of trafficking and antigen presentation by CD1 in AP-3-deficient cells. Immunity. 2002;16(5):697-706.

215. Jackman RM, Stenger S, Lee A, Moody DB, Rogers RA, Niazi KR, et al. The tyrosine-containing cytoplasmic tail of CD1b is essential for its efficient presentation of bacterial lipid antigens. Immunity. 1998;8(3):341-51.

216. Morita D, Hattori Y, Nakamura T, Igarashi T, Harashima H, Sugita M. Major T cell response to a mycolyl glycolipid is mediated by CD1c molecules in rhesus macaques. Infection and immunity. 2013;81(1):311-6.

217. Scott-Browne JP, Matsuda JL, Mallevaey T, White J, Borg NA, McCluskey J, et al. Germline-encoded recognition of diverse glycolipids by natural killer T cells. Nature immunology. 2007;8(10):1105-13.

218. Kjer-Nielsen L, Clements CS, Purcell AW, Brooks AG, Whisstock JC, Burrows SR, et al. A structural basis for the selection of dominant alphabeta T cell receptors in antiviral immunity. Immunity. 2003;18(1):53-64.

219. Gras S, Van Rhijn I, Shahine A, Cheng TY, Bhati M, Tan LL, et al. T cell receptor recognition of CD1b presenting a mycobacterial glycolipid. Nat Commun. 2016;7:13257.

220. Borg NA, Wun KS, Kjer-Nielsen L, Wilce MC, Pellicci DG, Koh R, et al. CD1d-lipid-antigen recognition by the semi-invariant NKT T-cell receptor. Nature. 2007;448(7149):44-9.

221. Matulis G, Sanderson JP, Lissin NM, Asparuhova MB, Bommineni GR, Schumperli D, et al. Innate-like control of human iNKT cell autoreactivity via the hypervariable CDR3beta loop. PLoS biology. 2010;8(6):e1000402.

222. Van Rhijn I, Young DC, Im JS, Levery SB, Illarionov PA, Besra GS, et al. CD1d-restricted T cell activation by nonlipidic small molecules. Proc Natl Acad Sci U S A. 2004;101(37):13578-83.

223. Altamirano MM, Garcia C, Possani LD, Fersht AR. Oxidative refolding chromatography: folding of the scorpion toxin Cn5. Nat Biotechnol. 1999;17(2):187-91.

224. Gadola SD, Karadimitris A, Zaccai NR, Salio M, Dulphy N, Shepherd D, et al. Generation of CD1 tetramers as a tool to monitor glycolipid-specific T cells. Philos Trans R Soc Lond B Biol Sci. 2003;358(1433):875-7.

225. Mansour S, Tocheva AS, Cave-Ayland C, Machelett MM, Sander B, Lissin NM, et al. Cholesteryl esters stabilize human CD1c conformations for recognition by self-reactive T cells. Proc Natl Acad Sci U S A. 2016.

226. Andreu N, Zelmer A, Fletcher T, Elkington PT, Ward TH, Ripoll J, et al. Optimisation of bioluminescent reporters for use with mycobacteria. PLoS ONE. 2010;5(5):e10777.

227. Carroll P, Schreuder LJ, Muwanguzi-Karugaba J, Wiles S, Robertson BD, Ripoll J, et al. Sensitive Detection of Gene Expression in Mycobacteria under Replicating and Non-Replicating Conditions Using Optimized Far-Red Reporters. PLoS ONE. 2010;5(3):e9823.

228. Workman VL, Tezera LB, Elkington PT, Jayasinghe SN. Controlled Generation of Microspheres Incorporating Extracellular Matrix Fibrils for Three-Dimensional Cell Culture. Adv Funct Mater. 2014;24(18):2648-57.

229. Snyder-Cappione JE, Nixon DF, Loo CP, Chapman JM, Meiklejohn DA, Melo FF, et al. Individuals with pulmonary tuberculosis have lower levels of circulating CD1d-restricted NKT cells. The Journal of infectious diseases. 2007;195(9):1361-4.

230. Apostolou I, Takahama Y, Belmant C, Kawano T, Huerre M, Marchal G, et al. Murine natural killer T(NKT) cells [correction of natural killer cells] contribute to the granulomatous reaction caused by mycobacterial cell walls. Proceedings of the National Academy of Sciences of the United States of America. 1999;96(9):5141-6.

231. Behar SM, Dascher CC, Grusby MJ, Wang CR, Brenner MB. Susceptibility of mice deficient in CD1D or TAP1 to infection with Mycobacterium tuberculosis. J Exp Med. 1999;189(12):1973-80.

232. Mansour S, Tocheva AS, Sanderson JP, Goulston LM, Platten H, Serhal L, et al. Structural and Functional Changes of the Invariant NKT Clonal Repertoire in Early Rheumatoid Arthritis. Journal of immunology. 2015;195(12):5582-91.

233. Langermans JA, Andersen P, van Soolingen D, Vervenne RA, Frost PA, van der Laan T, et al. Divergent effect of bacillus Calmette-Guerin (BCG) vaccination on Mycobacterium tuberculosis infection in highly related macaque species: implications for primate models in

tuberculosis vaccine research. Proceedings of the National Academy of Sciences of the United States of America. 2001;98(20):11497-502.

234. Sharpe S, White A, Gleeson F, McIntyre A, Smyth D, Clark S, et al. Ultra low dose aerosol challenge with Mycobacterium tuberculosis leads to divergent outcomes in rhesus and cynomolgus macaques. Tuberculosis. 2016;96:1-12.

235. Bienemann K, Iouannidou K, Schoenberg K, Krux F, Reuther S, Feyen O, et al. iNKT cell frequency in peripheral blood of Caucasian children and adolescent: the absolute iNKT cell count is stable from birth to adulthood. Scandinavian journal of immunology. 2011;74(4):406-11.

236. Javed S, Marsay L, Wareham A, Lewandowski KS, Williams A, Dennis MJ, et al. Temporal Expression of Peripheral Blood Leukocyte Biomarkers in a Macaca fascicularis Infection Model of Tuberculosis; Comparison with Human Datasets and Analysis with Parametric/Non-parametric Tools for Improved Diagnostic Biomarker Identification. PloS one. 2016;11(5):e0154320.

237. Van Kaer L. Regulation of immune responses by CD1d-restricted natural killer T cells. Immunologic research. 2004;30(2):139-53.

238. Fujii S, Shimizu K, Kronenberg M, Steinman RM. Prolonged IFN-gamma-producing NKT response induced with alpha-galactosylceramide-loaded DCs. Nature immunology. 2002;3(9):867-74.

239. Zhou LJ, Tedder TF. CD14+ blood monocytes can differentiate into functionally mature CD83+ dendritic cells. Proceedings of the National Academy of Sciences of the United States of America. 1996;93(6):2588-92.

240. O'Doherty U, Ignatius R, Bhardwaj N, Pope M. Generation of monocyte-derived dendritic cells from precursors in rhesus macaque blood. Journal of immunological methods. 1997;207(2):185-94.

241. Autissier P, Soulas C, Burdo TH, Williams KC. Immunophenotyping of lymphocyte, monocyte and dendritic cell subsets in normal rhesus macaques by 12-color flow cytometry: clarification on DC heterogeneity. Journal of immunological methods. 2010;360(1-2):119-28.

242. Xia H, Liu H, Zhang G, Zheng Y. Phenotype and function of monocyte-derived dendritic cells from chinese rhesus macaques. Cellular & molecular immunology. 2009;6(3):159-65.

243. Leslie DS, Dascher CC, Cembrola K, Townes MA, Hava DL, Hugendubler LC, et al. Serum lipids regulate dendritic cell CD1 expression and function. Immunology. 2008;125(3):289-301.

244. Sharpe SA, Eschelbach E, Basaraba RJ, Gleeson F, Hall GA, McIntyre A, et al. Determination of lesion volume by MRI and stereology in a macaque model of tuberculosis. Tuberculosis. 2009;89(6):405-16.

245. Sharpe SA, McShane H, Dennis MJ, Basaraba RJ, Gleeson F, Hall G, et al. Establishment of an aerosol challenge model of tuberculosis in rhesus macaques and an evaluation of endpoints for vaccine testing. Clin Vaccine Immunol. 2010;17(8):1170-82.

246. Rogers PR, Matsumoto A, Naidenko O, Kronenberg M, Mikayama T, Kato S. Expansion of human Valpha24+ NKT cells by repeated stimulation with KRN7000. Journal of immunological methods. 2004;285(2):197-214.

247. Jesudason S, Collins MG, Rogers NM, Kireta S, Coates PT. Non-human primate dendritic cells. Journal of leukocyte biology. 2012;91(2):217-28.

248. Nambiar J, Clarke AW, Shim D, Mabon D, Tian C, Windloch K, et al. Potent neutralizing anti-CD1d antibody reduces lung cytokine release in primate asthma model. MAbs. 2015;7(3):638-50.

249. Godfrey DI, Hammond KJ, Poulton LD, Smyth MJ, Baxter AG. NKT cells: facts, functions and fallacies. Immunol Today. 2000;21(11):573-83.

250. Lee PT, Benlagha K, Teyton L, Bendelac A. Distinct functional lineages of human V(alpha)24 natural killer T cells. The Journal of experimental medicine. 2002;195(5):637-41.

251. Cooper AM, Dalton DK, Stewart TA, Griffin JP, Russell DG, Orme IM. Disseminated tuberculosis in interferon gamma gene-disrupted mice. The Journal of experimental medicine. 1993;178(6):2243-7.

252. Tameris MD, Hatherill M, Landry BS, Scriba TJ, Snowden MA, Lockhart S, et al. Safety and efficacy of MVA85A, a new tuberculosis vaccine, in infants previously vaccinated with BCG: a randomised, placebo-controlled phase 2b trial. Lancet. 2013;381(9871):1021-8.

253. Bhatt K, Verma S, Ellner JJ, Salgame P. Quest for correlates of protection against tuberculosis. Clin Vaccine Immunol. 2015;22(3):258-66.

254. Kagina BM, Abel B, Scriba TJ, Hughes EJ, Keyser A, Soares A, et al. Specific T cell frequency and cytokine expression profile do not correlate with protection against tuberculosis after bacillus Calmette-Guerin vaccination of newborns. American journal of respiratory and critical care medicine. 2010;182(8):1073-9.

255. Fletcher HA, Snowden MA, Landry B, Rida W, Satti I, Harris SA, et al. T-cell activation is an immune correlate of risk in BCG vaccinated infants. Nat Commun. 2016;7:11290.

256. Scanga CA, Flynn JL. Modeling tuberculosis in nonhuman primates. Cold Spring Harb Perspect Med. 2014;4(12):a018564.

257. Im JS, Kang TJ, Lee SB, Kim CH, Lee SH, Venkataswamy MM, et al. Alteration of the relative levels of iNKT cell subsets is associated with chronic mycobacterial infections. Clinical immunology. 2008;127(2):214-24.

258. Emoto M, Emoto Y, Buchwalow IB, Kaufmann SH. Induction of IFN-gamma-producing CD4+ natural killer T cells by Mycobacterium bovis bacillus Calmette Guerin. European journal of immunology. 1999;29(2):650-9.

259. Ogawa LM, Vallender EJ. Genetic substructure in cynomolgus macaques (Macaca fascicularis) on the island of Mauritius. BMC Genomics. 2014;15:748.

260. Dhodapkar MV, Richter J. Harnessing natural killer T (NKT) cells in human myeloma: progress and challenges. Clin Immunol. 2011;140(2):160-6.

261. Kasmar A, Van Rhijn I, Moody DB. The evolved functions of CD1 during infection. Curr Opin Immunol. 2009;21(4):397-403.

262. Sutherland JS, Jeffries DJ, Donkor S, Walther B, Hill PC, Adetifa IM, et al. High granulocyte/lymphocyte ratio and paucity of NKT cells defines TB disease in a TB-endemic setting. Tuberculosis. 2009;89(6):398-404.

263. Gumperz JE, Miyake S, Yamamura T, Brenner MB. Functionally distinct subsets of CD1d-restricted natural killer T cells revealed by CD1d tetramer staining. The Journal of experimental medicine. 2002;195(5):625-36.

264. Lu W, Mehraj V, Vyboh K, Cao W, Li T, Routy JP. CD4:CD8 ratio as a frontier marker for clinical outcome, immune dysfunction and viral reservoir size in virologically suppressed HIV-positive patients. J Int AIDS Soc. 2015;18:20052.

265. Liu TY, Uemura Y, Suzuki M, Narita Y, Hirata S, Ohyama H, et al. Distinct subsets of human invariant NKT cells differentially regulate T helper responses via dendritic cells. European journal of immunology. 2008;38(4):1012-23.

266. Dougan SK, Kaser A, Blumberg RS. CD1 expression on antigen-presenting cells. Current topics in microbiology and immunology. 2007;314:113-41.

267. Sakamoto K. The pathology of Mycobacterium tuberculosis infection. Vet Pathol. 2012;49(3):423-39.

268. Dull T, Zufferey R, Kelly M, Mandel RJ, Nguyen M, Trono D, et al. A third-generation lentivirus vector with a conditional packaging system. Journal of virology. 1998;72(11):8463-71.

269. Bieber T, Rieger A, Stingl G, Sander E, Wanek P, Strobel I. CD69, an early activation antigen on lymphocytes, is constitutively expressed by human epidermal Langerhans cells. The Journal of investigative dermatology. 1992;98(5):771-6.

270. Tentori L, Graziani G, Porcelli SA, Sugita M, Brenner MB, Madaio R, et al. Rifampin increases cytokine-induced expression of the CD1b molecule in human peripheral blood monocytes. Antimicrobial agents and chemotherapy. 1998;42(3):550-4.

271. Beckman EM, Porcelli SA, Morita CT, Behar SM, Furlong ST, Brenner MB. Recognition of a lipid antigen by CD1-restricted alpha beta+ T cells. Nature. 1994;372(6507):691-4.

272. Beukes M, Lemmer Y, Deysel M, Al Dulayymi JR, Baird MS, Koza G, et al. Structure-function relationships of the antigenicity of mycolic acids in tuberculosis patients. Chemistry and physics of lipids. 2010;163(8):800-8.

273. Orme IM, Basaraba RJ. The formation of the granuloma in tuberculosis infection. Semin Immunol. 2014;26(6):601-9.

274. Ramakrishnan L. Revisiting the role of the granuloma in tuberculosis. Nature reviews Immunology. 2012;12(5):352-66.

275. Chackerian AA, Alt JM, Perera TV, Dascher CC, Behar SM. Dissemination of Mycobacterium tuberculosis is influenced by host factors and precedes the initiation of T-cell immunity. Infection and immunity. 2002;70(8):4501-9.

276. Brennan PJ, Besra GS. Structure, function and biogenesis of the mycobacterial cell wall. Biochemical Society transactions. 1997;25(1):188-94.

277. Vander Beken S, Al Dulayymi JR, Naessens T, Koza G, Maza-Iglesias M, Rowles R, et al. Molecular structure of the Mycobacterium tuberculosis virulence factor, mycolic acid, determines the elicited inflammatory pattern. European journal of immunology. 2011;41(2):450-60.

278. Kalergis AM, Nathenson SG. Altered peptide ligand-mediated TCR antagonism can be modulated by a change in a single amino acid residue within the CDR3 beta of an MHC class I-restricted TCR. Journal of immunology. 2000;165(1):280-5.

279. Guiard J, Collmann A, Garcia-Alles LF, Mourey L, Brando T, Mori L, et al. Fatty acyl structures of mycobacterium tuberculosis sulfoglycolipid govern T cell response. Journal of immunology. 2009;182(11):7030-7.

280. Wun KS, Cameron G, Patel O, Pang SS, Pellicci DG, Sullivan LC, et al. A molecular basis for the exquisite CD1d-restricted antigen specificity and functional responses of natural killer T cells. Immunity. 2011;34(3):327-39.

281. McCarthy C, Shepherd D, Fleire S, Stronge VS, Koch M, Illarionov PA, et al. The length of lipids bound to human CD1d molecules modulates the affinity of NKT cell TCR and the threshold of NKT cell activation. The Journal of experimental medicine. 2007;204(5):1131-44.

282. Garcia-Alles LF, Collmann A, Versluis C, Lindner B, Guiard J, Maveyraud L, et al. Structural reorganization of the antigen-binding groove of human CD1b for presentation of mycobacterial sulfoglycolipids. Proceedings of the National Academy of Sciences of the United States of America. 2011;108(43):17755-60.

283. Cheng TY, Relloso M, Van Rhijn I, Young DC, Besra GS, Briken V, et al. Role of lipid trimming and CD1 groove size in cellular antigen presentation. EMBO J. 2006;25(13):2989-99.

284. Ding YH, Smith KJ, Garboczi DN, Utz U, Biddison WE, Wiley DC. Two human T cell receptors bind in a similar diagonal mode to the HLA-A2/Tax peptide complex using different TCR amino acids. Immunity. 1998;8(4):403-11.

285. Coombs D, Kalergis AM, Nathenson SG, Wofsy C, Goldstein B. Activated TCRs remain marked for internalization after dissociation from pMHC. Nature immunology. 2002;3(10):926-31.

286. Barry CE, 3rd, Lee RE, Mdluli K, Sampson AE, Schroeder BG, Slayden RA, et al. Mycolic acids: structure, biosynthesis and physiological functions. Progress in lipid research. 1998;37(2-3):143-79.

287. Schiefner A, Fujio M, Wu D, Wong CH, Wilson IA. Structural evaluation of potent NKT cell agonists: implications for design of novel stimulatory ligands. J Mol Biol. 2009;394(1):71-82.

288. Liddy N, Bossi G, Adams KJ, Lissina A, Mahon TM, Hassan NJ, et al. Monoclonal TCR-redirected tumor cell killing. Nature medicine. 2012;18(6):980-7.

289. Tan MP, Gerry AB, Brewer JE, Melchiori L, Bridgeman JS, Bennett AD, et al. T cell receptor binding affinity governs the functional profile of cancer-specific CD8+ T cells. Clinical and experimental immunology. 2015;180(2):255-70.

290. Aleksic M, Dushek O, Zhang H, Shenderov E, Chen JL, Cerundolo V, et al. Dependence of T cell antigen recognition on T cell receptor-peptide MHC confinement time. Immunity. 2010;32(2):163-74.

291. Molloy A, Laochumroonvorapong P, Kaplan G. Apoptosis, but not necrosis, of infected monocytes is coupled with killing of intracellular bacillus Calmette-Guerin. The Journal of experimental medicine. 1994;180(4):1499-509.

292. Oddo M, Renno T, Attinger A, Bakker T, MacDonald HR, Meylan PR. Fas ligand-induced apoptosis of infected human macrophages reduces the viability of intracellular Mycobacterium tuberculosis. Journal of immunology. 1998;160(11):5448-54.

293. Festjens N, Vanden Berghe T, Vandenabeele P. Necrosis, a well-orchestrated form of cell demise: signalling cascades, important mediators and concomitant immune response. Biochimica et biophysica acta. 2006;1757(9-10):1371-87.

294. Grooten J, Goossens V, Vanhaesebroeck B, Fiers W. Cell membrane permeabilization and cellular collapse, followed by loss of dehydrogenase activity: early events in tumour necrosis factor-induced cytotoxicity. Cytokine. 1993;5(6):546-55.

295. Vercammen D, Vandenabeele P, Beyaert R, Declercq W, Fiers W. Tumour necrosis factor-induced necrosis versus anti-Fas-induced apoptosis in L929 cells. Cytokine. 1997;9(11):801-8.

296. Benam KH, Dauth S, Hassell B, Herland A, Jain A, Jang KJ, et al. Engineered in vitro disease models. Annu Rev Pathol. 2015;10:195-262.

297. Pampaloni F, Reynaud EG, Stelzer EH. The third dimension bridges the gap between cell culture and live tissue. Nat Rev Mol Cell Biol. 2007;8(10):839-45.

298. Parker MW, Rossi D, Peterson M, Smith K, Sikstrom K, White ES, et al. Fibrotic extracellular matrix activates a profibrotic positive feedback loop. The Journal of clinical investigation. 2014;124(4):1622-35.

299. Yamada KM, Cukierman E. Modeling tissue morphogenesis and cancer in 3D. Cell. 2007;130(4):601-10.

300. Lin PL, Ford CB, Coleman MT, Myers AJ, Gawande R, Ioerger T, et al. Sterilization of granulomas is common in active and latent tuberculosis despite within-host variability in bacterial killing. Nature medicine. 2014;20(1):75-9.

301. Barkan D, Hedhli D, Yan HG, Huygen K, Glickman MS. Mycobacterium tuberculosis lacking all mycolic acid cyclopropanation is viable but highly attenuated and hyperinflammatory in mice. Infection and immunity. 2012;80(6):1958-68.

302. Dao DN, Sweeney K, Hsu T, Gurcha SS, Nascimento IP, Roshevsky D, et al. Mycolic acid modification by the mmaA4 gene of M. tuberculosis modulates IL-12 production. PLoS pathogens. 2008;4(6):e1000081.

303. Hedhli D, Denis O, Barkan D, Daffe M, Glickman MS, Huygen K. M.tuberculosis mutants lacking oxygenated mycolates show increased immunogenicity and protective efficacy as compared to M. bovis BCG vaccine in an experimental mouse model. PloS one. 2013;8(10):e76442.

304. Watanabe M, Aoyagi Y, Ridell M, Minnikin DE. Separation and characterization of individual mycolic acids in representative mycobacteria. Microbiology. 2001;147(Pt 7):1825-37.

305. Davis JM, Ramakrishnan L. The role of the granuloma in expansion and dissemination of early tuberculous infection. Cell. 2009;136(1):37-49.